Polymer Field Effect Transistor as a probe to study Injection Barrier and Donor-Acceptor Interface

A Thesis

Submitted for the Degree of

Doctor of Philosophy

by

Manohar Rao N V

Chemistry and Physics of Material Unit
Jawaharlal Nehru Centre for Advanced Scientific Research
(A Deemed University)
Bangalore – 560 064

MAY 2010

To Spirit of Science,

LORD SAI

who taught, Learning is a way of Life

DECLARATION

I hereby declare that the matter embodied in the thesis entitled "**Polymer Field Effect Transistor as a probe to study Injection Barrier and Donor-Acceptor Interface**" is the result of investigations carried out by me at the Chemistry and Physics of Material Unit, Jawaharlal Nehru Centre for Advanced Scientific Research, Bangalore, India under the supervision of Prof. K. S. Narayan and it has not been submitted elsewhere for the award of any degree or diploma.

In keeping with the general practice in reporting scientific observations, due acknowledgment has been made whenever the work described is based on the findings of other investigators.

Manohar Rao

CERTIFICATE

I hereby certify that the matter embodied in this thesis entitled "**Polymer Field Effect Transistor as a probe to study Injection Barrier and Donor-Acceptor Interface**" has been carried out by Mr. Manohar Rao at the Chemistry and Physics of Material Unit, Jawaharlal Nehru Centre for Advanced Scientific Research, Bangalore, India under my supervision and it has not been submitted elsewhere for the award of any degree or diploma.

Prof. K. S. Narayan
(Research Supervisor)

ACKNOWLEDGMENT

It's the eternal quest of man and will always be i.e. search for permanent happiness. But the nature is so harmoniously balanced; that it permits happiness only as an interval in between pain. Laborious effort along with the ability to consistently learn precedes the fruit of happiness. The society has evolved ever since the dark ages, and its' only due to the effort mankind has put in to learn from his surroundings. Learning is one such endeavor that keep's a man intrigued about the nature and him. Society today reaps the benefits of multitude of people who has previously have attempted to seek the answer for the unknown. Passion drives an individual seeking to unravel the mystery and truth about the nature. PhD dissertation is one such small step that we as researcher get an opportunity to seek for the unanswered question about the nature. My attempt to understand the working principle of Organic Transistor is a just a mere drop in ocean of unanswered riddle and phenomenon of the nature.

The work presented in this thesis is the culmination of effort put down by me in the last five years under the able guidance of Prof K. S. Narayan, For learning in the company of learned individual always accelerate the process. I would like to express my sincere thanks to him for introducing me to field of Organic Electronics and providing me with necessary infrastructure and suggestion for carrying out my research problem. I would like to thanks him for the interesting hospitality at his home with family members during the festive season.

I would like to thank Prof C. N. R. Rao for setting up Research Institute with amazing work culture that has allowed many individual to excel in the field of science.

The ability to pursue science in an environment that allowed pursuing science as

fun was only possible by having interesting lab colleagues, who shared the same joy and passion alike. My sincere thanks to my past lab members Dr Soumya Dutta, Dr Dinesh Kabra, Dr Dhritiman Gupta, Dr Arun N, and my present lab members Monojit, Sabyasachi, Anshuman, Vini, Ravichandran, Arun Rao, Satya and Vijay. Along with various students and post doc's who worked in the lab, Dr Vasuda Bhatia, Dr Balarasu, Hemant, Jasmeet, Ankit, Radha and Shruti.

I would like to thank all the CPMU and TSU faculties, and Dr Vidyadiraja with whom, I had a good opportunity of discussing my work in details. I would also like to thank Mr. Srinath from electronics lab, Mr. Arokianathan from the workshop, Mr. Vasu from the measurement lab, whose help was quite instrumental.

The stay in campus was fruitful and symbiotic because of the special friends with whom I shared lots input and knowledge, Pavan, Sairam, Saswati, Vishwas.

I would like to acknowledge two of my school teachers, to whom I owe a lot for ensuring that I developed a interest in pursuing science, Mr. Sunil from Sri Sailam and Mr. Rajkumar Jain from Brindavan.

My deep hearted gratitude to my parent and brother for standing by me all through my research days and supporting me with constant support and encouragement. They supported me for all the important decision I took in my life.

And finally the support I have received from my life partner, 'Rashmi' with whom I have dreamt to walk the journey of my life.

SYNOPSIS

The central theme of this thesis is on fabricating and studying (p-channel, n-channel and bilayer) field effect transistor (FET) devices under dark, steady state and transient illumination conditions. This thesis probes injection barriers at metal-semiconducting polymer interface that determine the overall charge injection property of device. FET's consisting of n-channel acceptor with a coating of optically active donor polymers is studied. Presence of a D-A interface in FET showing n-channel transport is used to study the process charge separation and charge transport occurring in bulk of the acceptor upon photoexciting the donor polymer.

Inefficient charge injection/extraction process at the source/drain electrodes is responsible for contact resistance in polymer based FET's. The presence of the contact resistance in devices affect the ideal operation of PFET's especially in short channel devices, where contact resistance (CR) becomes comparable to channel resistance. CR in polymer FET's are studied using transmission line method, four-probe measurement and kelvin probe potentiometry. Local doping of polymer near metal interface improves charge injection property, by locally introducing charge carriers near polymer-metal semiconductor interface through a photodoping mechanism lowering of interfacial barrier is achieved. The approach to study injecting barrier present in a metal-semiconductor interface relies on selective illumination of polymer under the source and drain electrodes and monitoring the electrical characteristics. Observation of asymmetric threshold voltage shift in the electrical measurement for identical photon flux incident on the polymer under source and drain electrodes indicates the presence of higher injecting barrier present at the

source in comparison to barrier present at the drain electrode required for charge collection.

In order to study charge transfer and transport process at D-A interface, acceptor based FET were fabricated and optically active donor species were introduced using non-solvent deposition technique without altering the n type electrical characteristics. The possibility of exclusively exciting the donor species is used to decouple charge generation and charge transport in the acceptor bulk system. Steady state and transient pulse illumination are used to observe V_g dependent and independent processes at the D-A interface. Modified version of transient-time of flight is introduced to study the dynamics of photogenerated charge transport at the donor-acceptor interface. Poly(3-hexylthiophene) P3HT as the donor species and [6,6]-phenyl-C61-butyric acid methyl ester (PCBM) and naphthalene-bis(dicarboximide) (N2200) polymer as the acceptor system is chosen for the studies. Simple drift-diffusion transport analysis for photogenerated charge carriers at the D-A interface is carried out to model the transport of charge carriers from the D-A interface to the conducting channel. The highlight of the work shows existence of spatially separated charge-generating layer from charge-transporting layer that is used to extract simultaneous bulk and FET mobility.

PUBLICATIONS

1. Studies of photogenerated Charge carriers from Donor-Acceptor interface in a field effect transistor geometry., **Manohar Rao**, R. P. Ortiz, A. Facchetti, Tobin Marks and K. S. Narayan, *Manuscript Submitted*.

2. Studies of charge transfer process across Donor-Acceptor interface using Field effect Transistor Geometry., **Manohar Rao** and K. S. Narayan, *Appl. Phys. Lett.*, **95**, 183306 (2009).

3. Evaluation of electrode-semiconductor barrier in top contact polymer field effect transistor., **Manohar Rao** and K. S. Narayan. *Appl. Phys. Lett.*, **92**, 223308 (2008).

4. Control of single wall nanotube field effect transistor via indirect long range optically induced processes., K. S. Narayan, **Manohar Rao**, R. Zhang and P. Maniar. *Appl. Phys. Lett.* **8**8, 243507, 2006.

5. Electric field Induced steering of conducting polymer dispersion in microchannels., K. S. Narayan and **Manohar Rao**. *Appl. Phys. Lett.* **8**8, 073506, 2006.

CHAPTER 1

Organic/Polymer Field Effect Transistor

1.1 Introduction

Polymer semiconductors open up new opportunities for devices and applications that are not viable using conventional silicon technology. While polymers were known to be used broadly for a wide range of applications, their use in electronic applications due to the intrinsic semiconducting and metallic property is a recent phenomenon. These materials combine the electrical properties of semiconductors with the properties typical of plastics: low cost, versatility of chemical synthesis, ease of processing and flexibility. Polymeric semiconductors have lower fabrication costs and can be deposited on flexible substrates. Applications demonstrated for these material include their use in sensors[1], electrochromic devices[2], light emitting diodes[3], photovoltaics[4], batteries[5], field effect transistors[6] and radio-frequency identification circuitry[7]. A potential advantage of utilizing conjugated polymers in such applications is the ability to tune the electronic properties of the polymer at the molecular level. Wide range of electronic and optical properties can be fine tuned through chemical modification and this tunability allows us to facilitate the engineering of polymers to fit the specific requirements. The ability to modify the properties is of utmost importance for the efficient application of these materials along with the potential for low cost fabrication has driven

the field of polymer electronics. Prototype of major possible application based on PFET have been already demonstrated and as of now are getting close to being bought in market. The present thesis addresses important property like injection barrier and donor acceptor interface present in polymer FET and are relevant in understanding the efficient operation of organic devices.

Polymers are composed of long chains of monomer units, where the molecule units are linked to each other via a single carbon bond. Most polymers are large band gap insulators. The carbon-carbon bonds are primarily single bond, sp^3 hybridized. Conjugated polymers, on the other hand have alternating single and double bonds sp^2 hybridized. This bond alternation structure results in delocalized π electrons that give conjugated polymers their semiconducting or metallic properties. Saturated polymers (all the 4 valence electrons of carbon is used in bond) are insulating and aren't interesting as electronic material, while conjugated polymers have fundamentally different electronic configuration. Conjugated polymer has atleast one backbone chain consisting of alternating single and double bonds. The bonding in conjugate material leads to one unpaired π electron per carbon atom. In π bonding the carbon atoms are sp^2p_zhybridized, where the orbital of successive carbon atom overlap leading to electron delocalization along the backbone of the polymer. The π electron delocalization along the chain determine the optical and electronic property of the polymer, while sp^2 orbital's construct the skeleton of the polymer[8]. The conjugation between p orbitals result in splitting of energy collective orbitals into two levels π (bonding) and π^*(anti-bonding) orbitals with low and high energy respectively. Without an excitation the orbitals that are occupied are referred to as highest occupied molecular orbital (HOMO). The unoccupied orbitals are called the lowest unoccupied molecular orbital (LUMO). The intermolecular in-

teraction in long polymer chain leads to further splitting of each molecular orbital level resulting in the formation of narrow bands. The HOMO and LUMO are associated in the polymeric semiconductor as valence and conduction band respectively.

The unique properties of conducting polymers are a consequence of their electronic structure, the ground state of conjugate polymers can be either insulating or semiconducting. Conductivity in conjugated polymers increases due to doping. Doping of conjugated polymers leads to structural distortion (relaxation) of the polymer structure about the charge, which in turn stabilize the charge. The first highly conducting organic polymer, chemically doped polyacetylene, was reported in 1977[9]. Initially these doped conducting polymers were unstable in air, brittle, and difficult to process, but new generations of these materials are stable and easily processible from a wide variety of solvents. The electrical conductivities now range from those typical for insulators ($< 10^{-10}$ S/cm), to those typical of semiconductors such as silicon ($\sim 10^{-5}$ S/cm), to those greater than 10^4 S/cm (nearly that of copper, 5 x 10^5 S/cm)[10]. Doping [i.e., addition (or withdrawal) of electrons to (or from) the conjugated chains is the central process that governs the main properties of conducting polymers, in particular the crossover from an insulating to a conducting state. There are various ways to dope semiconductors, Chemical Doping: Here the double bond is broken, followed by a charge transfer between the polymer chain and the dopant, this leads to increase in conductivity. The ability to dope conjugated polymers involved charge transfer redox chemistry, oxidation (p-type doping) or reduction (n-type doping)[9]. Electrochemical Doping: Here the electrode supplies the redox charge to the conducting polymer, while ions diffuse into (or out of) the polymer structure from the nearby electrolyte to compensate the electronic charge. The doping level is determined by the voltage applied between

the conducting polymer and the counter electrode. Photogeneration is another process to increase the conductivity of the polymer; it involves creating a pair of oppositely charged carriers and dissociation into isolated charge carriers to contribute in the transport process. Charge injection into polymeric semiconductor, sandwiched between two metal electrodes with appropriate work function, results in electron injection into the π^* band from one electrode accompanied by electron removal from another π band from another electrode. This process is vastly used in organic light emitting devices, leading to radiative recombination of the injected electron and holes in the organic system. Field effect doping is another process that introduces additional charge into semiconductor via capacitive coupling. It's applicable in field effect transistor geometry, and is the basic principle of operation of FETs.

1.2 Charge Transport Model

In organic semiconductor materials, the molecules are kept together mainly by weak van der Waal's forces, which differ from the forces in inorganic semiconductors in which the atoms held together with very strong covalent bonds. When a large number of individual atoms are gathered together in a three dimensional lattice, the discrete atomic levels widen into bands and the charges move freely in delocalized bands with very high mobilities. The forces in the semiconductors determine the different charge transport. In inorganic semiconductors, charge transport occurs in delocalized states which are limited by the scattering of the carriers, mainly on phonons, that is, thermally induced lattice deformations. In inorganic semiconductors, the mobility is limited by phonons that scatter the car-

riers and thus it is reduced as the temperature increases. In organic materials, the transport differs from the band transport of inorganic semiconductors. Currently, there is a general agreement that it occurs via polaron (the deformation of the lattice around the electron or hole) hopping between localized states. In this model, charge transport occurs by hopping of charges between localized scatterers and carriers are scattered at every step. Hopping is assisted by phonons and the charge mobility increases with temperature in organic semiconductors. According to this model, small polarons move via thermally activated hopping, resulting in a simple activated dependence of the mobility with temperature. When the temperature is in the appropriate temperature range, normally above 100 K, the activation energy of the organic semiconductors is high. In this temperature range, the charge mobility is in good agreement with the small polaron model and the mobility is temperature dependent. At low temperatures, the activation energy is substantially reduced and the mobility is practically temperature independent or the mobility rises contrary to expectation. At low temperature charge transport occurs vis band transport, and this is attributed to narrow effective width of the electron and hole bands. Delocalized transport is unlikely in polycrystalline materials, since the evaluated mean-free path of carriers is shorter than the separation of two molecules rendering the concept of band transport less probable. The above observation is valid extensively for small molecules based organic semiconductors.

1.2.1 Hopping Mechanism

In disordered polymeric materials, transport is dominated by hopping mechanism. Disorder in a solid leads to localization of the states, the transport takes

places via hopping between the localized states with the assistance of phonons[11]. Two models that have been widely used are fixed range hopping[12] and variable range hopping. In fixed range hopping, proposed by Miller and Abrahams for lightly doped semiconductors at a low temperature[12], the hopping rates is given by

$$\Gamma_{ij} = \upsilon_0 exp(\frac{-2R_{ij}}{a}) exp(-\frac{E_i - E_j}{kT}) \tag{1.1}$$

Where υ_0 is a constant related to phonon density of states and other material properties, a is the localization length, R_{ij} is the distance between sites i and j with energy E_i and E_j. The first exponential term expresses the tunneling possibility, at low doping levels the probability for an electron on one site to jump to sites more distant than the nearest neighbors decreases exponentially. The second exponential term accounts for the temperature dependence of the hopping rate. The mobility is thermally activated, according to fixed range hopping.

Bassler model describes transport in a disordered organic solid assuming a gaussian density of states (DOS) and Miller-Abrahams hopping mechanism with neglected electron-phonon coupling[13]. Monte Carlo simulations reveal that the carriers relax to an equilibrium energy level, $-\sigma^2/kT$ below the center of the DOS. Here σ is the width of the gaussian DOS. The result is that the temperature dependence of mobility follows $\mu(T) = \mu_0 exp[-(T_0/T)^2]$. Later the model was extended to include spatial correlations of energetics disorder[14–16]. The temperature and electric field dependence of the mobility in this correlated Gaussian DOS model is given by

$$\mu = \mu_0 exp\left\{(-\frac{3\sigma}{5k_bT})^2 + 0.78\left[(\frac{\sigma}{k_bT})^{3/2} - 2\right]\sqrt{\frac{eaE}{\sigma}}\right\} \tag{1.2}$$

Where σ is the width of the gaussian DOS, k_b is the boltzmann constant, a is the localization length, T is the temperature, and E is the electric field. This equation correlated gaussian DOS shows a nonarrhenius temperature dependence of mobility, and Poole-Frenkel ($\mu \propto exp(\gamma E^{1/2})$) behavior for the electric field dependence.

In molecular solids and conjugated polymers, the transport model has to take into account the strong electron-phonon interaction. Charge carriers deform the surrounding lattices, thereby creating a quasiparticle called a polaron that corresponds to the charge carrier with its associated deformation. To move from one site to the next, the polaron has to 'hop' through an energy barrier, thereby the transport is thermally activated even without disorder. Based on the polaron hopping model, the mobility is given by,

$$\mu = \frac{ea^2}{k_bT}\frac{\sqrt{\pi}J^2}{h\sqrt{2E_bk_bT}}exp(-\frac{E_b}{2k_bT}) \tag{1.3}$$

where T is the temperature, J is the nearest-neighbor interaction energy, and E_b is the polaron binding energy. The activation energy of the mobility in a polaron hopping model is usually small.

1.2.2 Multiple Trapping and Release Model (MTR)

In the MTR model, a high concentration of localized states is associated within a narrow delocalized band as observed in schematics of the Fig. 1.1. The

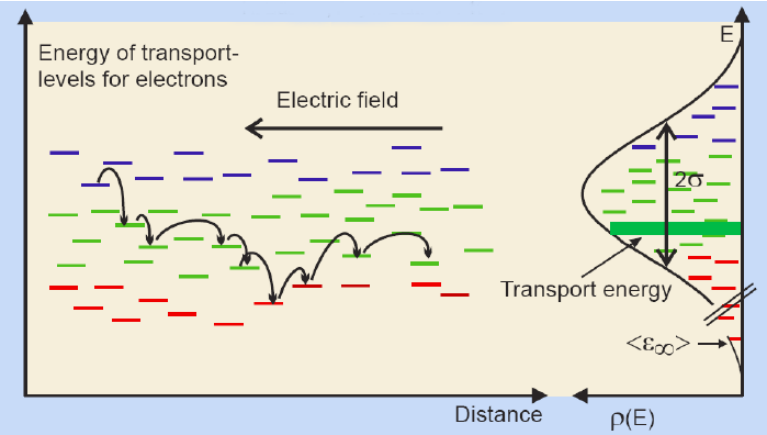

Figure 1.1: **Principle of charge transport limited by multiple trapping and thermal release.**

model was initially developed for understanding electrical transport in amorphous silicon[17]. For the charge carriers to transport through the delocalized bands, the carriers have to interact with the localized trapping states through a trapping and release mechanism. The possibility for a charge carrier to localize in a trap site is close to one, and the release of the carrier is thermally activated, thus the mobility is essentially determined by trapping and release in localized states. At relatively high temperatures, the mobility is thermally activated and is given by,

$$\mu = \mu_0 \alpha exp(-\frac{E_T}{k_b T}) \tag{1.4}$$

where μ_0 is the mobility at the band edge, α is the ratio of the delocalized to localized states, and E_T is the energy of the trap states. At low temperatures, the release of the charges at trap states is through a tunneling mechanism, and the low mobility becomes temperature independent.

1.2.3 Variable range hopping model

This model assumes that charges can hop a short distance with high activation energy or long distance with low activation energy, and has been used by Vissenberg and Matters[18]. The theory assumes an exponential distribution of localized states, which represent the tail of gaussian density of states that dominates the transport characteristics at low carrier density. The model predicts an increase of field effect mobility with increasing gate voltage, as the accumulated charge carriers fills the lower lying states of the organic semiconductors first and any additional charges in the accumulation layer will occupy states at relatively high energies. The additional charges will require lower activation energy to hop between sites. This dependence of the mobility on charge density and gate voltage has been observed for many organic semiconductors. For a series of isotropic, amorphous PPV polymers the large difference between the low mobility values extracted from space charge limited current measurements in LEDs and the comparatively higher field effect mobilities can be explained by the largely different charge carrier concentrations can be observed in the Fig. 1.2. This model is useful to predict charge carrier transport in organic diode and organic field effect transistor devices.

1.2.4 Meyer-Neldel Rule

Meyer-Neldel rule is observed in that phenomenon which are strongly diffusion dominated. M-N rule states that the activation energy for conduction can depend on various parameters ranging from the (partial) pressure[20] to applied bias. The phenomenon is observed in material that have abundant density of traps like amorphous silicon[21]. It was observed that conduction in α-sexithiophene

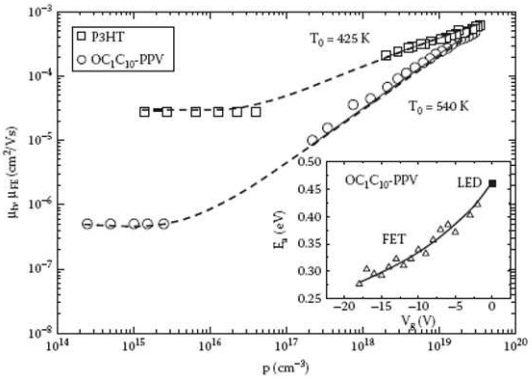

Figure 1.2: **Hole mobility as a function of charge carrier concentration in diode and field effect transistors for P3HT and a PPV derivative. Reproduced with permission from reference[19].**

(T6) was governed by traps and the M-N rule can be applied to such a organic systems also[22]. The Arrhenius behavior of conduction states that the conductivity is depending on the temperature in an exponential way,

$$\sigma = \sigma_o exp\,(-E_A/kT) \tag{1.5}$$

where with E_A the activation energy, k the Boltzmann constant and T the absolute temperature. The empiric Meyer-Neldel rule states that the pre-factor σ_o depends on the activation energy.

$$\sigma_o = \sigma_{oo} exp\,(-E_A/kT_{MN}) \tag{1.6}$$

with σ_{oo} a true constant and T_{MN} the iso-kinetic temperature. This implies that (1) The activation energy of current or carrier mobility depends on for instance the bias conditions but (2) there exists a temperature, T_{MN}, where the dependence on bias disappears. Exponential distribution of trap states results in an observation of the M-N rule in organic devices.

1.3 Field Effect Transistors

Semiconducting polymers offer a unique combination of properties that make them attractive alternatives for traditional, widely used inorganic semiconductor like silicon and gallium arsenide. Electrical conductivity in polymers can be controlled by several approaches as chemically manipulating the polymer backbone, modifying the nature of dopant, changing the degree of doping, blending conducting polymers with nanoparticles. Since the development of first polyacetylene transistors by Ebisawa et. al. in 1983 [23], a tremendous amount of research has been done in the field of organic/polymer field effect transistors FETs. In literature, small molecule based FET devices are referred to as organic FET's and the polymer based FETs as PFETs. In 1986, Koezuka et. al. reported a PFET based on electrochemically polymerized polythiophene[24]. Later in 1990, the all polymer thin film transistor was developed through evaporation technique[25], based on printing technology[26]. By the end of 2000, large scale all polymer integrated circuits[27] and complementary integrated circuits[28] based on OFET's is also reported. OFETs/PFETs have found use in application such as smart pixel[29], electronic luggage tags[30], sensors[31] and active matrix light emitting polymer displays[32].

FETs fabricated from conjugated material present several potential advantages. The techniques for depositing films for the semiconductor allows for large area to be coated. Organic/polymeric material can be deposited onto substrate using various techniques such as spin coating, thermal evaporation, inkjet printing, screen printing and micro-contact printing. Polymers are mechanically tough and thin films are flexible providing the ability to for non-planar flexible electronics. These

advantages are balanced by the disordered nature of organic semiconductors arising due to van der Waals bonded organic system resulting in low mobility of charge carriers in conjugated system in comparison to high mobility as observed in three dimensionally σ bonded crystalline semiconductor such as Si or Ge. Low mobility of organic system will ultimately limit the applications to low frequency electronics. Large scale micron size printing methods are used to realize state of the art, cheap organic electronics circuits. The emissivity nature of organic semiconductor allows for optical transmission element to be directly integrated with electronic circuitry[33], which is not possible with silicon circuitry.

1.3.1 Theory of Operation

In 1930, Lilienfeld introduced the operating principle of field effect transistors[34]. The transistor is a device that relies on an electric field to control the conductivity of a channel in a semiconductor material. FETs can be viewed as voltage controlled resistors. The main component in OFET/PFET is an organic semiconductor layer, which can be constituted either by an evaporated or solution-cast film, or by a thin single crystal, a dielectric layer, and three conducting electrodes. The device can be viewed as a plane capacitor where one of the plates is constituted by one electrode, the gate, while the semiconductor element composes the second plate; the two other electrodes, the source and the drain are directly in contact with the semiconductor. The role of the source and drain electrodes is to inject and retrieve charge carriers to and from the semiconductor. The source and drain electrodes used to inject charges into semiconductor are usually high work function metals like (Au, Pd, Pt, and Ag) but conducting polymers such as PEDOT:PSS and PANI

which can be printed are also routinely used. The gate electrode is a metal or a conducting polymer, but often highly doped silicon serves both as a substrate and gate electrode. Inorganic gate dielectrics like SiO_2, Al_2O_3, Si_3N_4 or polymeric dielectric like PMMA, PVP, PVA are commonly used.

Voltage is applied to gate electrode V_g and drain electrode V_d and the source electrode is grounded V_s=0. The potential difference between the source and gate voltage is called the gate voltage, while the potential difference between source and drain is called V_{ds}. The source is the charge injecting electrode, and is always more negative than the gate electrode when a positive gate voltage is applied (electrons are injected) and more positive than the gate electrode when a negative gate voltage is applied (holes are injected). Figure 1.3, depicts the basic operating regimes and associated current-voltage characteristics of FET. Assuming a simple metal-insulator-semiconductor (MIS) diode with a voltage V_g applied to gate electrode. A positive V_g will induce negative charges (electrons), while a negative V_g will induce positive charge (holes) at the dielectric-semiconductor interface. The number of accumulated charges is proportional to V_g and the capacitance C_i of the insulator. But not all induce charges are mobile and contribute to the current in FET. Deep traps have to be filled before the additionally induced charges can be mobile. Gate voltage greater than the threshold voltage V_{th} has to be applied, i.e. the effective gate voltage is V_g-V_{th}. When no source-drain bias is applied, the charge carrier concentration is the transistor channel in uniform. A linear gradient of charge density from the carrier injecting source to the extracting drain forms when a small V_{ds} is applied ($V_{ds}<<V_g$), this is the linear regime, where the current flowing through the channel is directly proportional to V_{ds}. The potential V(x) within the channel increases linearly from the source (x=0,V(x) =0) to V_{ds}

at the drain electrode (x=L, V(x)= V_{ds}).

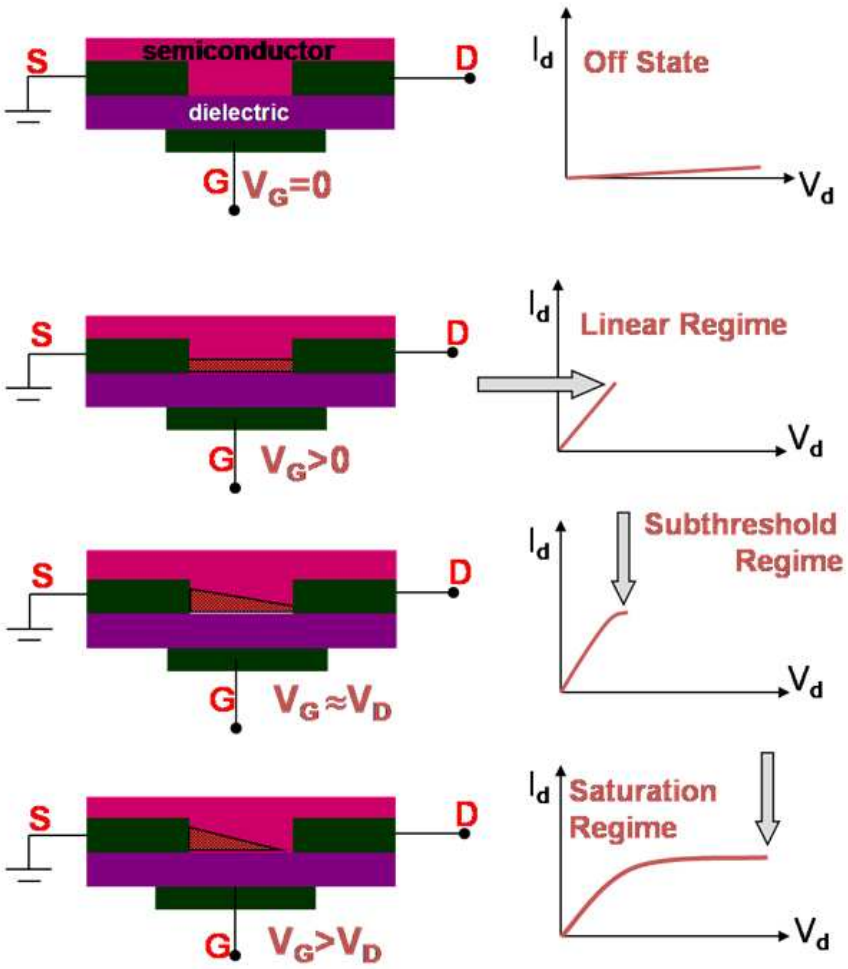

Figure 1.3: **Schematic structure of a field effect transistor and applied voltages, illustrating different operating regimes of the FET, (a) off state, (b) linear regime, (c) onset of saturation regime, i.e. subthreshold regime, (d) saturation regime and the corresponding current-voltage characteristics.**

When the V_{ds} is further increased at V_{ds}=V_g-V_{th}, the channel gets pinched off. This implies a depletion region forms next to drain electrodes because the difference between local potential V(x) and the V_g is now below the threshold voltage.

A space charge limited saturation current $I_{ds,sat}$ flows across the narrow depletion zone as carriers are swept from the pinch-off point to the drain by the high electric field in the depletion region. Further increasing the V_{ds} will not increase the current but leads to expansion of depletion region and thus a slight shortening of the channel. Since the potential at the pinch-off point remains V_g-V_{th} and thus the potential drop between that point and the source electrode stays the same and current saturates at a level $I_{ds,sat}$. FETs with short channel length require thin gate dielectrics, typically L < 10d dielectrics in order to ensure that field created by the gate voltage determines the charge distribution within the channel (gradual channel approximation) and is not determined by the lateral field due to V_{ds}. Else a space-charge limited bulk current will prevent saturation and the gate voltage will not determine the on-off state of the FET.

1.3.2 Current-Voltage Characteristics

The current-voltage characteristics in the different operation regimes of FET can be described analytically assuming gradual channel approximation; i.e. field perpendicular to the current flow generated by gate voltage is much larger than the electric field parallel to the current flow created by the drain voltage. At a given gate potential higher than the threshold voltage V_{th}, the induced mobile charges Q_{mob} per unit area at the source contacts are related to V_g via

$$Q_{mob} = C_i(V_g - V_{th}) \tag{1.7}$$

where C_i is the capacitance per unit area of the gate dielectric, the channel potential is assumed to be zero, the induced charge density depends on the position along

the channel (x),

$$Q_{mob} = C_i(V_g - V_{th} - V(x)) \tag{1.8}$$

Neglecting diffusion, the source-drain current (I_d) induced by carriers is

$$I_d = W\mu Q_{mob} E_x \tag{1.9}$$

Where W is the channel width, μ is the charge mobility and E_x is the electric field at x. Substituting for Q_{mob} and E_x we obtain,

$$I_d dx = W\mu C_i(V_g - V_{th} - V(x))dV \tag{1.10}$$

The gradual channel expression for the drain current can be then obtained by integration of the current increment from x= 0 to L, that is of the form V(x) = 0 to V_{ds}, assuming mobility is independent of carrier density thus

$$I_d = \frac{W}{L}\mu C_i[(V_g - V_{th})V_d - \frac{1}{2}V_{ds}^2] \tag{1.11}$$

In the linear regime with $V_{ds} \leq V_g$ this can be simplified to

$$I_d = \frac{W}{L}\mu_{lin} C_i(V_g - V_{th})V_{ds} \tag{1.12}$$

The drain current is directly proportional to V_g, and the field effect mobility in the linear regime (μ_{lin}) can be extracted from the gradient of I_d versus V_g

$$\mu_{lin} = \frac{\partial I_{ds}}{\partial V_g} . \frac{L}{WC_i V_{ds}} \tag{1.13}$$

The channel is pinched off when $V_{ds} = V_g$-V_{th}. The current cannot increase substantially anymore and saturates at ($I_{ds,sat}$). The saturation current now is obtained by substituting V_{ds} with V_g-V_{th}, giving

$$I_{ds,sat} = \frac{W}{2L}\mu_{sat}C_i(V_g - V_{th})^2 \tag{1.14}$$

In the saturation regime, the square root of the saturation current is directly proportional to the gate voltage. This assumes that mobility is gate voltage independent, a gate voltage dependent saturation mobility μ_{sat} can be extracted using

$$\mu_{sat} = \frac{\partial I_{ds,sat}}{\partial V_g} \cdot \frac{L}{WC_i(V_g - V_{th})} \tag{1.15}$$

The gradient of the current increase in the linear and saturation regime is directly proportional to the mobility and is constant if the mobility in the sample is gate voltage independent. Most organic semiconductors however shows gate voltage dependent mobilities, as a consequence shows deviation from linear curve in the saturation and linear regime in the transconductance curve.

1.3.3 Device Architecture

The physical nature of semiconductor and gate dielectric allows for different device structure that can show different transistor behavior. Commonly used structure are bottom contact/top gate (BC/TG), bottom contact/bottom gate (BC/BG) and top contact/bottom gate structures (TC/BG) as observed in the Fig. 1.4. FETs with same components but different geometries show different behavior. Major reason for the dissimilarity arises due to the position of inject-

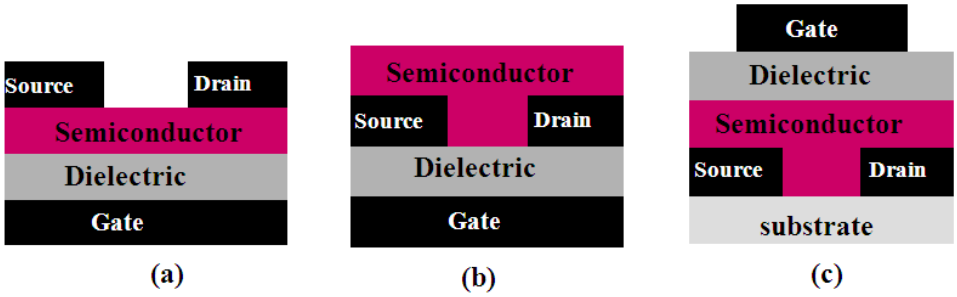

Figure 1.4: **Device architecture showing top contact-bottom gate (TC/BG), bottom contact-bottom gate (BC/BG) and top gate-bottom contact (TG/BC) structure.**

ing electrodes in relation to the gate. In BC/BG structure charges are directly injected into the channel of accumulated charges at the semiconductor-dielectric interface. In TC/BG and TG/BC structures, source drain electrodes and the channel are separated by the semiconducting layer. Charges are injected across several nanometer distance of undoped semiconductor before they reach the channel. Also in staggered BC/TG and TC/BG configuration, charges are injected not only from the edge of the electrodes but also from those parts of the electrode that overlap with the gate electrode, contributing to the current depending on distance from the edge. For top contact devices the charging of the insulator interface might also form an effective potential barrier under the drain electrode as observed in the Fig. 1.5, implying the difference between the top-contact and bottom contact devices can arise due to charging effects. Another difference arises due to different morphologies at the top and bottom surface of a semiconductor film[35] or introduction of trap states during metal evaporation on organic semiconductor for top contact transistors[36]. For top gate geometry the key parameter is the choice of insulator and solvent used for depositing the insulator material, while for bottom gate device performance is highly depended on interfacial properties which can be controlled using surface treatment[37].

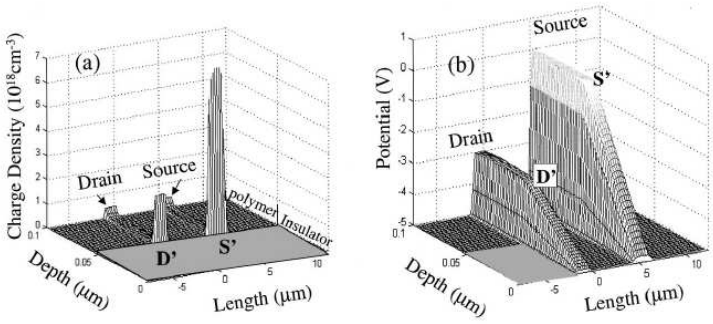

Figure 1.5: **Calculated 2D distribution of the hole density (a) and the electrostatic potential (b) 150 ns after the gate bias was set to -5 V (V_s 0 V, V_d -3 V. Reproduced with permission from reference[36].**

1.3.4 Threshold Voltage

Since OFETs/PFETs operate in the accumulation regime, where the gate voltage is polarized positively (negatively) for the n-type (p-type) semiconductor. Accordingly, the source and drain consist of simple ohmic contacts on a thin semiconductor film. In such geometry, there is no depletion layer to isolate the conducting channel from the substrate, and a very low conductivity is therefore required. Another consequence of the absence of a depletion layer is that in principle, the threshold voltage should be zero[38]. Threshold voltage is still observed in a-Si:H TFTs, the origin of which has been analyzed in detail by Shur[39]. Amorphous Si is characterized by a high density of localized states within the energy gap, the highest density occurring near the band edges. At equilibrium, the Fermi level is located close to the middle of the gap. Its position changes when carriers are induced via field effect. At low gate bias (below-threshold regime), practically all

the charge goes into the localized states, and transport occurs via activated hopping between these states, with a low mobility. With an increase of the gate bias, more states are filled, and the Fermi level moves closer to the conduction band, leading to an increase of the carrier concentration in this band and a subsequent rise of the mobility. In other words, the threshold voltage in a-Si:H corresponds to a gate-bias-dependent mobility, this is analogous to the observation of gate dependent mobility found in PFETs.

Threshold voltage can originate from several effects and depend strongly on the semiconductor and dielectric used. Built-in dipoles, impurities, interface states and charge traps contribute to the threshold voltage[40]. V_{th} can be reduced by increasing the gate capacitance and thereby inducing more charges at lower voltages. V_{th} is not constant for a given device, when organic/polymeric devices are operated for an extended time, V_{th} tends to increase. The bias stress behavior that arises due to change in V_{th} due to prolonged operation has a detrimental effect on the applicability of organic transistors in circuits.

1.3.5 Hysteresis

A key parameter for device operation, besides long term stability, is the reproducibility of the current voltage behavior, which may be affected by hysteresis phenomena. Hysteresis can be attributed to carrier trapping or migration of dopants. Traps and defects also cause a non-optimal behavior of FETs[41]. Reduction of such effects can be realized by using of patterned gate structures. Residual hysteresis can be attributed to border effects. Hysteresis effects are often observed

in organic transistors during sweeps of the gate V_{gs}. Hysteresis is a bistability in the operational transistor current. It appears as a difference in the I_{ds} values observed during forward and backward sweeps of the V_{gs}. Hysteresis is not an unwanted feature, but can be useful in nonvolatile memory, but should be avoided in standard integrated circuits. The possible origin of hysteresis in OFET can be attributed to presence of mobile charges at the channel, charge injection from the semiconductor into the dielectric, slow reactions of charge carriers in the organic semiconductor, and mobile ions in the semiconductor. Effects resulting in a polarization of the gate dielectric (ferroelectrics as dielectric or metastable polarization in the dielectric), and mobile ions in the dielectric and charge injection from the gate electrode into the dielectric[42]. A shift of V_{th} causes current hysteresis, large stable threshold shifts induced by polarization of a ferroelectric gate dielectric is used in organic memory devices[43].

Another important parameter of FETs that can be extracted from the transfer characteristics is the on/off ratio (I_{on}/I_{off}). It's the ratio of drain current in the (on) state at a particular gate voltage and the drain current in the (off) state.

$$\frac{I_{ds,on}}{I_{ds,off}} = \mu/\sigma \frac{C_i^2}{Ned_s^2} V_{ds}^2 \tag{1.16}$$

The above equation 1.16 suggests that high on/off ratio requires thin film of semiconductors with high ratio of mobility to conductivity and insulators with high capacitance per unit area. Lightly doped films will further enhance the on/off ratio due to very low off current brought about by depletion. The magnitude of (off) current is also determined by gate leakage current, especially for unpatterned gate electrodes and semiconductor layer, by the conduction pathway at the substrate

interface, and the bulk conductivity of the semiconductor, which can increase due unintentional doping.

1.4 Fabrication Methods

Most OFETs/PFETs reported are grown on silicon wafers or polymer dielectrics, the deposition of the semiconductor is the determining step of their fabrication. Depending on the nature of the semiconducting material, polymer or small molecule, various deposition techniques have been used. Small molecules are usually deposited using vacuum deposition, while macromolecule follows solution processing.

1.4.1 Solution Process Technique

One of the most simple and elegant ways to realize a good quality polymer film is through spin coating, it allows the formation of very homogeneous films with a perfect control of its thickness over relatively large area. Uniform thickness can be maintained by optimizing coating parameters such as viscosity of the solution and rotation speed. The requirement for this technique is good solubility of the polymer, since conducting polymers are not soluble the problem is overcome by grafting with solubilizing groups to the polymer backbone[44, 45] or the use of a soluble precursor polymer, which can then converted to the polymers by appropriate chemical or physical treatment[6, 46]. Solution-processed deposition has also been used with a short molecule, pentacene[47]. The main problem with spin coating is that it results in disordered amorphous films, which is not favorable for final mobility of devices, but can be circumvented in a post-bake stage resulting in

crystalline domains.

Drop casting is another deposition scheme in which solution is allowed to dry slowly in inert atmosphere. This is a slow growth process with natural evaporation of the solvent. Printing technology is the technique that has attracted recent interest for the developments of organics electronics toward future direction. It involves printing of conducting or conjugated polymers which can be used as a form of suspension or ink. Dip-coating is one of other technique to achieve large area device in both side of the substrate, here the substrate in dipped into polymer solution in a repeated and automated manner.

1.4.2 Vacuum Evaporation Technique

Spin coating requires high viscosity and is not applicable to small molecules, which can be appropriately deposited by vacuum evaporation by heating the material under reduced pressure. Advantages of vacuum deposition are the easy control of the thickness and purity of the film. Highly ordered films can be realized by monitoring the deposition rate and temperature of the substrate. The drawback being requirement of sophisticated instrumentation, which contrast the simplicity of low cost of spin coating.

The two other method used are Langmuir-Blodgett, (LB) technique allows for fine control of both structure and thickness of the film. The technique is however limited to amphiphilic molecules, composed of a hydrophobic chain and a hydrophilic head-group. Mixing of electrically active semiconductors with inactive

compounds leads to substantial decrease in the mobility compared to vacuum evaporated film. LB grown OFET have been reported with layers of quinquethiophene (5T) and arachidic acid[48]. Electrochemical polymerization was earlier one of the leading techniques for the synthesis of conducting polymers, and reports on electrochemically grown OFETs date back to late eighties[24]. The main advantage of this technique is the direct synthesis of the polymer in the form of a thin film. Drawbacks being electro polymerization occur only on conducting substrates, for which film is first grown of source-drain electrodes and its extension over the insulator occurring through the lateral expansion of the deposit, resulting in highly disordered film and poor quality of dielectric-semiconductor interface. And secondly the conducting polymer is obtained in oxidized form, so it must be reduced to become semiconducting resulting in additional disorder.

1.5 Materials

Organic semiconductors can be classified as p-type or n-type, and unlike inorganic materials they are not chemically doped. p-type or n-type behavior in FETs depends on the ability of the materials to transport the injected holes or electrons.

1.5.1 p-Type Semiconductors

Several p-type semiconductors have been developed to enable good mobility, chemical stability and solution processability. Commonly small molecule semiconductors include fused aromatic compounds, thiophene oligomers, metallophthalocyanines.

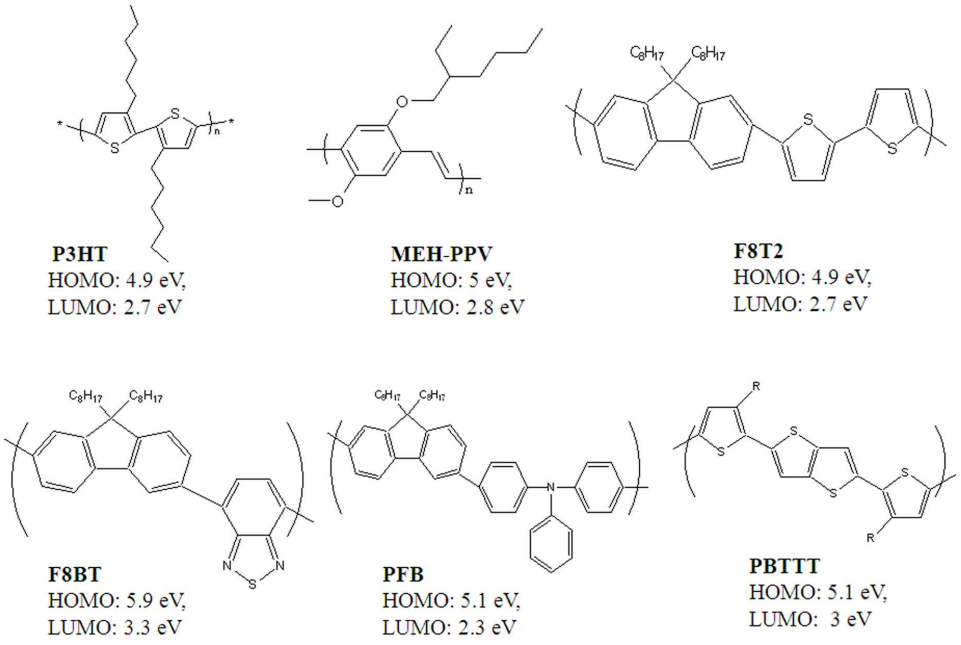

Figure 1.6: **List of important p-channel semiconductor (P3HT, MEh-PPV, F8T2, F8BT, PFB, PBTTT) with their highest occupied molecular orbital(HOMO) and lowest unoccupied molecular orbital (LUMO) levels.**

Polythiophene and polyfluorene are among the most studied polymeric semiconductors as observed in Fig. 1.6. Of these materials, the small molecule semiconductors usually exhibit the best performance, with mobility one or two orders of magnitude greater than polymeric semiconductors. Polymeric semiconductors offer the advantage of solution processability, contrary to the high vacuum vapor deposition used to fabricate small molecules films.

Pentacene is considered to be the benchmark materials for OFETs. The interplay between thin film growth, morphology and device performance of the transistors based on pentacene other vapor deposited small conjugated molecules has been studied extensively[49–52],and it's shown that the mobility and charge transport depends on the morphology of the polycrystalline thin films[53]. Parameters like na-

ture of substrate[54–56], substrate temperature[55, 57], deposition rate[55, 57, 58], and device geometry[57, 59], affects the morphology of the deposited film.

Thiophene oligomers are other promising p-type semiconductors; they give high device performance and can be tuned readily by chemical modification. The effect of alkyl side chain[60, 61], chromophore length[61], and deposition conditions[49, 62] on device performance of vapor deposited oligomer has been extensively studied. Polythiophene represent the most widely studied materials for polymer based FETs. Alkyl side-chains are introduced to enhance the solubility of polymers. The 3-alkyl side chains result in two different regioregularities, head-to-head or head to tail. A regiorandom poly(3-hexylthiophene) P3HT has both head-to-head and head-to-tail regioregularity in a random pattern, While regioregular P3HT has only one configuration either head-head or head-tail. Through well known chemical synthetic methods, polythiophene can be prepared with well-controlled regioregularity[63]. The performance of polythiophene FETs is influenced by chemical regioregularity[64–67], molecular weight[68, 69], side-chain length[50, 65, 67, 70, 71] and film morphology[64, 72–75]. Polythiophene films have microcrystalline and amorphous domains, In crystalline domains the polymer chain forms ordered $\pi - \pi$ stacking of thiophene rings. Continues films with high crystalline order with strong $\pi - \pi$ interaction and a $\pi - \pi$ stacking direction parallel to the substrate shows efficient charge transport.

Polythiophene has a low ionization potential (IP) resulting in p-doping in air due to the formation of reversible charge-transfer complex with oxygen[76]. As a result the devices tend to degrade gradually with time and cycling. To address this issues several groups have designed new polythiophene materials with more

air stability[72, 77–79]. The strategy to modify the IP is by controlling the extent of conjugation and the electron density of the conjugated system. Deviations from coplanarity with twisting adjacent thiophene rings through steric interactions result in shorter effective conjugation lengths and higher IP, thereby increasing its resistance to oxidative doping.

1.5.2 n-Type Semiconductors

Development of high performance n-type organic semiconductors is important for organic electronics because they provide routes to complementary circuits. n-type semiconductors are observed in material with high electron affinity and comprising of specific electron withdrawing groups. The inherent instability of organic anions (carbions) leads to chemical instabilities in n-type semiconductor when exposed to ambient environment. Also the electron affinities of most organic semiconductor are below 4 eV, while most metals used in OFETs have high work function, as a result the charge injection from high work function metal into the semiconductor is schottky barrier limited. Low work function metals get easily oxidized in air or react with organic semiconductors. This factor limits the availability of high mobility n-channel semiconductors.

n-type semiconductors are synthesized by adding strong electron-withdrawing groups, such as -F, -CN, -Cl to the known p-semiconductors. The presence of electron withdrawing group lowers both HOMO and LUMO level, resulting in electron injection and introducing stability in the presence of oxygen[80, 81]. Much of the n-type semiconductors have focused in compounds by adding electron withdrawing

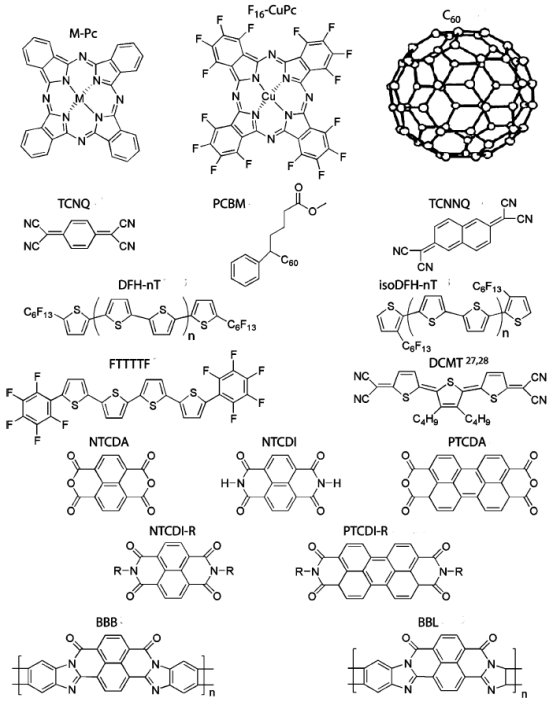

Figure 1.7: **Structures of n-channel semiconductors with known FET characteristics.**

dianhydride or diimide groups to naphthalene and perylene. FETs fabricated from napthalene derivatives have yielded mobilities of 10^{-4} cm^2/Vs and 10^{-3}cm^2/Vs for 1,4,5,8-napthalene tetracarboxylic diimides and 1,4,5,8-napthalenetetracarboxylic diianhydride[82–84]. High mobility solution processed and air stable n-type PTCDI-R derivatives, where the perylene core is functionalized by cyano groups to provide solubility for solution processing and stability for n-type conduction have shown an electron mobility of 0.64 cm^2/Vs[85].

Thiophene based n-type semiconductors can be synthesized by modifying p-type oligothiophenes. Quinoid terthiophene derivative with electro-withdrawing dicyanomethylene group have shown mobilities as high as 0.2 cm^2/Vs under vacuum conditions[86]. Fluorocarbon substituted oligothiophenes have good ther-

mal/chemical stability and exhibit strong π-π intermolecular interaction, and have exhibited electron mobility of 0.22 cm^2/Vs and I_{on}/I_{off} ratio of 10^5 for thermally evaporated α-ω-diperflurohexylquaterthiophene (DFH-4T) films[87]. Structure-property relationships in these materials show that change from p to n-type conduction is primarily due to electron withdrawing properties of flurocarbon substituent. Ladder type polymer, called poly(benzobisimidazobenzophenanthroline) BBL spun from Lewis acid ($AlCl_3$, $GaCl_3$, $FeCl_3$)[88] showed a mobility of 10^{-4} cm^2/Vs and was shown to increase upto 0.1 cm^2/Vs when spin coated from methanesulfonic acid instead of Lewis acid[89]. Recent reports [87] have shown synthesis of high mobility n-type polymer using napthalene-bis(dicarboximide) (NDI) core used as the building block to ensure a strong electron-depleted electronic structure and a regio-regular and highly π conjugated polymeric backbone. Figure 1.7 shows the list of commonly used n-type semiconductors reported to show n-channel transport.

1.5.3 Dielectric

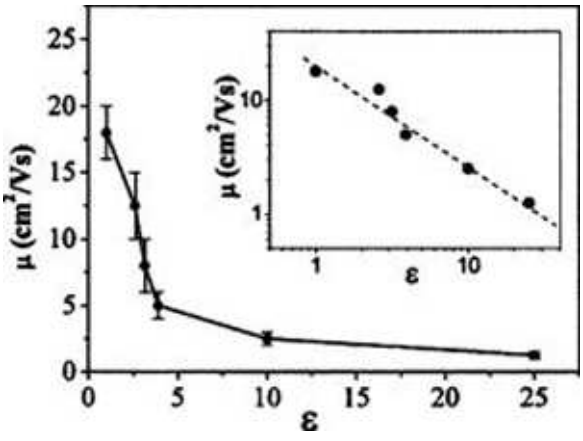

Figure 1.8: μ **as a function of dielectric constant for a single crystal rubrene FET, Inset shows the same data in log-log scale. Figure reproduced with permission from reference[90]**

The gate dielectric plays a critical role in performance of FETs. The interaction between the insulator and the semiconductor materials plays an important role in carrier transport. The crucial process of charge accumulation and transport in FET takes place at the dielectric-semiconductor interface and hence the properties of the interface and the semiconductor have a huge influence on device characteristics. The current flowing between source and drain electrode is directly proportional to induced charges (C_iV_g) at the dielectric-semiconductor interface. Important parameters to be considered while choosing a polymer dielectric are, dielectric breakdown field (E_b), capacitance per unit area C_i, $C_i = \epsilon_0\epsilon/d$ where ϵ is the dielectric constant, d is the dielectric thickness and most importantly leakage current. They should contain minimal concentration of impurities that could act as traps, environmentally stable and easily processible. High performance FETs require that the interface between dielectric and semiconductor to have low defect densities, low surface roughness and low interfacial mixing. Polymeric dielectric material can be solution processed and do not require high temperature processing and its characteristics can be tuned over a wide range by changing its chemical structure. The influence of gate dielectrics is more fundamental than changing morphologies or the amount of induced charges. The insulator is not only capable of affecting the morphology of the semiconducting layer, but can also change the density of states by local polarization effects. Carrier localization is enhanced by insulators with large permittivity, due to the random dipole field present at the interface. Mobility decreases about an order of magnitude when insulator from low dielectric constant to high dielectric constant is chosen as observed in Fig. 1.8 for single-crystal rubrene FET fabricated on various dielectric. Similar studies were carried out on conjugated polymer based on triarylmines on the dielectric constant of the employed gate dielectric[91]. This observation can be explained based on the

presence of random dipoles present at the interface that could modulate energies of localized states, leading to increased energetic disorder. It was observed that with additional energetic disorder at the interface induced by dipolar disorder in the dielectric, which increases with increasing ϵ. Increase in energetic disorder leads to broadening of Gaussian density of states which results in lowering of mobility based on mobility model for disordered semiconductors by Bassler[13]. Thus the use of polar gate insulators in PFETs can lead to increased temperatures activation in the field effect mobility, thus low-k gate insulators when used result in enhanced device performance by increased mobility, reduced threshold voltage, and lower hysteresis.

A graphical illustration of this phenomenon in Fig. 1.9 shows DOS as Gaus-

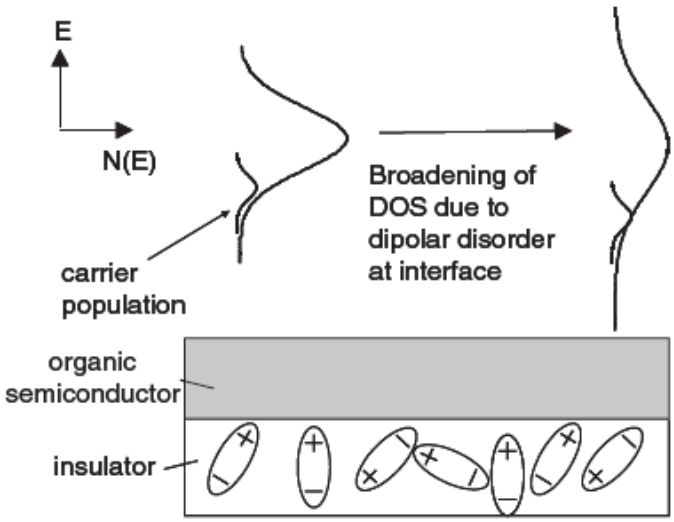

Figure 1.9: **Mechanism for enhancement of carrier localization due to polar insulator interface. Figure reproduced with permission from reference[91]**

sian distribution of localized states. These states would be totally isoenergetic in the absence of disorder. The broadening is due to number of intermolecular interaction, among them energy fluctuations due to the randomly oriented dipoles present

locally. Although neighboring dipoles in some insulators may well be strongly correlated, that can be enhanced due to applied gate voltage, sufficient variation in the electrostatic field appears to be present. Thus if the interface is polar, the DOS broadening becomes more severe, leading to more tail states. Carrier in equilibrium with the temperature and field will therefore, on average, face a higher potential barrier for upward hops into denser sites that lie closer. If one assumes that the DOS takes some other shape, the effect will still be similar, with many sites becoming trap states in the distribution. In effect as long as localized states are present, localization is likely to be enhanced by dipolar disorder. Even if the material is originally characterized by narrow bands, these may totally disintegrate by dipolar effects in the vicinity of the interface. Studies of charge transport on organic single-crystal FETs with different gate insulators have shown that the temperature dependence of the mobility evolves from metallic like to insulating like with increasing dielectric constant of the insulator. The phenomenon is accounted for by a two dimensional Frohlich polaron model that quantitatively describes the observations and shows that increasing the dielectric polarizability results in a crossover from the weak to the strong polaronic coupling regime[92]. Most organic materials are affected and improvement can be achieved using low-k insulators with almost any OFET/PFET. Disadvantage of low-k insulator is that the operating voltage required may be high, but a linear decrease in the on-state current is compensated by an exponential increase in the mobility, and reduced hysteresis and threshold voltages. The strategy of high permittivity gate insulators has been reduced operating voltages by high capacitance, and therefore high charge density, induced at low gate voltages[93, 94]. This leads to filling trap states at lower gate potential and reduced threshold voltages can be attained. In contrast in order to eliminate the trap states themselves by reducing energetic disorder and minimizing localiza-

tion enhancement due to interface, with this approach it's possible to use high-k materials. The use of multiple layer gate insulator comprising of a high permittivity layer to maximize the capacitance and a thin, low polarity layer adjacent to the semiconductor, minimizes trapping at the interface[91].

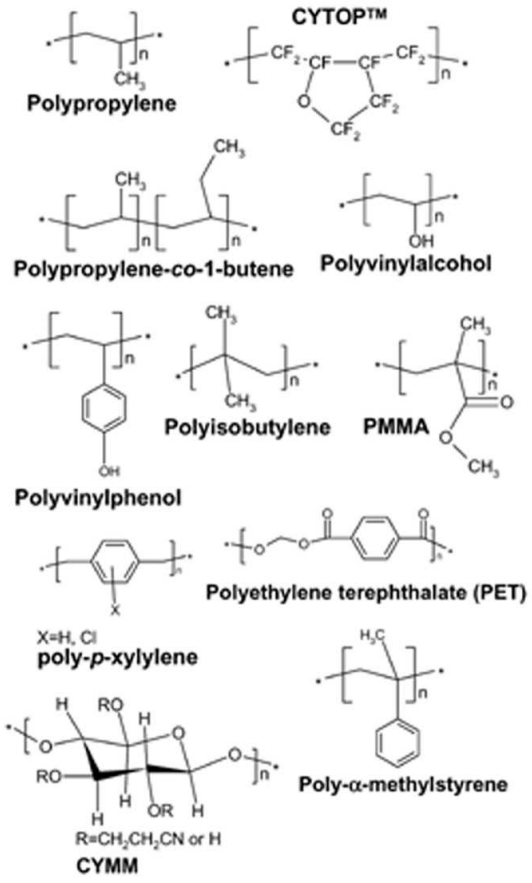

Figure 1.10: **Some of the organic polymers used as dielectric along with their dielectric constant, PVP(4.5), PMMA(3.5), CYTOP(2.1, PVA(10.4), Polypropylene(2.1), Polyisobutylene(2.2).**

A trap free gate dielectric siloxane-based compound, divinyltetramethyldisiloxane-bis(benzocyclobutene) (BCB) was demonstrated to be a promising dielectric material for FETs[95], which led to a general observation of n-channel and ambipolar characteristics in broad range of polymeric semiconductor[96]. The BCB polymer is crosslinked and film has good thermal and solvent stability and is readily integrated

into various processing schemes. Other polymeric dielectric include polyimide[97], silsesquioxane resins[98], polystyrene (PS)[99], polymethylmethacrylate(PMMA) and low k-dielectric materials[91] as shown in the Fig. 1.10 along with their dielectric constant.

1.5.4 Role of injecting electrodes

An electrical contact is generally referred to as a contact between metal and a non-metallic material which may be an insulator or a semiconductor and its functions is to enable or block carrier injection. When two materials with different Fermi levels are brought into contact, free charge carriers will flow from one material into the other until an equilibrium condition is established, until the Fermi levels of both materials are aligned. Such a net carrier flow will set up positive space charge and negative space charge on the other side of the interface, forming an electric double layer. The function of the double layer is to set up an electric field to stop any further net flow of free carriers from one material to the other. For a metal with work function Φ_m and semiconductor with work function Φ_s which are not equal, when they are bought into intimate contact with each other, based on the value of Φ_m and Φ_s different electrical contact are made.

Neutral contacts implies that the region adjacent to the contacts on both sides are neutral electrically. No space charge exists and band bending is present within the semiconductor. The requirement for neutral contact is $\Phi_m = \Phi_s$, because then the probability of electrons to flow from the metal to semiconductor is equal to the probability in reverse direction, thus there is no net flow and hence no space charge formed near the interface. A neutral contact can also be defined as one at

which the carrier concentration at the contact is equal to that in the bulk of the semiconductor.

Blocking contacts: The condition for a contact to be blocking as seen by electron from the metal is when $\Phi_m > \Phi_s$, for a metal n-type semiconductor junction. Under such a condition the electrons will flow from the semiconductor to the metal, leaving a positive space charge region (depletion region) in the semiconductor. Φ_b is the height of the potential barrier which an electron in the metal has to surmount in order to pass into the semiconductor. Such contacts are referred to as rectifying contacts because under forward bias electrons can flow easily from semiconductor to the metals, while under reverse bias the flow of electrons from the metal is limited by the electrons available over the schottky barrier. Thus a blocking contact can be defined as one which creates a depletion region extended from the interface to the inside of the semiconductor.

Ohmic contact between metal and semiconductor is defined as one which has a negligible small impedance as compared with the series impedance of the bulk of the semiconductor. This results in free carrier density at and in the vicinity of the contacts much greater than that in the bulk of the semiconductor. In order to achieve ohmic contacts, (a) choose metals of low work function such that $\Phi_m<\Phi_s$ for metal n-type semiconductor for electron injection or to choose metals of high work function such that $\Phi_m>\Phi_s$ for metal p-type semiconductor for hole injection. (b) To dope the semiconductor surface heavily near the contact to make potential barrier thin enough for efficient quantum mechanically tunneling. The resistivity of most organic semiconductors is very large so that the electrical contact impedance is negligibly small as compared with the resistance of the organic semiconductor.

For current to flow through the transistor channel, charges have to be injected from the source electrode into the semiconductor, i.e. for p-channel transistor injection of holes into the HOMO level of the semiconductor and for n-channel injection of electrons into LUMO level of semiconductor. Metal-semiconductor interface is treated as a Mott-Schottky barrier, where the barrier height is given by the difference between metal work function (ϕ_m) and the semiconductor HOMO or LUMO level. A good ohmic contact is expected when the work function of the injecting metal is close to the HOMO or LUMO level of the semiconductor[100]. Otherwise a potential barrier is formed, leading to poor charge injection and non-ohmic contacts. Comparing the work function of the injecting metal with the HOMO/LUMO levels of a semiconductor can help to determine whether charge injection is likely or whether high/low contact resistance is to be expected. But the simple Mott-Schottky model is not always sufficient to describe contacts. The interface exhibits an additional dipole barrier that tends to change the metal work function[101] and hence the interfacial barrier. Intentionally introduced dipoles at the metal surface through self-assembled monolayers are useful to improve charge injection into organic semiconductors[102, 103]. Although the simple Mott-Schottky model provides a guideline for choosing appropriate injecting electrodes, it is not sufficient to properly describe charge injection into organic semiconductor.

1.6 Ambipolar Field Effect Transistor

Organic FETs are generally used as an unipolar devices, and this has limited the design of integrated circuits to unipolar logic. From a performance point of view, complementary logic is superior to unipolar logic as it shows low power

Material(p/n type)	**Dielectric**	**Mobility (cm^2/Vs)**	**I_{on}/I_{off}**	**Reference**
Polyacetylene (p)	polysiloxane	N/A	N/A	[23]
Pentacene (p)	SiO_2	0.5	10^7	[104]
8-Thiophene (p)	SiO_2	0.33	N/A	[105]
Didecylsexithiophene (p)	SAM	0.07	N/A	[106]
Copper phthalocyanine (p)	SiO_2	0.02	4 x 10^5	[107]
Poly(3-octylthiophene)(p)	SiO_2	2 x 10^{-5}	N/A	[108]
Poly(3,4-ethyylenedioxythiophene)(p)	SiO_2	0.8	10^5	[109]
Poly(9,9-dioctylfluorene-co-bithiophene(p)	polyimide	0.02	10^5	[75]
Poly[5,5'-bis(3-dodecyl-2,2'-bithiophene](p)	SiO_2	0.06	10^6	[110]
α-Sexithiophene (p)	polyimide	0.01	N/A	[29]
Poly(hexylthiophene)(p)	SiO_2	0.01	10^8	[111]
Poly(aniline-co-N-propane-sulfonic acid aniline (p)	SiO_2	2.14	N/A	[112]
1,4,5,8-Napthalenetetracarboxylic dianhdride (n)	SiO_2	10^{-3}	N/A	[84]
Tetracyanoquinodimethane (n)	SiO_2	3 x 10^{-5}	N/A	[113]
Hexadecafluorophtalocyanine (n)	SiO_2	0.03	3 x 10^5	[114]
Dialkyl-substituted PPV (n)	BCB	10^{-3}	N/A	[96]
Copper hexadecafluorophthalocyanine (n)	polyimide	0.001	N/A	[29]

Table 1.1: Characteristics of organic/polymer FETs based on different materials, selected from representative publications.

dissipation, wide noise margin and robust operation[28]. The first organic complementary logic circuits, 48-stage shift register, were created by combining discrete p-channel and n-channel transistors[28]. A step forward for the development of complimentary logic is the realization of ambipolar transistor based on a single semiconducting film and single type of electrodes. Ambipolar device architecture or materials provide both n-channel and p-channel performance, advantage being it work for both positive and negative V_{ds} and the appropriate gate voltage V_g as observed in Fig. 1.11, while unipolar device works for only one polarity. The disadvantage in ambipolar FETs neither transistor are fully switched off, thus leakage current increases power dissipation and lowers the switching speed compared to those of complementary inverters fabricated with unipolar p or n-channel FETs.

An ambipolar FET is one in which both electron and holes are accumulated depending on the applied voltage as observed in Fig. 1.12. In an ideal ambipolar transistor with one semiconductor layer, the ambipolar regime is characterized by a hole and electron accumulation layer next to respective electrode which meets at some point within the channel region, undergoing recombination and for electroluminescent material this leads to light emission from within the channel. The transfer characteristics of ambipolar FET exhibit a characteristic V-shape with one arm indicating electron and other hole transport. For positive (negative) applied voltages, the effective gate voltage for hole(electron) depends upon applied source-drain voltage, which give rise to characteristic dependence of the transfer characteristics on the source-drain voltage. The output curves as seen in Fig. 1.12 are characterized by a superposition of standard behavior for one carrier at high V_g and a superlinear current increase at low V_g and high V_g due to injection of the opposite carrier.

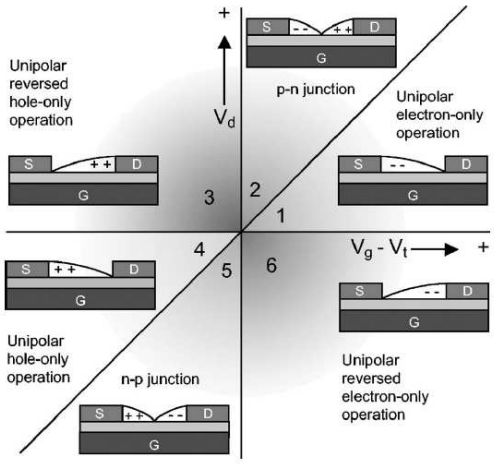

Figure 1.11: **A sketch of all operating regimes for a typical ambipolar transistor as a function of drain and gate biasing. Figure reproduced with permission from reference[115].**

Challenges of fabricating ambipolar transistors lies in efficient injection of both type of charge carriers. Optimal charge injection takes place when the work function of the metal electrode lines up with the HOMO level of the semiconductor for hole injection and LUMO level for electron injection. Most of the organic semiconductors are wide band gap material with 2-3 eV, the injection of one carrier becomes contact limited for a given electrode. Another difficulty arises due to trapping of one type of carriers, especially electron due to the presence of impurities or chemical moieties at the dielectric-semiconductor interface. The stability of hole and electron transport under ambient conditions and exposure to moisture and oxygen is detrimental for ambipolar operation.

Ambipolar transport was achieved by using n-channel and p-channel semiconducting materials either in bilayer or blend configuration or a single component material with appropriate injecting electrodes. Hole conducting α-hexathienylene

($\alpha - 6T$) and electron conducting C_{60} were sublimed on top of silicon oxide layer with appropriate source-drain electrode, the device exhibited lower electron and hole mobility than those of each material on its own[116]. Bilayer structure of pentacene and PTCDI-$C_{13}H_{27}$ with gold electrode for hole injection and magnesium electrode for electron injection exhibited ambipolar characteristics with electron mobility of 3 x 10^{-3} cm^2/Vs and hole mobility of 10^{-4} cm^2/Vs[117].

Bilayer approach yields impressive device characteristics, but the main disadvantage being the need to deposit two layers on top of each other. Solution processing becomes challenging due to the unavailability of orthogonal solvent for the deposition of second layer. Thin films of polymer blends are easily processible and well suited for application in integrated circuits, and their microstructure can be tuned by choice of solvent and spin conditions[118]. The first demonstration of polymer blend transistor with appreciable ambipolar mobilities was achieved by blending poly(2-methoxy-5-(3,7-dimethyl-octoxy)-p-phenylene vinylene)OC_1C_{10}-PPV) and [6,6]-phenyl C_{61}-butyric acid methyl ester (PCBM) with hole and electron mobility of 7 x 10^{-4} cm^2/Vs and 3 x 10^{-5} cm^2/Vs[119].

Overcoming contact resistance and suitable choice of gate dielectric is important for achieving ambipolar characteristics, bottom contact/top gate structure is used to inject holes and electron from Au electrode into F8BT polymer semiconductor showing a stable and balanced electron and hole mobility of 8 x 10^{-4} cm^2/Vs[121]. A recent breakthrough on ambipolar transport in most of the p-type semiconductor has received considerable attention, where the origin of unipolar transport is attributed to presence of hydroxyl group (OH) that can act as a trap centers for electron and oxygen having high electron affinity, replaces the hydrogen ion of OH

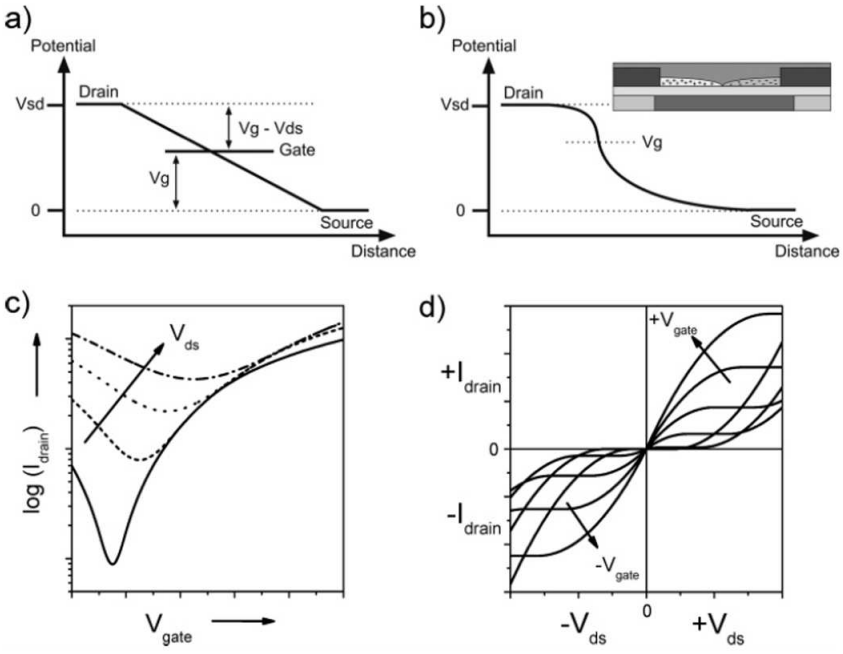

Figure 1.12: **(a) Illustration of the source, drain, and gate potentials with respect to each other in a field-effect transistor. (b) Channel potential in a field-effect transistor in the ambipolar regime with two separate channels of holes and electrons that meet within the transistor channel, where opposite charge carriers recombine (inset). (c) Transfer characteristics for an ambipolar transistor with equal hole and electron mobilities and slightly different threshold voltages in a semilog plot for positive gate voltages and different positive source drain voltages. (d) Ambipolar output characteristics for the same transistor for positive (first quadrant) and for negative (third quadrant) V_g and V_{ds}, respectively. Figure reproduced with permission from reference[120]**

with induced electrons providing hole only transport. However, the inclusion of hydroxyl free insulator, divinyltetramethylsiloxane-bis(benzocyclobutene) (BCB) has allowed ambipolar transport in almost all the well known p-type conjugated polymers[96].

1.7 Photoresponsive Polymer Field Effect Transistors

Photoresponsive polymer field effect transistor was first studied and demonstrated at JNCASR[122] nearly a decade ago. The effect of light incident on a polymer-based field-effect transistor and demonstrate the utility of light as an additional controlling parameter of the transistor state. The transistor exhibits large photosensitivity indicated by the sizable changes in the drain-source current at low levels of light[122]. The control aspect of the light is similar to the gate bias in a standard FET. The ON state for instance, in photoFET can be arrived through different routes; (a) normal FET mode without light with only gate bias, (b) FET mode at low light intensity with smaller gate bias values and, (c) FET mode at high illumination without any gate bias. The ability to use light as an additional parameter to control charge density in polymer devices has attracted lot of attention for its use as efficient photodetectors[123, 124]. In comparison to photodiode, the phototransistor exhibits larger photosensitivity induced by the sizable changes in the I_{ds} at low level of light intensity. The photo-induced response is considerably higher than that of a efficient conventional 2-terminal organic/polymeric photodiode due to process of internal amplification. In PFETs the incident light intensity can act as an added control parameter on the transistor operation, adding a novel aspect to the variety of application of PFETs. Apart from the large photoinduced changes in transport processes, interesting long-lived relaxation behavior is observed upon switching off the photoexcitation. A V_g dependence of photocurrent relaxation in the intermediate stage of the decay in phototransistor is observed. The asymmetrical charge distribution, which is inherent in this device geometry upon low level intensity photoexcitation, can be manipulated by V_g, and this is exploited

to obtain optical memory effect in PFETs[125, 126]. The writing process involves optical excitation of FET under depleted mode, while the reading and erasing procedure involves applying appropriate V_g bias conditions. These results also provide a measure of the carrier distribution profile and the electric field prevalent in the semiconducting layer.

Upon illumination two different effects are observed in the active layer of transistors, i.e. photoconductivity and the photovoltaic effect as observed in Fig. 1.13, when the transistor is in the ON-state the photocurrent is dominated by the photovoltaic effect and is given by Equation

$$I_{ph} = G_m \Delta V_{th} = \frac{AkT}{q} ln \left(1 + \frac{\eta q \lambda P_{opt}}{hc I_{pd}}\right) \tag{1.17}$$

where η is the quantum efficiency (i.e. the number of charge carriers generated per incident photon), q is the elementary charge, P_{opt} the incident optical power, I_{pd} the dark current for electrons, hc/λ the photon energy, G_m the transconductance, ΔV_{th} the threshold voltage shift, and A is a fit parameter. The photovoltaic effect together with the shift of the threshold voltage is caused by the large number of trapped charge carriers under the source contact. When the transistor is in the OFF-state, the photocurrent is dominated by photoconductivity

$$I_{ph} = (q\mu nE)\ Wd = BP_{opt} \tag{1.18}$$

where μ is the charge carrier mobility, n is the carrier density, E the electrical field in the channel, W the gate width, and d the thickness of the active layer. $I_{ph,pc}$ is therefore directly proportional to P_{opt} with a proportionality factor B.

The photocurrent is characterized by a high gain and fast saturation especially

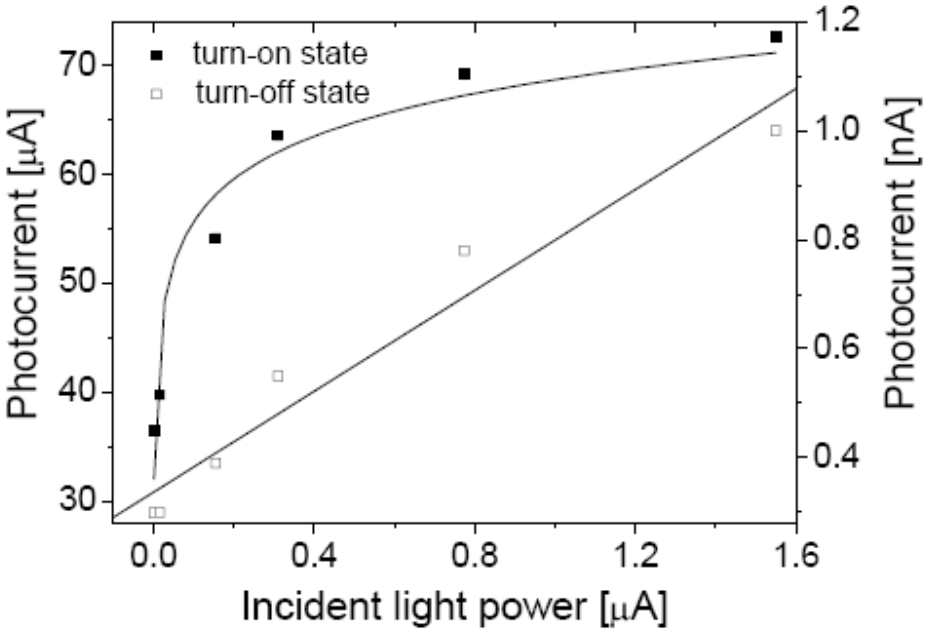

Figure 1.13: **Photocurrent as a function of incident light power from a p-channel CuPC organic phototransistor under enhancement mode(V_g=-50 V closed square) and depletion mode(V_g= 50 V, open square) showing Photovoltaic effect and Photoconductive effect. The figure has been reproduced with permission from reference[127].**

at low illumination intensities. Useful figures-of-merit for phototransistor are: The responsivity, R (expressed in A/W) of the device, which is defined as

$$R = \frac{I_{ph}}{P_{opt}} = \left(\frac{I_{ds,illum} - I_{ds,dark}}{P_{inc} A} \right) \tag{1.19}$$

where I_{ph} is the drain-source photocurrent, P_{opt} is the incident optical power, P_{inc} the power density of the incident light per unit area, $I_{ds,illum}$ the drain-source current under illumination, $I_{ds,dark}$ the drain-source current in the dark and A the effective device area.

The photosensitivity, P or signal (photocurrent) to background (dark current) ratio of the device, which is defined as

$$P = \frac{I_{ph}}{I_{ds,dark}} = \left(\frac{I_{ds,illum} - I_{ds,dark}}{I_{ds,dark}} \right) \tag{1.20}$$

The photoresponse, $R_{l/d}$, or the ratio of the total drain-source current under illumination to the drain-source current in the dark, which is defined as

$$R_{1/d} = \frac{I_{ds,illum}}{I_{ds,dark}} \tag{1.21}$$

The photoresponse exhibits a power law dependence on the illumination according to Equation

$$R_{1/d} \propto (P_{inc})^{\alpha} \tag{1.22}$$

In equation (9), P_{inc} is the power density of the incident light per unit area and the α is the exponent, which is a function of the applied voltage V_{gs}. Photoresponsive FET are important from technological point of view, but apart from that they also serve as a platform to study important photophysical features important in understanding the operation of efficient organic devices. The present thesis highlights the use of such photoresponsive FETs to study important interfaces present in PFETs.

1.8 Thesis Outline

The possibility of modifying PFET and controlling it with light has opened up several interesting problems. Several groups have studied novel materials that are photoresponsive and can be used as polymer phototransistors. Another direction for such studies that is carried out in the present lab is the nature of relaxation and memory effect that are observed in such photoresponsive PFETs. The present

thesis focus on the use of photoexcitation of the polymer to study various interfaces that is present in a top contact FET. Important property like injection barrier and donor-acceptor interface, which are relevant in understanding the efficient operation of organic devices can be studied closely.

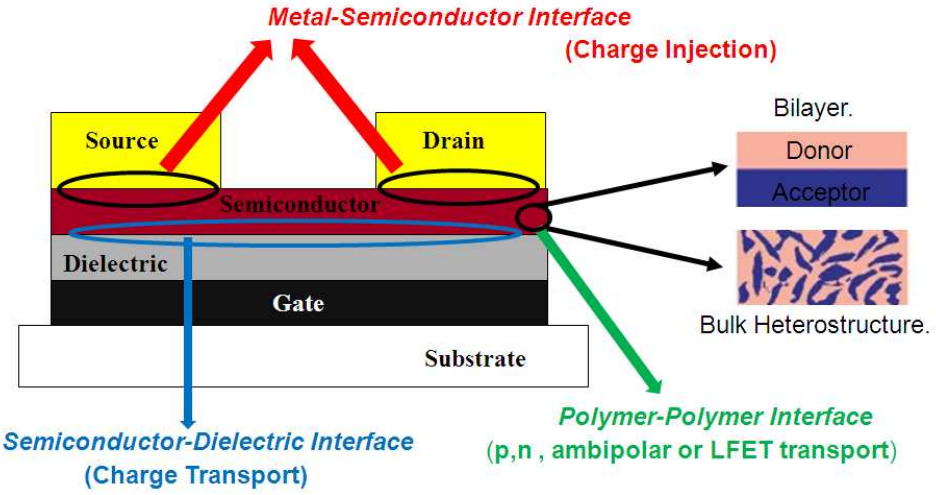

Figure 1.14: **Important interface in top contact FET depicting different process that occur at this interface.**

The Fig. 1.14 shows important interfaces present in a top contact FET, the source-drain electrode form a important metal-semiconductor interface, which determines the crucial charge injection property for the FET. The presence of polymer-polymer interface that arises in a blend or bilayer structure in FET determines p-channel, n-channel or ambipolar transport along with the charge injection property of the electrodes. The next most important crucial interface is the dielectric-semiconductor interface; this determines the overall film morphology and the general transport property. In the present thesis, Metal-Semiconductor interface and Polymer-Polymer(Donor Acceptor) interface has been extensively studied.

The interfacial barriers are the bottlenecks for charge injection and severely

limit the performance of FETs. They manifest in the form of contact resistance in the devices. We study the interfacial barrier using optical excitation directed specifically beneath the electrodes in top contact FET without optically perturbing the channel. We probe P3HT and P3HT-PCBM blend FET using this approach. A systematic shift in threshold voltage with intensity of the photoexcitation is observed for the devices. The difference in the response at the source and drain electrode regions provide an additional insight into the injection and collection processes of charge carriers at the metal-semiconductor junction.

Donor-Acceptor interface are important to study charge transfer and charge transport process that are important to understand the efficient operation of organic solar cell. We have use a methodology of fabricating acceptor based FET and introducing an optically active donor using non-solvent deposition technique, without affecting th n-channel transistor response. We selectively excite the donor species and study the process of charge transfer that occurs across the D-A interface by monitoring the n-channel FET characteristics. Series of steady state illumination and transient pulse illumination were carried to observe V_g dependent and independent process. We have used PCBM and N2200 as the n-channel acceptor system and P3HT as the optically active donor species for the studies.

CHAPTER 2

Materials, Fabrication and Measurements

2.1 Introduction

The methods adopted in this thesis revolves around the interaction of light with the semiconducting polymer in order to study the various interface present in a top contact field effect transistor. The choice of the materials and the fabrication method determines the operation of the PFETs. Poly(3-hexylethiophene) (P3HT), [6,6]-phenyl-C_{61}-butyric acid methyl ester (PCBM) and Naphthalenedicarboximide(N2200) were used as active material along with various other conjugated polymers. Insulators such as silicon dioxide, polyvinyl alcohol (PVA) and benzocyclobutene (BCB) were chosen for the studies. Devices were fabricated on glass substrate or Indium Tin Oxide (ITO) coated glass substrate as transparent gate electrode based on the experimental needs. A detailed description of the materials, the fabrication method of PFET and the experimental techniques that were used throughout the study, are discussed in the following sections.

The key components required for fabricating a polymer field effect transistor are, (a) Active semiconducting layer, (b) Dielectric layer followed by the surface treatment and (c) Metal electrodes used for injecting and collecting charges.

2.1.1 Semiconducting polymer layer

Poly(3-hexylthiophene): P3HT belongs to the group of alkyl-substituted thiophene compounds and usually is referred to as poly(3-alkylthiophene) (P3AT). Polythiophene is a leading candidate for optoelectronic application with sufficient thermal stability ($T_g > 150^o$ C). Depending on the relative position of alkyl group attached in the two consecutive chains, the polymer chains form head-to-head (HH) or head-to-tail (HT) or tail-to-tail (TT) combinations. According to the degree of orientation, P3HT is divided in two categories; regiorandom, where the HH and HT are randomly distributed and the other regioregular, which contains either HH or HT. Self-organized supramolecular structures of P3HTs upon coating on the insulating surface is normally observed and thought to be an indicator of 2-dimensional charge transport in FET structure. The structural orientation of P3HT is very sensitive to degree of regioregularity and the way of deposition techniques. The direct correlation between the mobility and the interchain interaction in P3HT was clearly reflected in the degree of regioregularity[64]. Chemical structure of P3HT is observed in the Fig. 2.1. P3HT was procured from american dye society (ADS), Catalog no: ADS306PT. Polymer was dissolved in cholorbenzene solvent (GR) grade and filtered from a 0.22 μm pore filter paper and was then used for device fabrication.

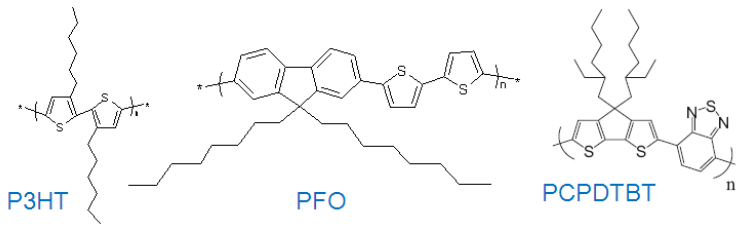

Figure 2.1: **p-type polymers used for device fabrication in the present thesis.**

[6,6]-phenyl-C_{61}-butyric acid methyl ester (PCBM): PCBM as seen in Fig. 2.2 is the soluble derivative of buckminsterfullerene. Functionalized fullerene has found extensive use mainly in two field, plastic solar cell and optical limiting glasses[128]. The high electronegativity of C_{60} makes this material a good acceptor material for solar cells. The high PL quenching efficiency was observed when C_{60} was added to polythiophene derivative[129] and PPV derivative[130]. Photophysical and electron spin resonance studies revealed that electron transfer occurred from the excited state of conjugated polymer to C_{60} and, the forward electron transfer was in the high femtosecond regime but the back electron transfer was only in the millisecond range. PCBM is an excellent electron acceptor, able to accept up to six electrons per molecule. According to the symmetry of the energy levels, the HOMO-LUMO transition is optically forbidden leading to a weak absorption at wavelengths above 500 nm. PCBM is highly soluble in organic solvents, and has a solubility of 40 mg/mL in chlorobenzene and 10 mg/ml in toluene. PCBM-C_{60} was procured from american dye society (ADS) and after filtration using a 0.22 μm pore filter paper was used for device fabrication. PCBM purity was verified by independently fabricating P3HT-PCBM blend solar cells with a reported efficiency of $\approx$ 2 % used for area dependent studies[131].

Napthalenedicarboximide N2200: Among the most interesting electron-depleted cores used for n-channel polymer building blocks, perylenes have demonstrated the greatest potential. The electron-poor NDIR co-monomer was selected because of the large electron affinity of this core, comparable to that of the far more π extended PDIR systems. Proper alkyl (R) functionalization at the rylene nitrogen atoms, here 2-octyldodecyl (2OD), result in highly soluble and processible, yet charge transport-efficient, polymers. The dithiophene (T2) unit is utilized

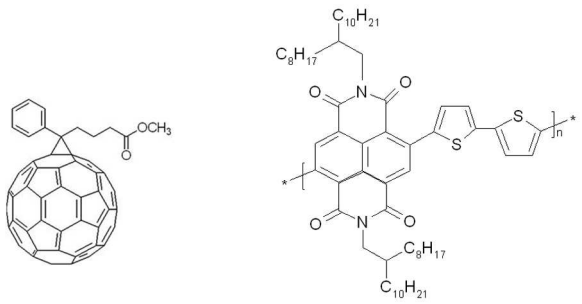

1 PCBM-C_{60} P(NDI20D-T2)

Figure 2.2: **n-type polymers used for device fabrication in the present thesis.**

because of the commercial availability, stability, and known electronic structure and geometric characteristics of this core providing highly conjugated, planar, and rod-like polymers. The optical and electrochemical properties of these new systems reveal important aspects of the polymer electronic structures and NDIR vs PDIR co-monomer effects. The thin-film polymer optical absorption spectra exhibits two/three main absorptions located at λ max at 697/391 nm. The corresponding (optical) energy gaps E_g are estimated from the spectrum low-absorption band edge as $\sim$ 1.45. Chemical structure of the polymer N2200 is seen in the Fig. 2.2. The polymer was procured from Polyera ActivInk Inc., was used for device fabrication without any further purification, after dissolving in dicholorobenzene at a concentration of 20 mg/ml.

2.1.2 Dielectric layer

Divinyltetramethyldisiloxane-bis(benzocyclobutene) (BCB): In this thesis, divinyltetramethyldisiloxane-bis(benzocyclobutene) (BCB) see Fig. 2.3 is chosen as gate-insulator, because of its excellent dielectric properties. BCB deliver highly transparent films, an important prerequisite for optical active devices. BCB

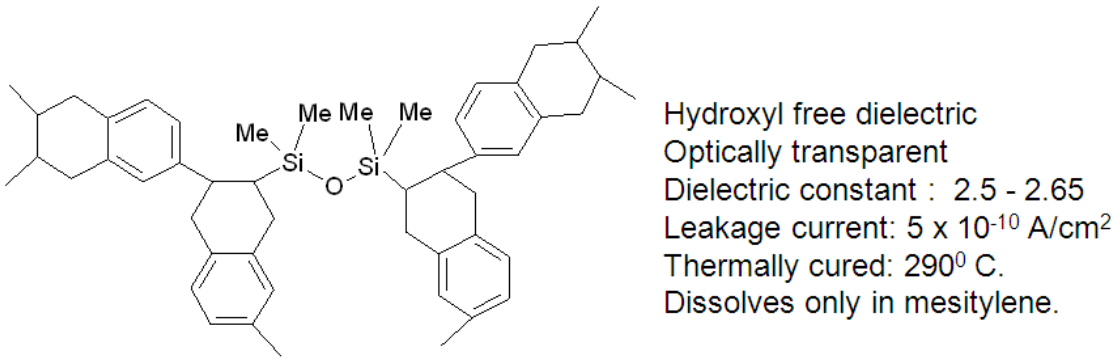

Figure 2.3: **Chemical structure of BCB polymer along with its electrical characteristics.**

belongs to a family of thermosetting polymer materials based on benzocyclobutene chemistry, developed by Dow Chemical company. The material features simple processing, superior dielectric properties, excellent gap-fill properties, polarization, low moisture absorption, and rapid curing without the emission of reaction by-products. The BCB monomer cures (crosslink's) thermally activated and forms a polymer network. One hour is required as the usual cure temperature of 250^o C [132]. The dielectric constant of BCB has negligible dispersion over a wide temperature and frequency range with a value close to *2.65*. The surface treatment of dielectric prior to semiconducting polymer deposition was based upon the choice of polymer used, For P3HT devices, HMDS treatment was followed, for PCBM based devices, (3-aminopropyl) trimethoxysilane (APTMES) treatment was applied and for N2200 based FET devices octadecyltrichlorosilane (OTS) treatment was carried out.

2.1.3 Silane Treatment

(a) **HMDS**: In solution-processed deposition technique, the interface between the polymer semiconductor and insulator is a crucial factor for deciding the field-effect mobility. Hexamethyldisilazane (HMDS) is a silane (silicon-based) chemical, which typically acts as a bridge between the inorganic substrate and the organic materials increasing the van der Waals interaction between the two surfaces. The main purpose of using HMDS layer is to convert the insulator surface from hydrophilic to hydrophobic. The common problem of oxide-coated silicon substrate (Si/SiO_2) is the appearance of hydroxyl group in the form of silanol (Si-OH) that makes the surface hydrophilic. The treatment SiO_2 with HMDS replaces the hydroxyl groups at the SiO_2 surface with methyl groups, forming $(CH_3)_3$Si-Si compound on the surface and ammonia as byproduct. The apolar nature of the modified surface containing methyl groups apparently attracts the hexyl side chains of P3HT, which in turn leads to the assembly of lamella structure with b-axis oriented parallel to the substrate. HMDS treatment on insulating surface can be performed either by projecting HMDS vapor for 2 minutes at 120^{o}C[133, 134], or by spin-coating HMDS, followed by annealing at 120^{o}C for 1 hour[135]. HMDS was obtained from sigma-aldrich was spin coated on BCB dielectric at a speed of 1500 rpm for 1 minutes, followed by baking of the substrate at 120^o C.

(b) **APTMES**: (3-aminopropyl) trimethoxysilane (APTMES) procured from Fluka chemicals was dissolved in toluene with a concentration of 1 mM, and dielectric coated substrate were then immersed in this solution for 1 minute, followed by rinsing of the substrate in toluene solvent to wash off excess of silane from the substrate. The substrate were then blown dry under N_2 gas and then transferred to glove box for semiconducting polymer deposition.

(c) **OTS**: octadecyltrichlorosilane (OTS) was procured from sigma-aldrich was dissolved in n-hexane (LR) grade to give concentration of 1 mM, substrate is then immersed in the solution for 1 minute followed by rinsing procedure in n-hexane solvent and blow drying in N_2 gas, prior to polymer deposition.

2.2 Device Fabrication

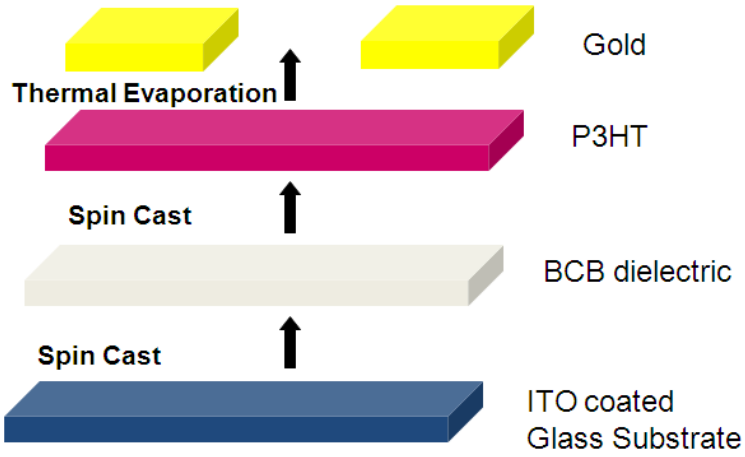

Figure 2.4: **Fabrication of Top contact FET, on BCB dielectric and ITO gate electrode with Au as S-D electrodes. Channel Length (L) 40 μm and channel width (W) (2 mm)**

Polymer field-effect transistors in top-contact configuration were fabricated using the standard protocol, as follows: (a) cleaning of the substrates (plain glass, ITO-coated glass plate, commercially available Si/SiO_2), (b) deposition of gate electrode (Al) electrode (only for glass and PET), (c) filtration of BCB monomer (d) spin-casting of BCB films on top of gate electrode's surface (exception in Si/SiO_2 substrate), (e) surface treatment using HMDS, (f) spin-casting of P3HT films on top of the gate dielectric, (g) post-coating thermal treatment and finally (h) controlled and uniform deposition of drain-source (Au) electrodes. Glass plates were

pre-cleaned with isopropyl alcohol, acetone, and distilled water and finally in acetone to remove any traces of water and the films were kept in a heat bath to dry out all the solvents. ITO coated glass plates were also cleaned using standard RCA cleaning, where the substrates were dipped into a mixture of ammonium hydroxide, hydrogen peroxide and distilled water (1: 1: 5) and heated around 80^o C for 15 minutes. Finally the substrates were cleaned in distilled water and acetone and dried. Similar treatment was also applied to Si/SiO_2 substrate.

For a typical P3HT FET device, this was the following procedure. Aluminum was coated on top of glass substrate using thermal evaporation technique. The spun-cast film of BCB was obtained using with spinning speed of about 1500 revolutions per minute (rpm) to maintain the thickness of $\approx$ 1 μm. The thin film was thermally cured at 290^o C for 30 minutes. Prior to semiconducting polymer coating, the dielectric is surface treated with HMDS followed by annealing at 90^o C for 2 hours to achieve hydrophobic surface. The as obtained P3HT was dissolved in chlorobenzene and the solutions were filtered using 0.2 μm pore size filter papers. A thin layer of P3HT was spin coated (1500 rpm for 1 minute) from chlorobenzene solution (10 mg/ml) in nitrogen atmosphere (<1 ppm O_2, <1 ppm H_2O) to obtain the thickness of 100-200 nm. After a thermal treatment process at 150^o C for 30 minutes in nitrogen environment. Gold was thermally evaporated (under a vacuum level $\sim 10^{-6}$ mbar) through a shadow mask to form drain and source electrodes with separation of 40 μm (L) and width (W) of 2 mm (W/L $\sim$ 50). The whole process of device fabrication is displayed in Fig. 2.4. Finally electrical contacts were made to the three electrodes and the device was transferred to a vacuum chamber (10^{-3} mbar) for electrical and optoelectronic measurements.

2.3 Measurement

Two identical sourcemeters SM1 and SM2 (Keithley 2400) along with a high impedance Electrometer (Keithley 6514) was used for measuring the transfer and output characteristics of PFETs. All the instruments were interfaced parallelly with the computer by means of general purpose interfaced bus (GPIB). The data acquisition was done using computer-controlled LabVIEW (version 6.1) programming. The schematic diagram of the set-up is shown in Fig. 2.5. The scan was done with sufficient interval between two successive data points depending on the response of PFET. In case of output characteristics, drain voltage V_d was varied through SM1 for different sets of voltage (gate voltage V_g) in the SM2. For measuring transfer characteristics V_g was changed through SM2 by keeping SM1 fixed. Prior to measure the transistor characteristics, we ensured that in all the cases the magnitude of leakage current as low as 100 pA was maintained to obtain the typical features. The Fig. 2.6 shows typical leakage current that existed in device specially fabricated in sandwich structure with Al bottom and top contacts. FET measurement was also carried out with using a Keithley semiconductor parameter analyzer 4200. The parameter that was varied was the scan rate and delay in between measurement, depending upon the response time of PFET. The added advantage of using semiconductor parameter analyzer over independent source units involves, faster measurement, capability for capacitance-voltage (C-V) measurement. Sweep rates and delay between data measurement could be independently controlled for V_g and V_d sweeps. Setting used for the measurement were as follow, sweep delay: 2 s, hold time: 0.01 s and the sequence of measurement was the gate voltage was first applied followed by drain voltage.

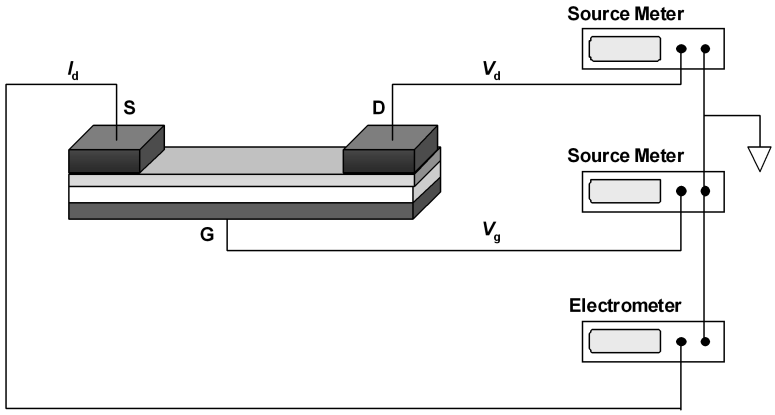

Figure 2.5: **Schematic diagram for Transistor characteristics measurement.**

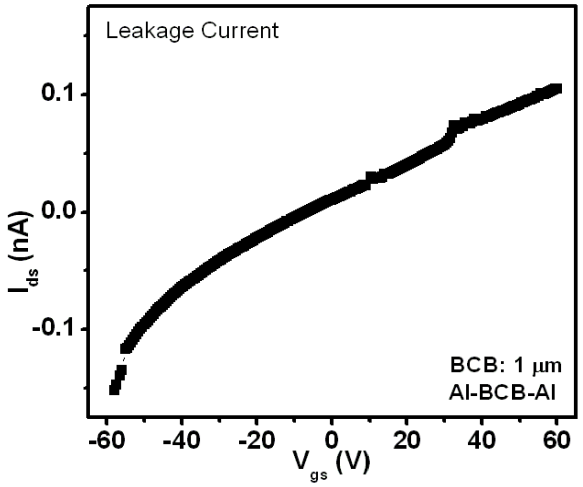

Figure 2.6: **Leakage current observed in Al-BCB-Al sandwich structure for the typical dimension of BCB film used for device fabrication.**

2.3.1 Absorption Characteristics

In case of organic polymers, absorption spectrum that measures the absorption coefficient α as a function of energy or wavelength λ, carries the primary information about the energy level of the polymer and provides various information about the sub-gap states arising due to the impurities or defects. Absorption coefficient $\alpha(\lambda)$ is essentially one of the important order parameters for detecting

opto-electronic properties. Here $\alpha(\lambda)$ of P3HT film was obtained using Hitachi U-3400 spectrophotometer and Perkin Elmer spectrophotometer. The absorption coefficient is determined using Beer-Lambert's law $I = I_0 exp(-\alpha d)$, where d is the thickness of the sample, and I and I_0 are the incident and transmitted beam intensity. The relation between $\alpha(\lambda)$ and the thickness of the film can be written of the form,

$$\alpha(\lambda)d = 2.303 log(I_0/I) \tag{2.1}$$

A typical value of $\alpha \approx 2$ x 10^5 cm^{-1} was observed at $\lambda \sim 525$ nm. The vibronic features for P3HT were observed around 2.36 eV and 2.24 eV (with shoulder around 2.1 eV) along with the onset of the bandgap around 1.9 eV. Estimation of α near the band-edge is particularly important. Band-edge is determined from the intercept of the tangent at λ corresponding to the derivative $|\partial\alpha/\partial\lambda|$ near the long wavelength region. Band edge position gives an estimate of the band gap of the polymer.

2.3.2 Intensity modulated photocurrent spectroscopy (IMPS)

Intensity modulated photocurrent spectrum is a powerful tool to measure the photoresponse, filed distribution, location of photoinduced charge generation.[137] The measurement is carried out in frequency domain. In this case a lock-in amplifier (SRS 830) was used instead of electrometer to detect weaker signal, it has an advantage of high signal to noise ratio. IMPS involve chopping of illuminated light and measuring the photocurrent using lock-in amplifier that is synchronized with the chopping frequency. The integration time constant of lock-in amplifier and so the speed of data acquisition were varied according to the chopping frequency.

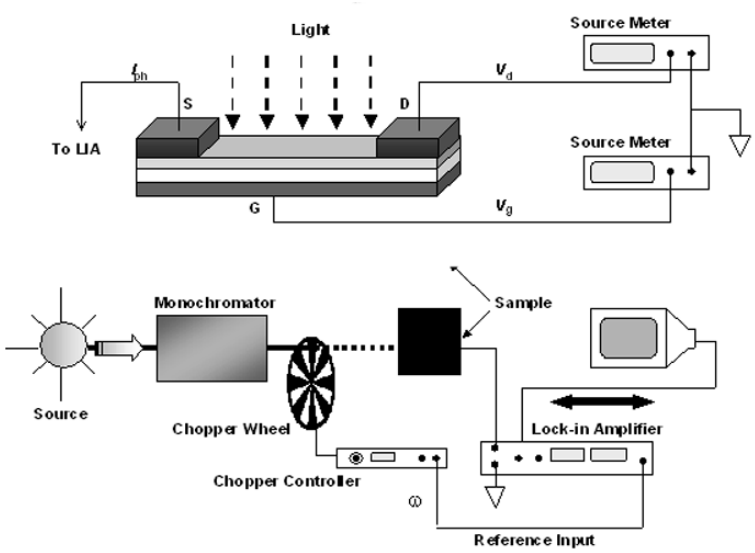

Figure 2.7: **Schematic diagram of the set-up for intensity modulated photocurrent spectroscopy(IMPS) measurement. Figure has been adapted from[136].**

Tungsten lamp, coupled with a monochromator was used to get a wide spectral window for this typical photocurrent measurement. The schematic diagram of the experimental set-up is shown in the Fig. 2.7. The photocurrent measurement can be performed also by measuring DC current value using electrometer, but the DC measurement introduces errors due to stray incident light, electrical noise, drift of I_{ds} with time and hysteresis of the sample.

2.3.3 Specific Device Details

The detailed fabrication method for each of the semiconducting polymers and dielectric polymer used for fabricating top contact FET is summarized below.

Semiconducting polymers

- P3HT: Polymer was cast from 20 mg/ml solution of chlorobenzene, and annealed at 150^o C in glove box environment for 30 minutes.
- Poly(9,9-dioctylfluorene-alt-bithiophene) (PFO): Polymer was casted from 40 mg/ml from THF solution and annealed at 100^o C in vacuum.
- poly[2,6-(4,4-bis-(2-ethylhexyl)-4H-cyclopenta[2,1-b-3,4-b]dithiophene)-alt-4,7-(2,1,3-benzothiadiazole)] PCPDTBT: Polymer was cast from 10 mg/ml solution from 1-2,dichlorobenzene and annealed at 150^o C in vacuum.
- PCBM: 20 mg/ml of PCBM in cholorobenzene solution was spin casted and annealed in glove box for 30 minutes
- N2200: 30 mg/ml of polymer was spin cast from toluene solution and annealed at 150^o C in vacuum.

Dielectrics

Following procedure were adopted for the dielectric layer:

- Polyvinyl alcohol (PVA): 4 mg/ml of PVA by weight was dissolved in warm water 60^o C and then filtered using 0.22 μm millipore filters. The solution was spin cast in ambient environment at 500 rpm and then kept for annealing at 100^0 C for 12 hours, prior to semiconducting polymer deposition.
- BCB dielectric: BCB monomer is spin cast at 1500 rpm in glove box environment, and then cured at 290^o C for 30 minutes in vacuum.
- $Si/Si0_2$: Commercially available p doped Si wafers, with $\sim$ 100 nm oxide coating were used for device fabrication.

Semiconductor	**Dielectric**	**On/Off**	**mobility** cm^2**/Vs**
P3HT (p)	PVA	∼100	10^{-4}
P3HT (p)	Si/SiO_2	∼100	10^{-3}
P3HT (p)	BCB	$\sim 10^4 - 10^6$	10^{-1}
Polyfluorene (PFO)(p)	BCB	100-200	10^{-3}
PCPDTBT (p)	BCB	$\sim 10^3$	10^{-2}
PCBM (n)	BCB	100	10^{-5}
Perylene Derivatives (n)	BCB	∼100	10^{-5}
N2200 (n)	BCB	$\sim 10^3$	10^{-2}

Table 2.1: Performance of transistors with different combination of semiconducting materials

2.4 Summary

The details of the semiconducting polymer, dielectric layer used for top contact FET for device fabrication have been summarized. Various measurements that have been carried out on the devices along with schematics have been outlined. Finally a brief summary of various procedures implemented for different polymers has been enumerated.

CHAPTER 3

Metal-Semiconductor Interface

3.1 Introduction

The operation of organic electronic device is determined by charge injection properties of the metal-organic interface. Understanding the mechanism that control the energetics of interface, in particular the magnitude of energy barrier between the metal fermi level E_F and the HOMO(LUMO) levels across the interface is important as it determines the injection of charge carrier across the interface. A primary difference in organic FET and inorganic FET is the type of metal contacts used as injecting and collecting electrodes. Inorganic structures typically uses heavily doped semiconductor as injecting electrodes[138], in contrast organic FET use metallic contacts instead of doped organic materials. The energy barrier between metal and organic films gets reflected as contact resistance in the device current-voltage characteristics.

From conventional semiconductor electronics, it is known that creating a low resistance ohmic contact requires alignment of the metal Fermi level E_F with the energy levels (bands) of the semiconductor. Figure 3.1(a) shows a simple diagram depicting energy level alignments at a metal-organic semiconductor junction. This diagram assumes that the Mott Schottky rule holds: namely, that the vacuum

levels of the metal and organic semiconductors are aligned. The outcome of this assumption is that one can easily estimate the conduction band and valence band offsets from the Fermi level. For example, the valence band offset, $E_F - E_V$, is the difference between the work function of the metal Φ_m and the ionization potential (IP) of the organic semiconductor, or

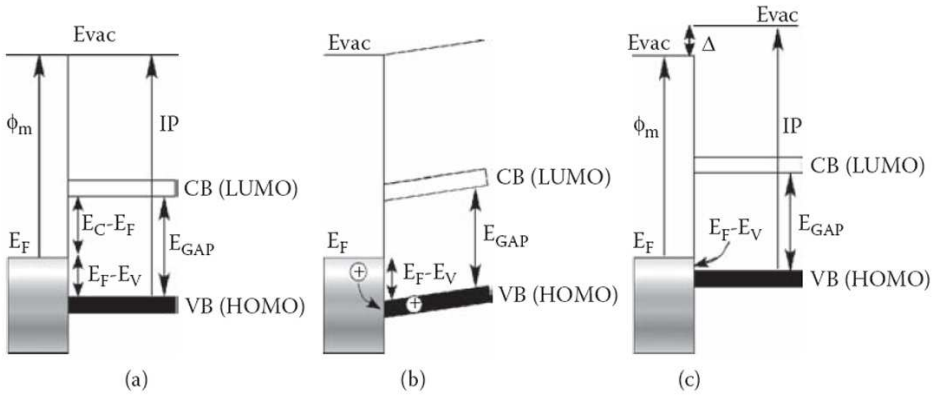

Figure 3.1: **(a) Simple band line-up diagram for a metal-organic semiconductor interface assuming that the Mott-Schottky rule holds and that the vacuum levels for the metal and semiconductor are aligned. (b) Application of a positive bias to the metal can result in hole injection into the semiconductor by thermionic emission over the barrier. (c) Band line-up diagram in the case where an interface dipole is present, causing a shift Δ in the vacuum levels across the junction.**

$$E_F - E_V = \Phi_m - IP \tag{3.1}$$

This offset is in turn a good estimate of the potential barrier to hole injection from the metal to the semiconductor. As shown in Fig. 3.1(b), applying a positive bias to the metal relative to the semiconductor can result in hole injection (thermionic emission) into the valence band if the holes can surmount the barrier E_F - E_V. A similar discussion holds for electron injection into the conduction band, but in that case the metal is biased negative and the barrier is determined by E_C-

E_F. Thus, the electronic structure of metal organic semiconductor interfaces plays a crucial role in determining the charge transport characteristics of the contact.

In reality, many metal-organic semiconductor interfaces do not follow the Mott-Schottky rule and the electronic structure is significantly more complicated than depicted in Fig. 3.1(a)[139]. Often, an interface dipole Δ is present that shifts the vacuum level of the semiconductor with respect to the metal, as shown in Fig. 3.1(c). Interface dipoles have several possible origins, including charge transfer between the semiconductor molecules and the metal. Reduction of the metal work function by adsorption of the organic layer (even absorption of a noble gas on a metal modifies the metal work function by pushing back the metal surface electrons and population of metal-induced mid-gap states (new energy levels) at the interface. The magnitude of the potential change due to the dipole Δ must be included in the calculation of the valence band offset,

$$E_F - E_V = \Phi_m - IP \pm \Delta \tag{3.2}$$

where the mathematical sign in front of Δ is chosen to reflect the direction of the interfacial dipole. Studies of electronic structure of metal-organic interface can be carried out using ultraviolet photoelectron spectroscopy (UPES) and inverse photoemission spectroscopy (IPES), which probes filled and empty electronic states. The techniques allows us to measure HOMO and LUMO energy level of polymer with respect to the metal fermi position and also the presence of interfacial dipoles. The interface between P3HT and Au has been investigated using photoemission spectroscopy, the results indicating that the P3HT interface has a smaller hole injection barrier 0.59 eV[140]. Evaluation of UPS and XPS of P3HT-Au interface

yields the electronic structure of the P3HT polymer and is used to estimate the presence of barrier required for hole injection as seen in the Fig. 3.2.

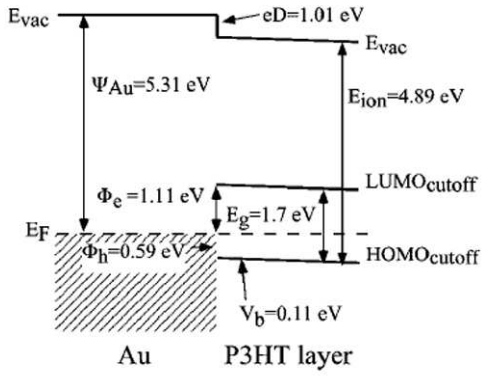

Figure 3.2: **Orbital lineup at the P3HT/Au interface as determined from the XPS and UPS data set. Figure reproduced with permission from the reference[140].**

The process of local doping of the semiconductor interfacial region to provide a tunneling contact is more associated with inorganic semiconductors, though few examples can be found in organic semiconductors[141]. Despite the fact that significant potential barriers (> 0.3 eV) exist at many metal-organic semiconductor interfaces, it is possible to fabricate ohmic source and drain contacts in PFETs. A likely reason for this is that the charge injection mechanism is probably not simple thermionic emission in which carriers must surmount the full potential barrier, as originally indicated in Fig. 3.1(b). Instead, at large interfacial electric field strength, field emission (tunneling) through the barrier can become possible; this is a process that effectively lowers the potential barrier. Another possible injection mechanism involves defect-assisted transport in which carriers bypass the barrier by hopping through midgap states[142]. Injection of charge carriers from metal into semiconductor is an important issue, and low mobility of organic semiconductor makes injection an inefficient process, since the mean free path is very small

resulting in trapping by the attractive part of the image potential thereby flowing back into the metal. Charge injection into semiconductor has to rely on proper alignment of metal Fermi level with HUMO (LUMO) level for achieving ohmic contacts with holes (electron) as observed in Fig. 3.3(a)(b) Relying on energy level alignment forces restriction on the choice of OSC which can be used for device fabrication, since the work function of easily processible metal is limited. The Fig. 3.4 shows commonly used various metals used for injecting hole and electron into the semiconducting P3HT polymer. The morphology of OSC in the region close to the interface can be disordered giving rise to bad electrical contact[59]. The origin of surface dipoles at the metal interface also modifies the energy level alignment. The above process results in non-ideal metal-semiconductor interfaces for charge injection and get reflected as contact resistance in organic devices.

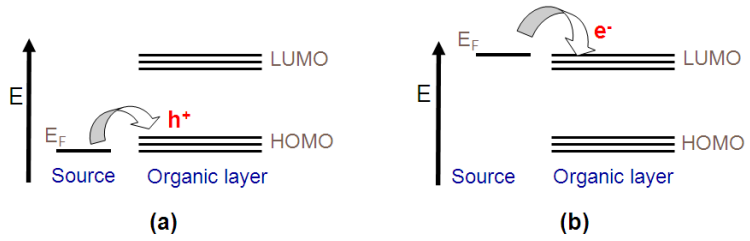

Figure 3.3: **(a) Energy level alignment of source metal fermi level with HOMO for hole injection, (b) with LUMO for electron injection into semiconductor layer.**

3.2 Origin of Contact Resistance

In PFET's if contacts are non-ohmic, externally applied voltage partly drops across the contact region and the channel. This can be modeled by adding contact

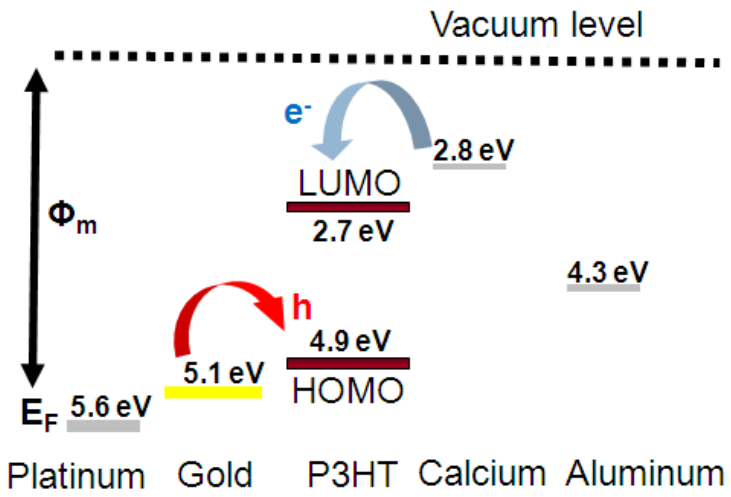

Figure 3.4: **Work function of various metals with respect to HUMO and LUMO level of P3HT used for injecting electrons and holes in the polymer.**

resistance in series to the source and drain electrodes. In traversing an OFET channel from source to drain, charge carriers are (1) injected from the source contact into the semiconductor channel; (2) transported across the length of the channel; and (3) extracted from the channel into the drain. These processes can be roughly thought of as three resistors in series. The resistances associated with carrier injection and collection steps can be grouped into the contact resistance R_c, while the resistance associated with crossing the channel length in the semiconductor is termed the channel resistance $R_{channel}$. Keeping the contact resistance small compared to the channel resistance is crucial to the realization of "ohmic contacts" in OFETs (i.e., for an ohmic contact, $R_c << R_{channel}$). If the contacts are ohmic, then they are not bottlenecks for current to flow and they can source and sink all the current that can be transported by the channel under the given bias conditions. Importantly, nominally high-resistance contacts can still be ohmic as long as they are able to source or sink the current driven through an even more resistive channel.

This definition also implies that contacts that function ohmically for a given channel length may no longer be ohmic as the channel length shrinks. This is because $R_{channel}$ scales proportionally with length, so making smaller channel length PFETs results in smaller channel resistances and puts a smaller upper bound on the acceptable value of contact resistance. R_{source} and R_{drain} contact resistances are gate voltage dependent and, they decrease with increasing gate voltage. Gate voltage dependence on the source, drain, and channel resistances also indicates that contact resistance depends on film transport properties near the contact. The observation can be explained on the basis that the R_{source} is the sum of (a) resistance arising from charge injection over or through the potential barrier and (b) resistance due to transport in the disordered depletion region near the contact while R_{drain} arises just due to contribution from (b). The presence of a strong gate field facilitates field emission through the barrier. Resistance due to charge injection is not limited for the source electrode, instead resistance due to disordered polymer dominates for drain electrodes. This description provides a qualitative description of different resistance present at the source-drain electrodes. Various deposition technique which determines the film morphology affects the total contact resistance of the device.

Contact resistances have been heavily studied in inorganic FETs, but models developed for single-crystalline devices are of limited application since they do not take into account properly the dependence of mobility on the gate voltage which is peculiar to organic and, in general, to amorphous and polycrystalline semiconductors. The estimate of CR is typically obtained by studying the FET characteristics using the scaling-law method by fabricating set FETs of varying channel length (L). Large statistical variations are commonly observed in the R(L) plots for poly-

mer FETs unlike the case of small molecule FETs or amorphous Si TFTs. R(L) profile is less reliable in PFETs to arrive at an accurate estimate of CR. In this regard, a direct assessment for CR from the polymer device would be quite valuable. In the literature on organic TFTs various strategies have been developed to deal with the effect of contact resistances on TFT: numerical fitting[143, 144] the scaling law approach[145, 146], the four probe measurement[147, 148],which is an effective and direct measurement of the potential drop on a portion of the TFT channel far from the interface regions; and the Kelvin probe measurement[149, 150], which is a powerful method to directly measure the surface potential of the channel.

The above mentioned methods either require preparation of many samples or use of high end scanning probe set-up in order to estimate the presence of CR in the FET devices, From the literature, it has been observed that locally doping the polymer at the metal interface has resulted in improved charge injection property[151]. Our approach to study interfacial barrier is through local perturbation of the polymer using optical excitation beneath the source and drain electrodes and then monitor the FET electrical characteristics. This is equivalent to photodoping, where in the polymer is optically doped near the metal-semiconductor interface. These results are used to estimate the presence of barrier present at the metal-semiconductor interface.

3.2.1 Device Fabrication

One of the key difference for top contact devices fabricated for these studies involved, having a larger source-drain electrode span over the polymer, which al-

lowed us to selectively excite the polymer far away from the channel region, without optically perturbing the channel region as observed in Fig. 3.5. It is to be noted, the presence of large electrode span does not affect the FET characteristics, since channel length and channel width are the geometric parameters of the device that determine the FET operation. Aluminum was coated on top of glass substrate using thermal evaporation technique. The spun-cast film of BCB was obtained using with spinning speed of about 1500 revolutions per minute (rpm) to maintain the thickness of $\approx$ 1 μm. The thin film was thermally cured at 290^0 C for 30 minutes. Prior to semiconducting polymer coating, the dielectric is surface treated with HMDS followed by annealing at 90^0 C for 2 hours to achieve hydrophobic surface. The as obtained P3HT was dissolved in chlorobenzene and the solutions were filtered by 0.2 μm pore size filter papers. A thin layer of P3HT was spin coated (1500 rpm for 1 minute) from chlorobenzene solution (10 mg/ml) in nitrogen atmosphere (<1 ppm O_2, <1 ppm H_2O) to obtain the thickness of 100-200 nm. After a thermal treatment process at 150^0 C for 30 minutes in nitrogen environment. Gold was thermally evaporated (under a vacuum level $\sim 10^{-6}$ mbar) through a shadow mask to form drain and source electrodes with separation of 40 μm (L) and width (W) of 2 mm (W/L $\sim$ 50). Finally electrical contacts were made to the three electrodes and the device was transferred to a vacuum chamber (10^{-3} mbar) for electrical and optoelectronic measurements. P3HT and P3HT-PCBM blend (1:1) by weight ratio FET devices were fabricated under identical processing conditions and device dimensions.

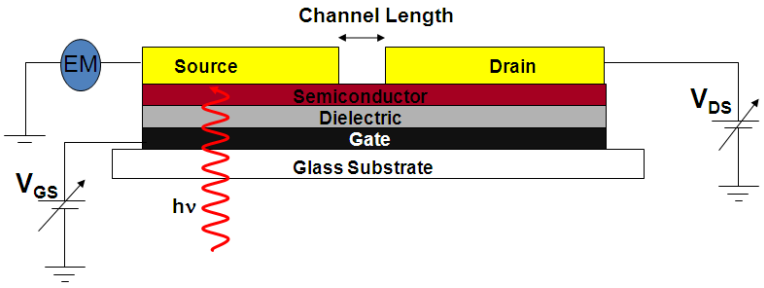

Figure 3.5: **Top contact FET, with transparent dielectric and wide source-drain electrodes photoexcited using 633 nm excitation far away from channel (3 mm) to avoid contribution coming from photogenerated charge carriers from channel region.**

3.2.2 Dark I-V Characteristics

The polymer transistors were primarily tested in vacuum 10^{-3} mbar under dark condition to extract the device parameters. The device parameters such as field-effect mobility, on/off ratio etc. are essential factors not only to speculate the nature of the interface between the insulator and semiconductor but also to understand the photophysical feature. The output and transfer characteristics are shown in the Fig. 3.6 and Fig. 3.7 respectively. Typical p-channel unipolar (hole-only) feature was observed in all the FET structures, operating under accumulation mode.

3.2.3 Measurement Methodology

In our work we have introduced an approach to study interfacial barrier by selective illumination of the polymer at the electrode region and monitor the variation in the transconductance characteristics. The method is applicable for top contact FET's where substrate dielectric is transparent and electrodes are wide enough to have excitation far away from the channel region, thereby avoiding the

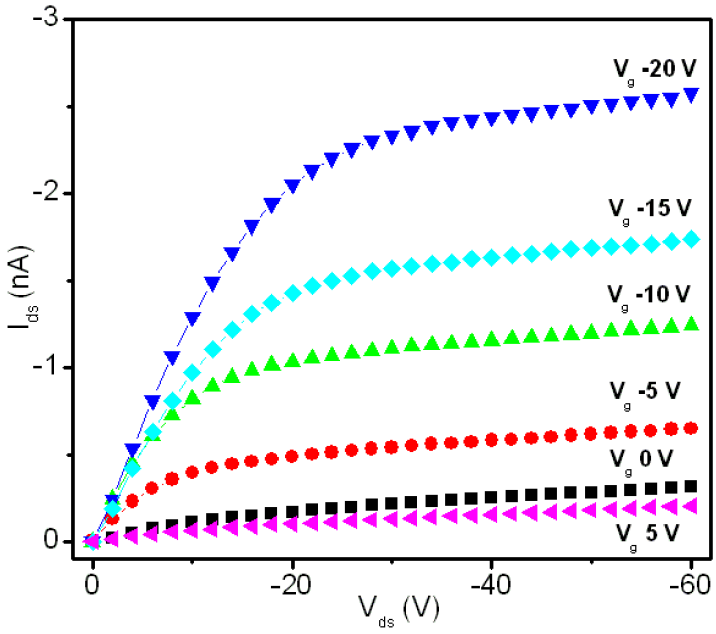

Figure 3.6: **Transistor characteristics for top contact P3HT FET measured in dark and vacuum conditions showing p-channel operation.**

direct contribution from the photogenerated charge carriers to the channel current. We carry out these studies for FETs based on (poly3-hexylthiophene) P3HT and (methanofullerene [6,6] Phenyl-C61-butyric acid methyl ester) PCBM, blend FETs. The optical beam size (b) from a 633 nm He-Ne source incident from glass side was much less than channel width (w) for the measurements. The channel region between the S-D electrodes was suitably masked from top to avoid any collection of direct and scattered light, while from the bottom side, Al gate electrode serve as a suitable mask to avoid collection of stray light as shown in the Fig. 3.5.

The P3HT based FET characteristics as seen in the Fig. 3.6 and Fig. 3.7 depicts transfer characteristics and transconductance characteristics. The transfer curves did not exhibit any appreciable hysteresis for the range of sweep rates used.

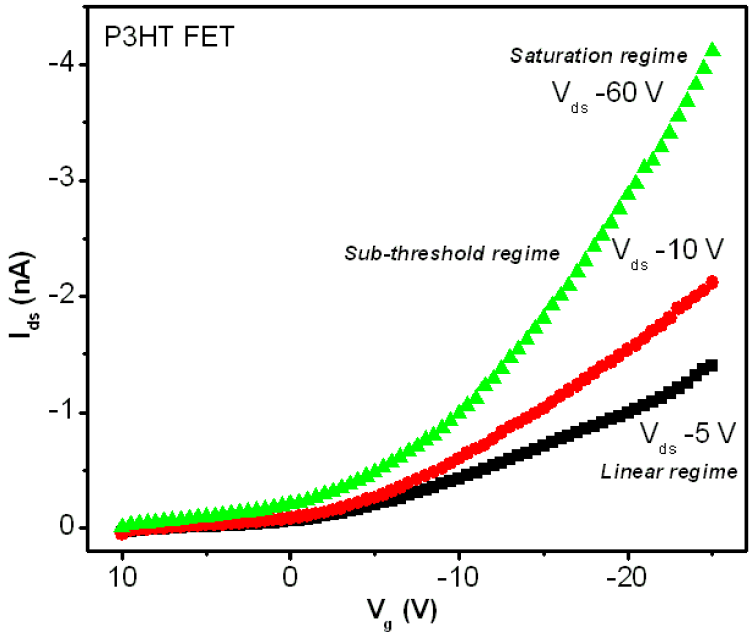

Figure 3.7: **Transfer characteristics for top contact P3HT FET measured in dark and vacuum conditions indicating different regime measured at V_{ds} -5V, V_{ds} -10 V and V_{ds} -60 V.**

The hole mobility μ_h in the saturation regime was obtained from

$$I_{ds} = \frac{W\mu C_i}{2L}(V_g - V_{th})^2 \tag{3.3}$$

where C_i is the capacitance per unit area of the gate dielectric 2.3 nF/cm^2. The measured μ_h for the saturation regime and V_{th} obtained by plotting $\sqrt{I_{ds}}$ versus V_g for a large number of devices were in the range of 0.2 - 5 x 10^{-3} cm^2/Vs and 0-7 V, respectively. The introduction of PCBM moieties in the P3HT matrix in case of the P3HT-PCBM blend FETs did not vary but resulted in a shifted V_{th} to higher positive voltages as observed in the electrical characteristics as observed in Fig. 3.8 and Fig. 3.9. Addition of PCBM to P3HT to form blend FET did not vary the dark electrical characteristics, but upon photoexcitation results in efficient charge separation due to the presence of donor-acceptor interface. The details of

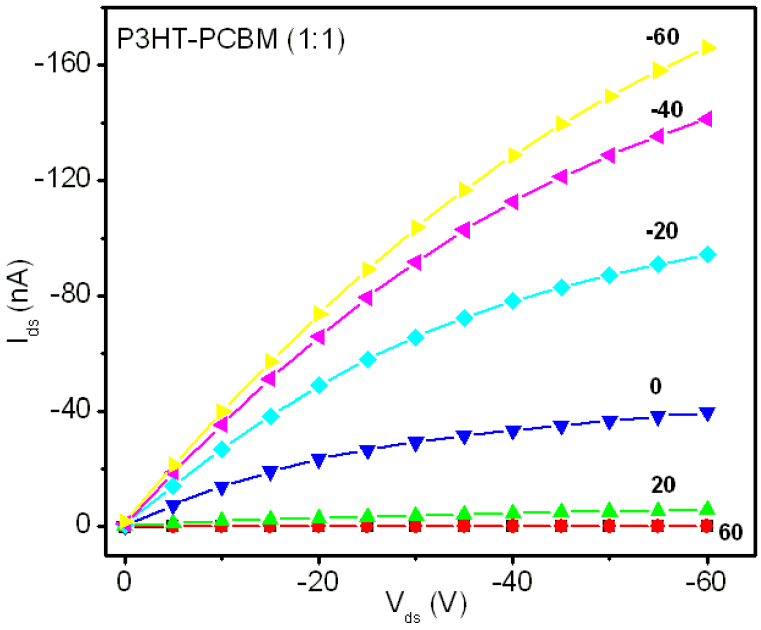

Figure 3.8: **Transistor characteristics for top contact P3HT-PCBM (1:1 blend) FET measured in dark and vacuum conditions showing p-channel operation.**

the P3HT-PCBM donor-acceptor interface has been extensively studied in the next chapter.

3.2.4 Light I-V Characteristics

The measurements involving photoexcitation of the electrode region were carried out by ensuring dark-conditions in the channel region. The dark current characteristics and the history of the device prior to illumination at the source and drain regions were identical. The changes introduced by the photoexcitation of channel region arise from a complete different set of photophysical processes leading to large variations in I_{ds} (by several orders) which is not the main theme of this work and is discussed in detail in labs previous work[122, 125]. The illumina-

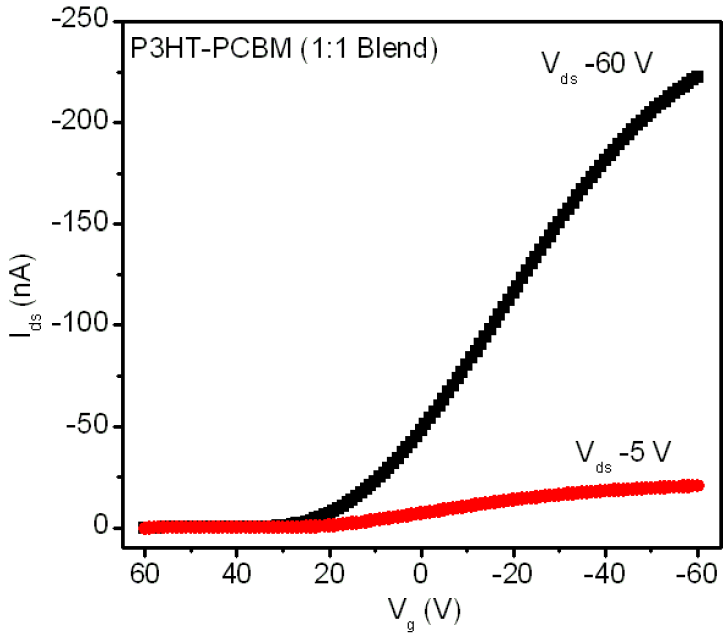

Figure 3.9: **Transfer characteristics for top contact P3HT-PCBM (1:1 blend) FET measured at V_{ds} -5V and V_{ds} -60 V.**

tion volume in this case was confined to region beneath the source electrode and the drain electrode, which was at a sufficient and equal distance of 3 mm away from the channel edge. At $\lambda = 633$ nm (low absorption region) for P3HT with light incident from the substrate side, the photoactivity is largely restricted at the P3HT-electrode interface region. The zone of activity at the interfacial region was ascertained by comparing the responses using $\lambda = 633$ nm and $\lambda = 532$ nm (where absorption is high, see Fig. 3.10) sources for films with different thickness and observing minimal changes in I_{ds} for the latter case. With $\lambda = 532$ nm excitation zone of activity is throughout the bulk of the semiconductor resulting in optical generation of charge carriers in the bulk, while it's important to have photo-doping of semiconductor near the metal-semiconductor interface to study injection barrier.

At low incident power (< 1 nW), subtle changes in I_{ds}-V_g characteristics are

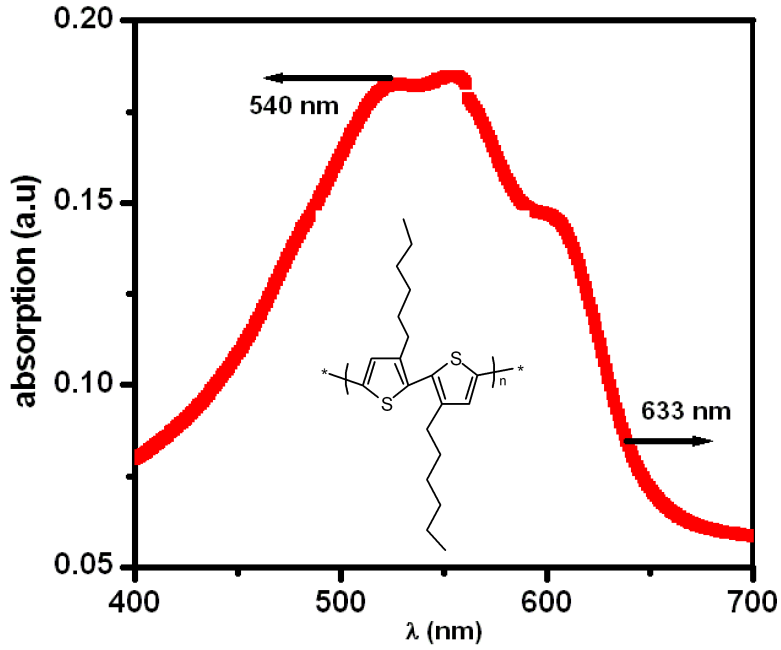

Figure 3.10: **The absorption spectra of P3HT indicating the 2 excitation wavelength used in the measurement. Inset shows the chemical structure of the polymer.**

observed, and at higher incident power (P), a clear trend in the I_{ds}(P) and V_{th}(P) is present. Fig. 3.11(a)(b) shows the transconductance behavior of the PFET under selective illumination at the source and drain electrodes regions with identical power illumination at the sample at identical distance away from the channel region. The transconductance characteristics for varying light intensity at both the electrodes region were measured for the linear, subthreshold and saturation regimes. The general trend of a larger I_{ds}(P) and dI_{ds}/dP for illumination under the D-region was observed and compared to S-region for both linear, subthreshold (Fig. 3.12) and saturation regime. The dI_{ds}/dP (at V_g = -25 V) showed a linear response and was in the range of 0.004 nA/ μW and 0.02 nA/μW for light incident at source and drain electrode respectively.

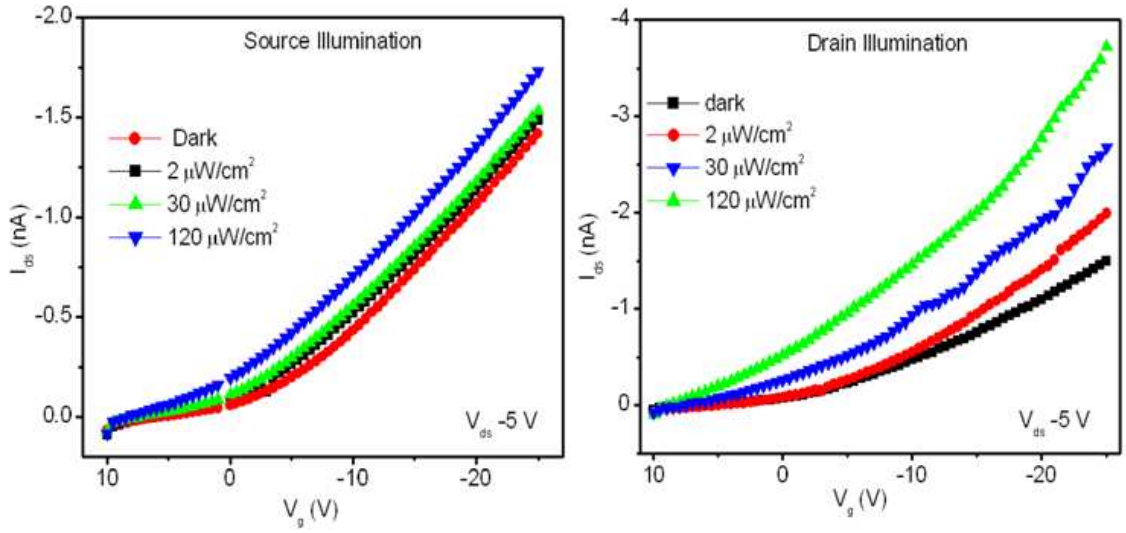

Figure 3.11: **Transfer characteristics of P3HT FET taken at V_{ds} -5 V with light selectively incident under source and drain electrode at different power incident at the sample.**

The selective increase of I_{ds} upon photoexcitation on the drain electrode region compared to the source electrode region was observed only in the enhancement mode of operation and changes were not noticeable in the depletion mode. This observation is strikingly in contrast from the changes observed in pristine polymer FET's when the entire channel is illuminated, and where a significant I_{light}/I_{dark} (up to 10^6) is observed in the depletion mode with the photoinduced current magnitude approaching values corresponding to the current in the enhancement mode. The significant increase in I_{ds} in the off state for polymer FETs is attributed to the enhancement of the carrier density due to the photogeneration of charge carriers in the polymer. The increase in carrier density can originate due to the following possibilities[152],:(1) Exciton formation and subsequent dissociation (due to electric field, surface, or impurity induced) into free carriers. (2) Direct, band-to-band excitation of electrons. (3) Photoinjection of carriers from the metal source/drain electrodes into polymer. (4) Detrapping of carriers trapped in localized gap states

in the polymer. The only possibility of excess charge generation in PFET can be attributed through excitonic route, while photoinjection from metal and detrapping of carriers and band-to-band excitation can be ignored, due to the observation of asymmetric I_{ds} response for drain and source excitation.

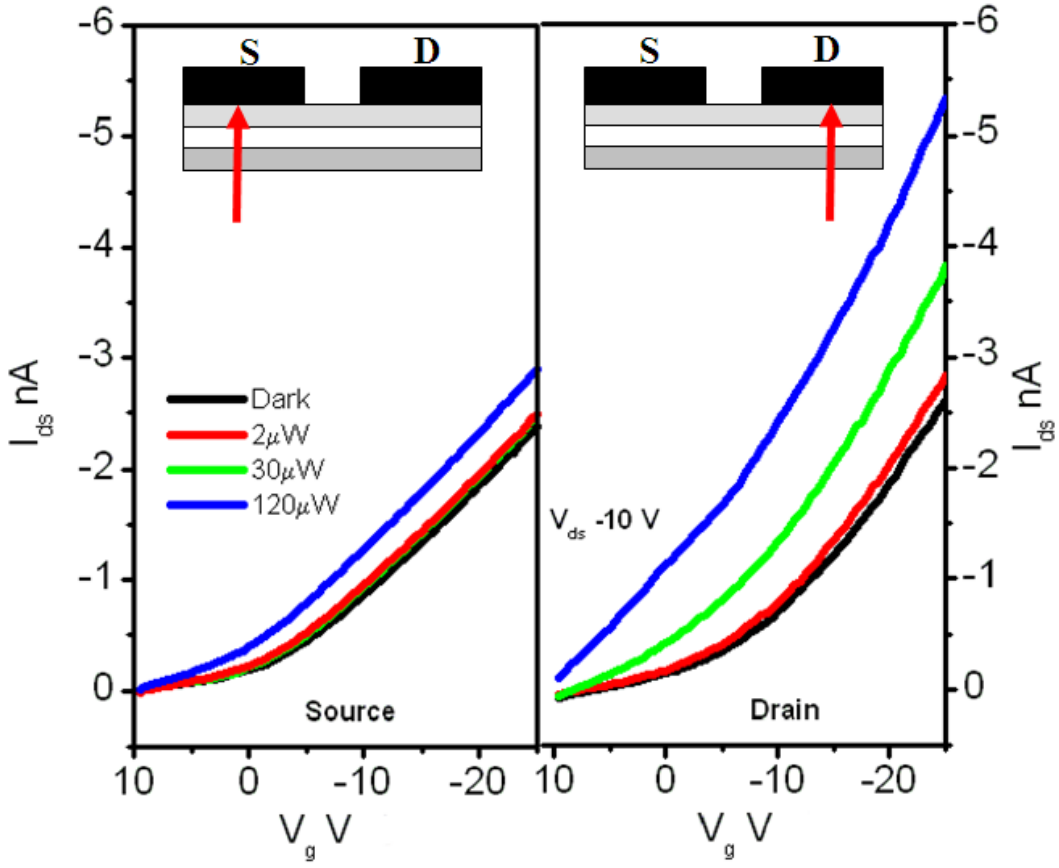

Figure 3.12: **Transfer characteristics of P3HT FET taken at V_{ds} -10 V with light selectively incident under source and drain electrode at different power incident at the sample.**

The transconductance relation $I_{ds} = w/2L\mu\ C_i\ (V_g - V_{th})^2$ which incorporates the modified V_{th} can be assumed good for the range of measurements. It is to be noted that μ which can be extracted from the transconductance curve does not change upon photoexcitation, as observed from the Fig. 3.14. C_i also does not

modifies upon photoexcitation. A clear linear shift in V_{th} as a function of incident power can be inferred from the Fig. 3.13. The device exhibits $\Delta V_{th} \sim 8.2$ V when illuminated with P = 120 μW at the drain electrode region compared to $\Delta V_{th} \sim$ 3.1 V at the source electrode for the same incident power (P). A linear dependence of the ΔV_{th} with increasing light intensity is observed with slope of 0.03 V/μW for source illumination and slope of 0.06 V/μW for drain illumination Fig. 3.14. The observation of larger changes in I_{ds} brought about by large enhancement V_g and/or large incident power is consistent with this simplistic treatment.

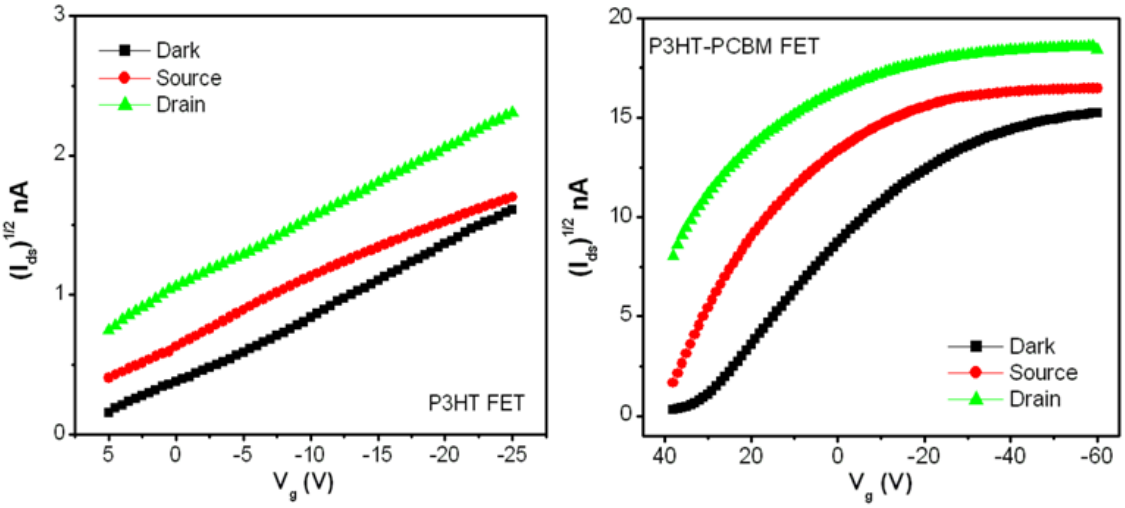

Figure 3.13: $\sqrt{I_{ds}}$-V_g **plot for P3HT FET and P3HT-PCBM FET observed at dark and with light incident selectively at source and drain electrodes (power 120 μW, V_{ds} -10 V).**

This behavior and trend in S and D illumination was verified by interchanging the S-D electrodes (S $\rightarrow$ D, D $\rightarrow$ S), to discount sample-electrode variations and other asymmetric inhomogeneities. These results and observations were confirmed by measurements on six independently fabricated devices. The effect was also present upon changing the gate electrode, and for a wide range gate-source overlap. These features were magnified for the P3HT-PCBM devices that have a

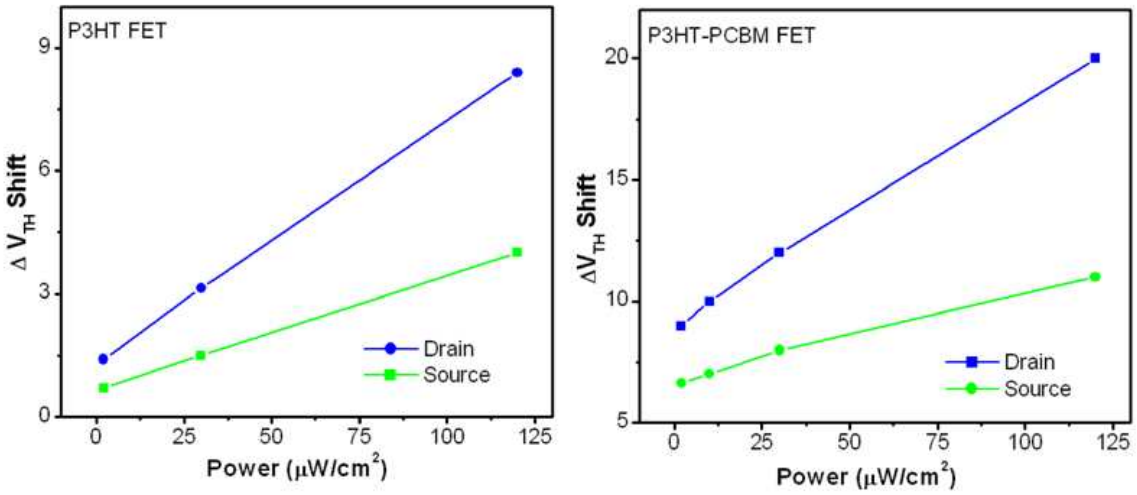

Figure 3.14: **ΔV_{th} shift observed for P3HT and blend FET with increasing light incident on the samples.**

higher degree of photoinduced charge separation and provides a larger photogenerated carrier density. The features for the P3HT-PCBM devices are $V_{th} \sim 19$ V and $V_{th} \sim 10$ V when illuminated (P = 120 μW) at the drain electrode and source electrode respectively. The intensity dependence indicates a linear response of V_{th}(P), with slope of 0.02 V/μW for source illumination and 0.07 V/μW for drain illumination. These trends in P3HT-PCBM devices point to processes which are more prominent but qualitatively analogous to the ones prevailing in P3HT devices.

3.2.5 Threshold Voltage Shift

Among the various electrical parameters that can be extracted from the transfer characteristics, parameter V_{th} has a contribution that can be related to the metal-semiconductor interface. V_{th} in organic transistors has been analyzed in terms of two major contributions[153]; V_{th}=V_{fb}+V_{sc}, where V_{sc} corresponds to voltage drop across the semiconductor and V_{fb} corresponds to flat band potential

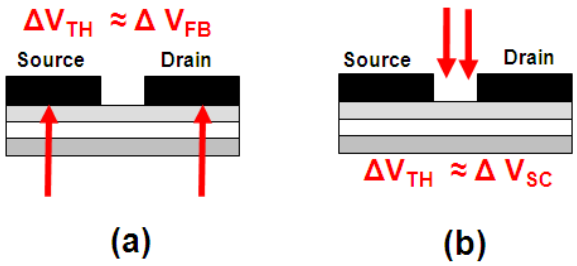

Figure 3.15: **Schematics showing excitation of polymer under metal electrodes result in change in V_{th} arising due to change in flat band potential, while excitation of polymer in channel result in change in V_{th} arises due to change in V_{sc}.**

arising from any mismatch between work function of metal electrodes and semiconductor. For channel illumination, the change in V_{th} arises due to the change in the V_{sc}, since zone of activity is confined near the dielectric-semiconductor interface. While for polymer excitation under the metal electrodes, the V_{th} shift that observed arises due to the change that occurs in the flat band potential at the metal-semiconductor interface i.e. V_{fb}. The schematics in Fig. 3.15 explains the observed trend. For identical intensity of light incident on source and drain electrode, maximum V_{th} shift is observed for D-electrode compared to S-electrode, implying the maximum lowering of barrier for charge collection at D-electrode is observed in comparison to lowering of barrier required for charge injection that occurs at the S-electrode.

The absence of V_{th} shift in dark for pristine P3HT and P3HT-PCBM devices as a function of V_d and the near-symmetric response upon interchanging S-D polarity is indicative of an absence of schottky-type barrier at the metal-semiconductor interface. However, the V_{th}(P) dependence and the difference in S-D response under illumination can be viewed in terms of a barrier which is accessible by photoexcitation. The illumination and generation of charge carriers at sufficient distance away

from the channel region primarily affects V_{fb} but not V_{sc}. The flat-band potential gets modified as the photogenerated carriers close to the metal-polymer interface enters the metal electrodes and shifts the band level so as to lower the barrier required for charge injection and collection. The results then can be interpreted in terms of an additional/higher resistance at the reverse biased source contact for a transport model consisting of $R = R_{bulk} + R_{source} + R_{drain}$. The asymmetric photogenerated carrier kinetics at S and D electrodes can lower R_{drain} compared to R_{source}. The observation is consistent with results obtained from scanning probe potentiometry where CR manifests itself as sizable potential-drop at the source and drain regions[149, 154]. Contact resistance for P3HT FETs have been estimated based on differential model as reported by Sampietro et.al. [155], the total contact resistance of the device under dark conditions has been estimated to be 9000 KΩ-cm. Upon exciting the polymer under the source electrode with (P) 120 μW, the CR is calculated to be 7100 KΩ-cm while for the drain electrode illumination, CR is found to be 6000 KΩ-cm. This observation validates the presence of lower CR at the drain electrode required for charge collection in comparison to higher CR present at source electrode required for charge injection.

3.2.6 Summary

In conclusion, we observe subtle changes in the FET characteristics for light incident selectively on the electrodes. A distinct difference and trend is observed in top contact field effect transistor, the photoresponse shows asymmetric response when light perturbs the interfacial region beneath the source-drain electrodes. The results were interpreted in terms of a lower barrier for extraction compared to in-

jection of charge carriers. The approach can be generalized and extended to probe other combination of metal-semiconductor interfaces to yield useful information.

CHAPTER 4

Donor-Acceptor Bilayer Structures

4.1 Introduction

This chapter deals with processes of charge transfer and charge transport originating from the Donor-Acceptor interface in the FET geometry. These studies have been used to characterize charge transfer processes at the **D-A** interface, which are important in understanding the photoinduced charge transfer process, central to the working of efficient organic solar cells and light emitting transistors. The key emphasis in the work includes the novel approach of a bilayer FET consisting of **D-A** interface, with n-channel transport in the A-layer. Photoexcitation of donor layer results in photocarrier generation and electrical transport that primarily occurs in the acceptor forming layer. The device allows us to simultaneously estimate field and bulk mobility, field dependence of carrier generation and transport from the **D-A** interface.

4.1.1 Excitonic Process

The bandgap of conjugated polymers usually lie in the range of 2-3 eV.. Photoinduced charge transport in semiconducting polymers follows the route through

(a) exciton formation, (b) exciton diffusion to a dissociation site, (c) exciton dissociation into positive and negative charge carriers and (d) charge transport under the influence of applied field. Exciton being a electrically neutral species, does not contribute to charge transport but it transports the energy from one site to the other depending upon the diffusion length ($\sim$ nm). The extent of delocalization of excitons strongly depends on the interplay between intermolecular interaction and the coulomb interaction. Depending upon the degree of delocalization and the binding energy, the excitons are classified as Frenkel, Wannier-Mott or charge transfer.

Frenkel excitons are generated due to strongly correlated electron-hole pair localized on a single molecule. The radius of these excitons are comparable to size of the molecule or sometime smaller than the intermolecular distance (< 5 A^0). The local electric field of the exciton polarizes the surrounding lattice, eventually generating polaron-type of quasiparticles.

Wannier-Mott (WM) excitons are generated in uncorrelated crystalline materials in which overlap between neighboring lattice atoms reduces the columbic interaction between the electron and hole involved. These have large exciton radius ($\sim$ 40-100 A^0) with relatively weak binding energy. At room temperature WM excitons in most of the inorganic semiconductors are dissociated and the associated energy levels are broadened too strongly to suppress the signatures as compared to the regular optical absorption.

Charge transfer (CT) exciton belongs to an intermediate between a Frenkel and a WM state, being neither extended nor tightly bound to a single molecular site.

The energy or charge transfer takes place depending on the relative energies of the intra acceptor chain and intra donor chain exciton. The fate of a bound CT state is either to decay to ground state by radiative/nonradiative recombination channel or to escape the mutual columbic potential by electric field (F) and temperature (T) activated diffusion process.

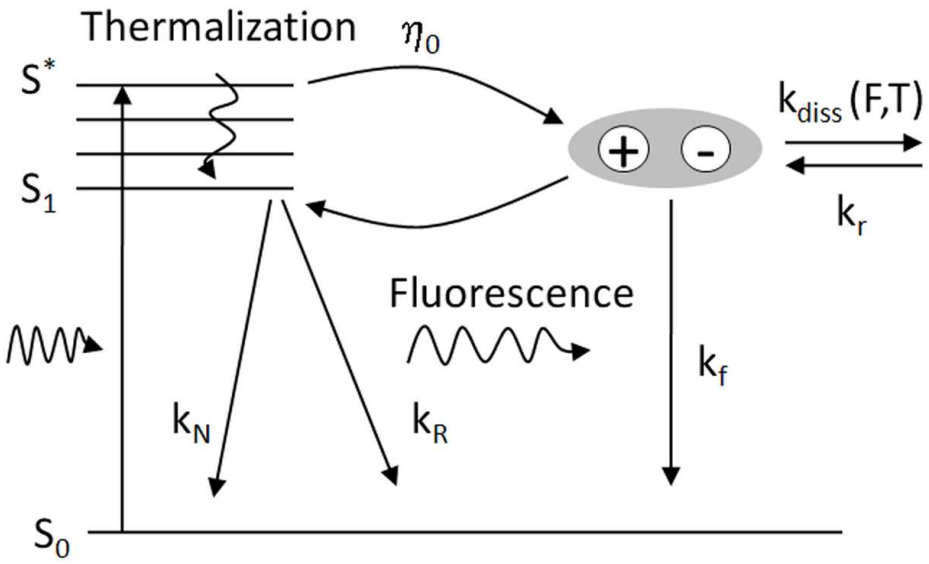

Figure 4.1: **Schematic representation of carrier photogeneration process as described by Onsager model[156] and later modified by Braun[157]. The carrier after bimolecular recombination is not essentially lost but it can form an intermediate bound polaron pair which can act as a precursor for free charge carrier generation.**

The created exciton has two fates during its temporal evolution. One set of excitons that separates and escapes from recombination. These separated charge

carriers contributes to the total photocurrent. The probability is termed as quantum yield or quantum efficiency (η) and by definition the amount of free charges collected per absorption of a single photon. The other possibility is that exciton may recombine, which results in fluorescence (radiative recombination) or an increase in thermal energy of the medium (non-radiative recombination). Excitons can be dissociated by either thermal energy or electric field or both.

Onsager Theory[156], attempts to understand the interplay between the exciton dissociation into charge carriers and recombination process in disordered system. In this theory, as observed in Fig. 4.1, the electrons that are excited from neutral S_0 state to a highly excited state S^*, thermalize at a distance r_0 (thermalization length) to form the exciton. The fraction is called the primary quantum efficiency. The ultimate probability for dissociation into free carriers is Ω(r,Θ,E), where Θ is the angle between vector of the bound pair (r) and the applied electric field E. The recombination rate is determined by R = 1 -Ω(r,Θ,E). Some of the states S^* may relax to the first excited singlet state S_1 with probability of 1- η_0 and then decay to ground state S via radiative or non-radiative route with rate constant of k_R or k_N respectively. The overall quantum efficiency is given by

$$\eta = \eta_0 \int \Omega(r, \Theta, E) g(r, \Theta) d\tau \tag{4.1}$$

Where g(r,Θ) is the initial spatial distribution of thermalization length. The main outcomes of this model are: (i) a strong dependence on the electric field in the middle regime, nonzero values at low field and saturation at high field, (ii) a weak increase with temperature, (iii) a strong dependence on the incident photon, (iv) a large thermalization length of about few nanometers. The drawbacks of this

model are the strong influence of incident energy on photogeneration and the large thermalization length.

4.2 Donor Acceptor Interface

The novel concept for photovoltaic devices, based on interpenetrating blends of donor and acceptor sandwiched between two asymmetrical contacts (two metals with different work functions), has been used successfully for solar cell applications. The presence of acceptor facilitates dissociation of the donor exciton into free charge carriers. Under the influence of the built-in-field caused by the asymmetrical contacts, separation of the opposite charges takes place, with the holes being transported in the donor phase and electrons in the acceptor phase. In this way, an interpenetrating blend can be considered as a network of **D-A** heterojunction that allows efficient exciton dissociation and balanced bipolar transport throughout the volume. The performance of this type of device is very sensitive to the morphology of the blend since as exciton dissociation occurs only at the **D-A** interface. To ensure efficient exciton dissociation, an acceptor species should be within the exciton diffusion range, from any donor species and vice versa. To put differently, the characteristic sizes of the channels of the phases should be matched to this diffusion range. Moreover, both the donor and acceptor phases should form a continuous network to allow bipolar charge transport. Since the exciton diffusion range is typically about 10 nm and hence shorter than the light absorption depth, a properly dimensioned network of **D-A** heterojunction should be more efficient in terms of the exciton dissociation than a double-layer structure with a single, planar donor-acceptor heterojunction. However, such a system of spatially distributed donor-acceptor heterojunctions may contain imperfections

Process	**Time scale**
Exciton formation	10 fs
Intrachain vibrational relaxation	0.1 ps
Exciton diffusion towards interface	1-10 ns
*Charge separation at **D-A** interface*	1-10 ps
Free charge carrier transport	1-100 μs

Table 4.1: Time scale for photoconduction process

that degrade performance, such as fully dispersed domains and discontinuities of the donor and/or acceptor phases. Furthermore, an enlarged phase boundary volume accompanies this extended interface area in which donor and acceptor species are molecularly mixed. This is likely to result in increased energy level disorder, causing an increase of the charge trap density and a reduction of the electron or hole mobility. Hence, though exciton dissociation may be enhanced, transport is impeded by the circuitous geometry of the interface. Donor-Acceptor blend FET have been fabricated and known to show both unipolar and ambipolar transport based on the choice of injecting electrodes and the ratio of **D-A** used for fabricating the FET. P3HT-PCBM blend FETs have been fabricated and studied in the previous chapter, and have shown a larger quantum efficiency for photo carrier generation compared to pristine P3HT FET. The presence of PCBM result in efficient exciton dissociation and increase in net carrier density upon photoexciting the blend PFET.

The characteristic time scale of charge transfer across **D-A** interface occurs in sub-picosecond range[130], and the charge separated pairs can be stable up to micro-milliseconds[158]. The Table 4.1 shows the time scale for the various processes associated with charge generation following photoexcitation of the semiconducting polymer. The intrinsic power conversion efficiency limiting factors essen-

tially arise from incomplete carrier generation processes and barrier in the transport processes. The other predominant loss mechanism is the recombination of charge carrier subsequent to exciton dissociation via exciplex formation[159] resulting in lower charge collections. Photoinduced charge separation at **D-A** interface occurs through a series of intermediate steps involving photogeneration of coulomb bound pair occupying a charge transfer complex state[160] and below-gap polaron states[161] that increases power conversion efficiency. The use of terahertz time-domain spectroscopy to investigate photoinduced charge generation via exciton dissociation in conjugated polymer field-effect transistors have been reported in the accumulation mode, with a quantum efficiency of ~ 0.1[162].

Solution processed p-channel and n-channel with high mobility and operational stability under ambient conditions have been achieved. Ambipolar charge transport in PFET's is of interest both from fundamental science and application point of view and has been achieved in bilayer[163], blend[164] and single component polymer system[121]. The combination of p and n semiconductor to form a donor-acceptor interface has been also used to study light-emitting field effect transistors (OLET) combining emission properties along with switching characteristics[165]. The use of a p-channel/emitter/n-channel trilayer semiconducting heterostructure in OLET, provides a new approach to markedly improve OLET performance. In this architecture, exciton charge annihilation and electrode photon losses are prevented and is reported to have better efficiency compared to previous reports[166]. The use of p and n semiconductor in PFET's can also be used to address another important issue related to **D-A** interface extensively studied to fabricate efficient organic solar cell. **D-A** interface plays an important role in determining the dissociation of excitons into free charge carriers, when excitons interact with

interfaces, impurities, defects or in the presence of external electric field[167]. In bilayer structure the **D-A** interface is spatially well defined and results in lower exciton dissociation due to smaller interfacial area compared to bulk heterostructure. Bilayer structure consists of D,A semiconductors provides attractive device architecture if suitable D and A materials with complementary optical and electronic properties are used, since the photogenerated charges are confined to either side resulting in spatial separation of carriers and minimizing the recombination probability[168] and facilitating the transport of charge carriers. It determines the fate of excitons and other charge transfer complexes that either get stabilized or destabilized at the interface[161]. Exciton dissociation process at interfaces competes with charge recombination mechanism where charge separated states decays backs to the ground states of the blend, apart from the existence of weakly bound charge transfer complex state at the interface limits the efficiency of charge generation. Figure 4.2 shows the existence of various CT complexes that are stable following exciton formation. Spectroscopic and electrical evidence of such CT complex at interface can be used to understand efficiency of exciton dissociation into free charge carriers.

Exciton dissociation in bulk hetrojunction and bilayer structure has been extensively studied in diode structure as seen in the Fig. 4.3, Here in this structure electric field induced exciton dissociation in conjugated polymers is limited by charge injection contacts[170] and extrinsic charge generation at the contacts[171]. For polymer FET such contact effects gets reduced due to large channel lengths and gate contacts being electrically insulated from the polymer films. Illumination of PFET's has shown to increase the I_{ds}, which is explained on the basis of exciton dissociation in the bulk of semiconductor under the influence of large electric field

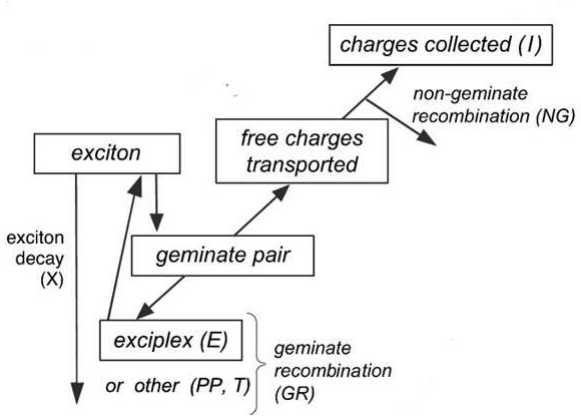

Figure 4.2: **Kinetic model of electronic transitions at the heterojunction. Excitons can either decay (depicted as X) or can reach the heterojunction to form geminate pairs. These can either be trapped (forming exciplexes (E), dark polaron pairs (PP) or triplets (T)) or separate into charges to be transported and collected at the electrodes (I). During charge transport, non-geminate recombination (NG) might occur. Figure reproduced with permission from reference[169]**

present in the depletion mode of operation[122, 172]. For a better understanding of the mechanism underlying the photocurrent generation, a study of exciton dissociation in PFET's is required. The I-V characteristics are the measure of device performance in FET, but the charge carrier densities and mobilities is often hampered by contact resistance effects[149, 173]. PFET provides an interesting architecture to study the mechanism of excitation dissociation into charge carriers. In PFET's the use of donor-acceptor either in blend or bilayer structure has been extensively used to study ambipolar transport or light emitting field effect transistor (LFET). Bulk heterojunction in FET arises out blending of more than 1 semiconductor, while bilayer structure in FET can be fabricated using sequential deposition of semiconductor solution, soft lithography or vacuum sublimation. We have studied the exciton dissociation into free charge carriers that contribute to total I_{ds} in bilayer FET structure, but based on the choice of the electrode used, the structure is used to transport only single charge carrier.

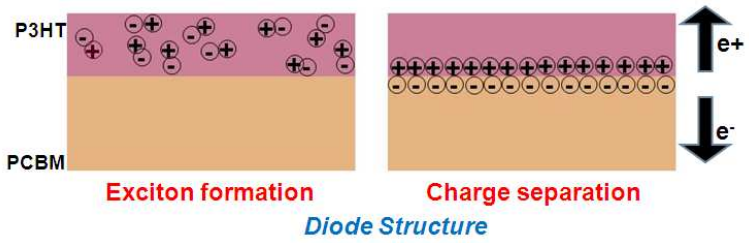

Figure 4.3: **Exciton separation into free charge carriers in diode structure.**

We have proposed a technique and a device structure incorporating FET geometry which is used to probe and address some of the issues related to the extent of carrier generation and its dependence to the external electrostatic field. The technique relies on fabrication of a top contact acceptor-molecule based FET and the possibility of introducing a layer of the donor medium on the acceptor layer. The channel current in the acceptor layer is well defined spatially, thus the process initiated by photoexciting the donor layer can be followed closely by monitoring the underlying I_{ds} in the acceptor-FET. Upon photoexciting the donor layer, exciton formation and diffusion in the donor polymer layer is followed by the charge transfer (CT) at the **D-A** interface. Interfacial charge transfer properties can be followed under combination of steady state and transient illumination studies. The n-photocarrier spread in the acceptor layer then can be monitored as the $I_{ds}(t)$ characteristics of the device. This device architecture enables the studies of transport processes under different gate voltage V_g conditions and can be utilized to examine the **D-A** interfacial processes as well as the bulk acceptor characteristics.

In FET architecture as observed in Fig. 4.4, the added advantage of studying exciton separation arises from the fact that we have access to V_g, where we

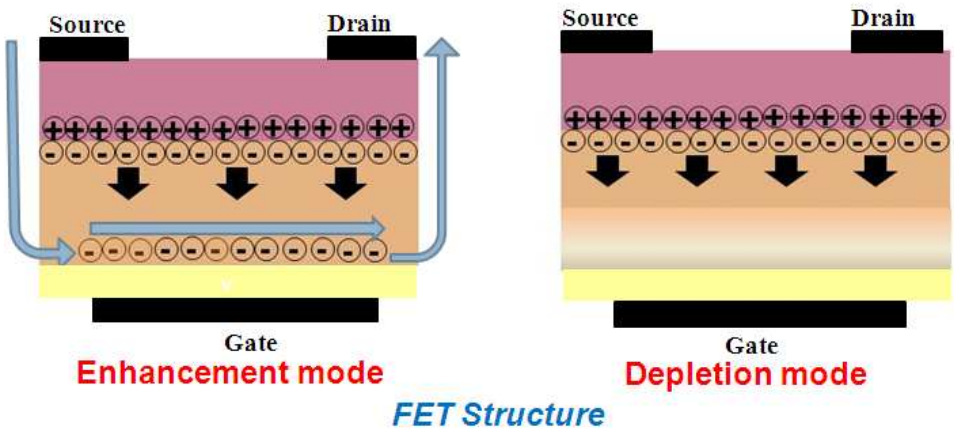

Figure 4.4: **Exciton separation into free charge carriers in FET structure in enhancement and depletion mode of operation. Note that the channel length (L) << semiconductor thickness.**

can introduce additional charge carriers at the dielectric-semiconductor interface (i.e. enhancement mode) or on the reversal of V_g we can deplete the dielectric-semiconductor interface of charges (i.e. depletion mode). Thus the presence of two type of charge carriers, photogenerated charge carriers at the donor-acceptor interface arising due to exciton dissociation occurring at the **D-A** interface and electrostatic induced charge carriers introduced due to V_g can be temporally characterized using $I_{ds}(t)$ studies. In diode structure, the charge carrier generation due to photon absorption and charge carrier transport plane lies along the same direction. While in FET structure charge carrier generation and charge transport plane are normal to each other, and thus are decoupled from each other. The presence of well defined **D-A** interface where photocharge generation and dielectric-semiconductor (D-S) interface where charge transport occur is spatially well defined and can be followed using a combination of steady state and transient illumination studies. These studies cannot be carried out in bulk heterojunction based phototransistor FET, since in such architecture upon photon absorption exciton will be generated throughout the bulk of the polymer sample and cannot be distinguished from the

V_g induced charge carriers.

4.2.1 Optically inactive PCBM FET fabrication

Regioregular poly(3-hexylthiophene) RR-P3HT is used as the donor species and [6,6]-phenyl-C61-butyric acid methyl ester (PCBM) as an acceptor species having excellent electron transporting and film forming property. PCBM is used as the active semiconducting material for fabricating the n-channel FET. Top contact PFET is fabricated using PCBM as the active material. Pre-cleaned glass substrate with thermally deposited aluminum c.a 50 nm is used as the gate electrode. Hydroxyl free polymer dielectric BCB is spin coated in N_2 filled glove box environment at 1500 rpm and thermally annealed at 290^o C for 1 hour. Dielectric coated substrate was treated with 1 mM solution of (3-aminopropyl) trimethoxysilane (APTMES) in toluene for 1 hour. PCBM is then spin coated from 25 mg/ml chlorobenzene solution and thermally annealed at 150^o C for 30 min. Aluminum source-drain electrode was thermally evaporated through shadow mask to form channel length (L) of 40 μm and channel width (W) of 2 mm. The transistor characteristics and output characteristics were carried out using Keithley 2400 semiconductor analyzer in dark and vacuum conditions. FET's fabricated from PCBM with Al as S-D electrode showed n-channel transport in dark. The calculated electron mobility from the linear regime was found to be in the range of 10^{-5} cm^2/Vs and the threshold voltage V_{th} was in the range of 0-10 V for most of the devices characterized.

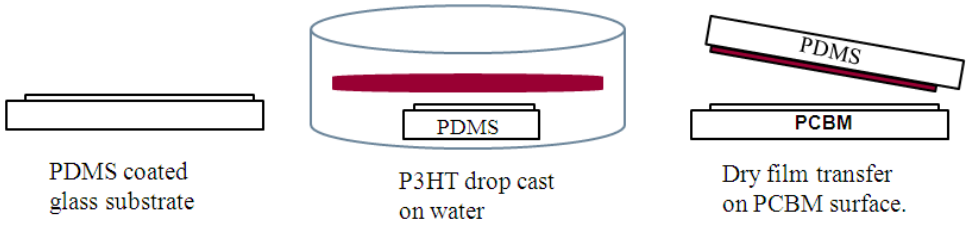

Figure 4.5: **(a) PDMS patterned on glass substrate (b) P3HT drop cast from chloroform solution onto water forming a suspended film. (c) Scooped P3HT film using the PDMS structure is then laminated on PCBM film forming a bilayer structure**

4.2.2 Bilayer FET fabrication

In order to fabricate a bilayer structure using a solution processed technique is a challenging, provided the solvent used to deposit both the component are orthogonal to each other. Thus in order to deposit multilayer component in order to tune the electronic property from solution process requires that each layer being soluble in orthogonal solvent so that the sequential deposition of solvent does not adversely affect the underlying layer. So in order to deposit P3HT polymer on solution processed PCBM film, a modified version of Transfer Printing Method (TPM) was deployed[174]. P3HT being soluble in most of the polar solvent has to be deposited via non solvent method onto PCBM to avoid dissolution of the PCBM film, which in turn might affect the electrical characteristics upon film swelling. TPM was used to form the bilayer structure consisting of P3HT film laminated on PCBM film, see Fig. 4.5. An elastomeric substrate polydimethylsiloxane (PDMS) is used to lift-off P3HT film suspended on water through drop cast from a chloroform solution and after drying in vacuum at 100^o C for 30 minutes is laminated over the PCBM film and then thermally annealed at 150^o C for 30 min in N_2 filled glove box environment. The structural integrity of the laminated film was verified by observing it under an optical microscope (Fig. 4.6) and obtaining high resolu-

tion atomic force micrograph(Fig. 4.7) of both bilayer structure and PCBM film.

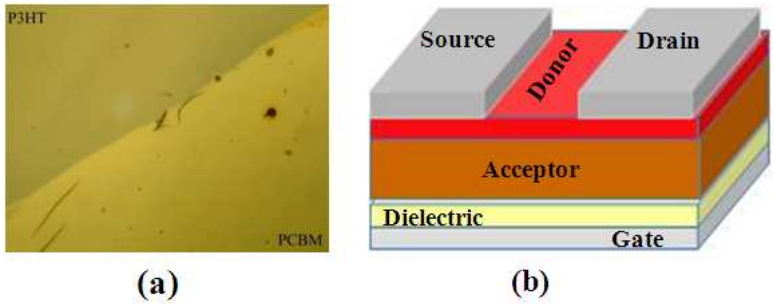

Figure 4.6: **(a) Optical Micrograph of bilayer structure. (b) Schematic of bilayer FET fabricated using non-solvent lamination methodology.**

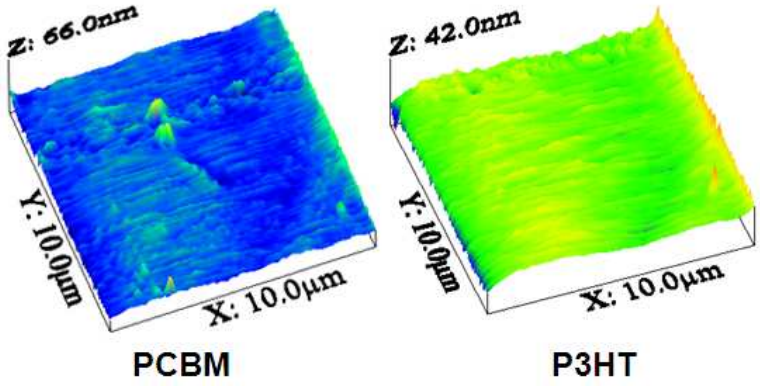

Figure 4.7: **AFM images of a bilayer structure taken over PCBM film showing a rms roughness of 1.9 nm and P3HT film showing a rms roughness of 2.9 nm**

4.2.3 Dark I-V characteristics

The dark electrical characteristics of PCBM transistor and donor laminated acceptor based FET showed identical electrical characteristics. Separate electrical characterization of laminated P3HT on BCB dielectric showed p-channel characteristics with Au source-drain electrodes, implying good structural integrity of

laminated P3HT films, which were also observed using optical micrograph Fig. 4.6. The use of aluminum electrode as source drain with P3HT film did not reveal any FET characteristics; this feature can be attributed to large injecting barrier associated with charge injection from aluminum into P3HT polymer, while gold makes ohmic contact with P3HT. FETs based on PCBM with aluminum as the source-drain electrode shows n-channel transfer response and the introduction of an additional donor polymer layer on PCBM merely introduces marginal changes in the electrical characteristics as seen in Fig. 4.8(a). The presence of P3HT layer does not adversely affect the n-channel transport transistor characteristics of PCBM. The magnitude of I_{ds} remains unchanged in all the devices in the bilayer structure and corresponds to the single layer PCBM FET. Electron mobility and on/off ratio obtained from the FET characteristics of bilayer device in dark was similar to that of single layer PCBM FET(Fig. 4.8(b)).

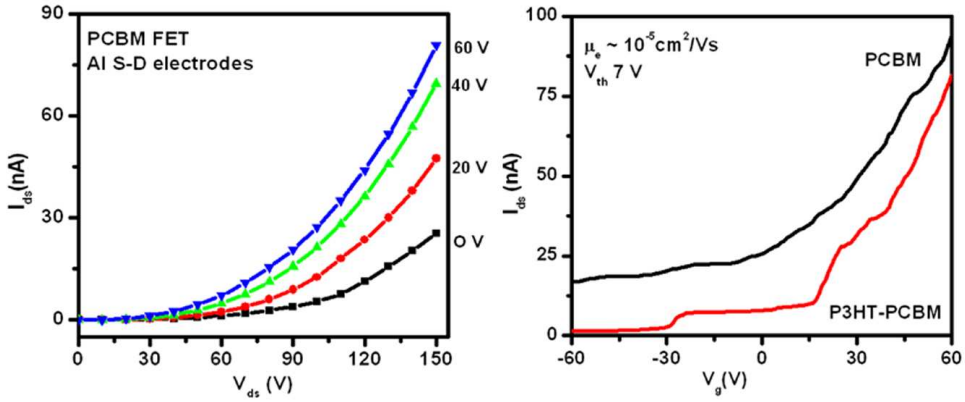

Figure 4.8: **Dark electrical characteristics of PCBM FET depicting n-channel transport and the transfer characteristics of bilayer and PCBM FET indicating identical electrical characteristics.**

In this bilayer FET structure, P3HT plays the role of optically active donor and is spatially separated from optically inactive PCBM channel as seen in the optical absorption features seen in Fig. 4.9. The figure shows optical absorption of PCBM

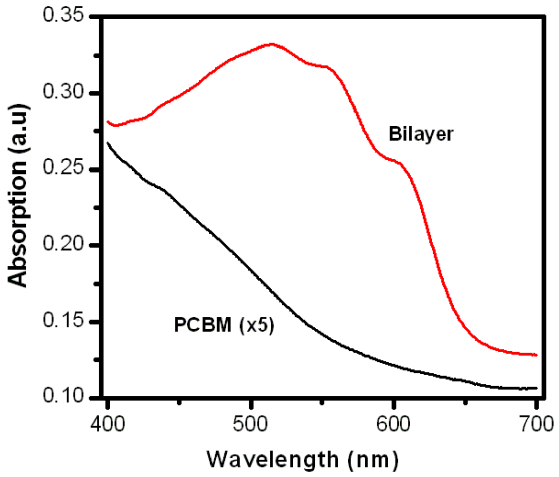

Figure 4.9: **Optical absorption for PCBM and P3HT-PCBM bilayer film.(Note the multiplicative 5X factor for the PCBM film)**

which is inactive in the visible range of the spectra, in comparison to the P3HT-PCBM bilayer structure. Note the multiplicative (5X) on the PCBM absorption profile. The dark electrical characteristics of bilayer and single layer PCBM FET are seen to be identical, but in the presence of 532 nm continuous wave (CW) illumination the bilayer FET shows large change in electrical characteristics. Several reports have suggested that large change in electrical characteristics upon photoexcitation of polymer even under low level illumination intensity. The device architecture in pristine and blend PFET allows for photogeneration of charge carrier throughout the bulk of the sample upon photoexcitation. In case of pristine and blend PFET, photoexcitation shows large change in I_{ds} in the depletion mode of operation compared to enhancement mode of operation. This feature arises since the photogenerated excitons are generated throughout the bulk of the sample, and the large electric field $E_{gs} > 10^6$ V/cm in depletion mode facilitates dissociation of photogenerated excitons into free carriers thereby increasing the charge carrier concentration in the sample.

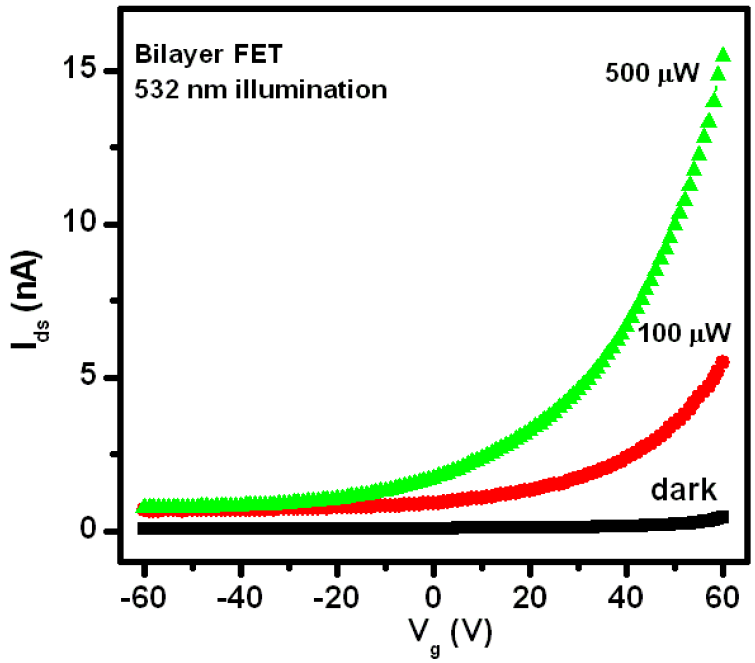

Figure 4.10: **Transfer characteristics of bilayer FET upon photoexciting with λ 532 nm at different intensities.**

4.2.4 CW illumination of bilayer FET

In the present case of bilayer FET, P3HT plays the role of optically active layer and is spatially separated from the underlying PCBM layer with the n-channel at the dielectric-semiconductor interface. Additional carriers upon photoexcitation exclusively originate from the photogenerated excitons in the top P3HT layer. Thus this device structure allows us to decouple the charge generation and charge transport processes. These features are evident from the observations noted for bilayer FET under CW illumination as observed in Fig. 4.10. The increase in I_{ds} in steady state illumination in bilayer FET occurs only in the enhancement mode of operation. I_{ds} increases linearly with increasing intensity of channel illumination

and do not show photoconductivity and photovoltaic effects as seen in pristine FET. The photocurrent $I_{ph}(\lambda)$ spectra of bilayer FET at different V_g follows $\alpha(\lambda)$ of P3HT as observed in Fig. 4.11.

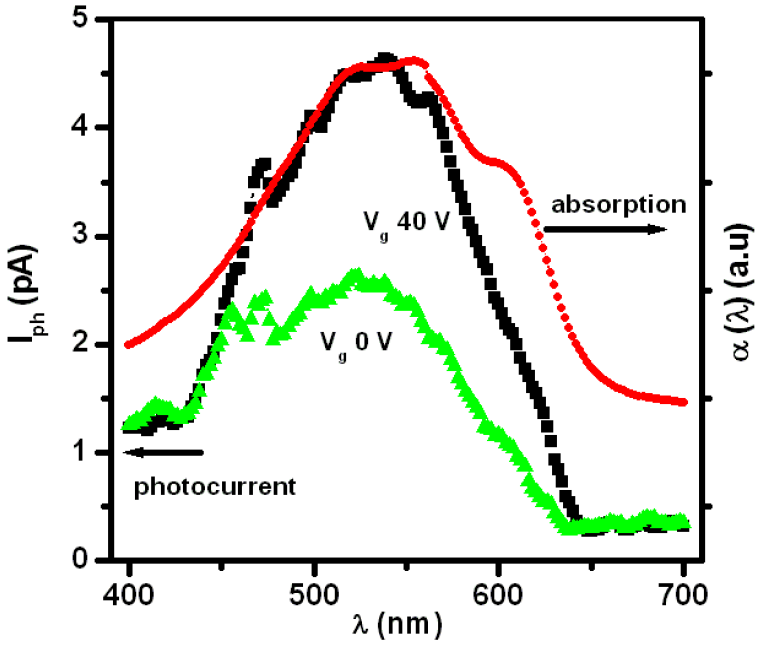

Figure 4.11: **Photocurrent spectra of bilayer FET observed at V_g 40 V and 0 V, and it follows the absorption profile for P3HT.**

The transconductance characteristics of bilayer FET shows no change in I_{ds} in depletion mode of operation as seen in Fig. 4.10, and only increase in the enhancement mode of operation. The light intensity incident on the sample was controlled using a set of neutral density filters. The device active area consists of (40 μm X 2 mm) over which the entire photon are incident corresponding to a photon flux/unit area sec $\sim 10^{15}$. The linear increase in I_{ds} in enhancement mode can be rationalized in terms of photoconductive effect, with a marginal change in V_{th}. The increase of I_{ds} in bilayer FET upon photoexcitation is purely due to transport of n-carriers from the **D-A** interface to the PCBM channel. The corresponding

change in pure P3HT FET with aluminum electrode to identical light intensity does not show any change in current, thereby indicating that the changes in the transfer characteristics comes only from the transferred photogenerated electrons into the PCBM film. The efficient conversion of photon into free carriers at the **D-A** interface is limited by several factors such as conformal contact of polymer onto PCBM induced by lamination and among all the photon absorbed by P3HT, only those exciton generated at the **D-A** interface will dissociate into free charge carriers at the interface.

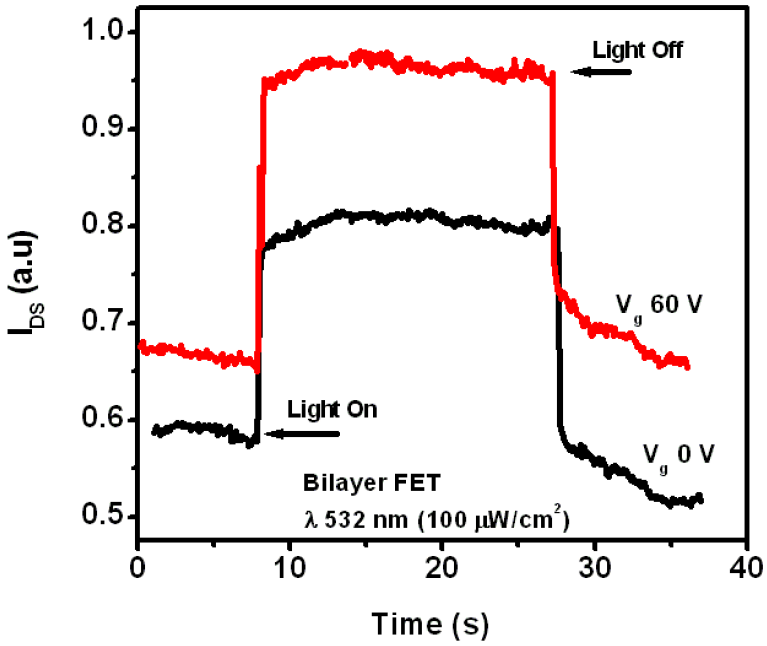

Figure 4.12: **Build up and decay of I_{ds} in bilayer FET upon photoexciting (CW, λ 532 nm, Power 100 μW/cm^2 at different V_g.)**

The photo induced features are reversible, i.e. I_{ds} traces back to the dark value upon switching off the illumination as observed in Fig. 4.12, this feature is in sharp contrast to existence of persistent current that shows a slow relaxation upon switching off the excitation. Such optical responsivity in the devices has been used

to demonstrate optically induced memory effects[126]. Upon switching off the excitation, current reverts back to the dark value. This key aspect of the spatially separated charge distribution at the **D-A** interface and transport process at the conducting channel provides an ideal platform to study evolution of charge carriers and its trajectory to the channel region as a function of V_g using a transient-time of flight techniques. The transient current studies of this bilayer structure can be considered to be modified version of the conventional TOF and planar transient current techniques. The time resolved transient signals upon pulsed photoexcitation provides and an insight into the different stages of the carriers transport and transport.

4.2.5 Transient-TOF studies of Bilayer FET

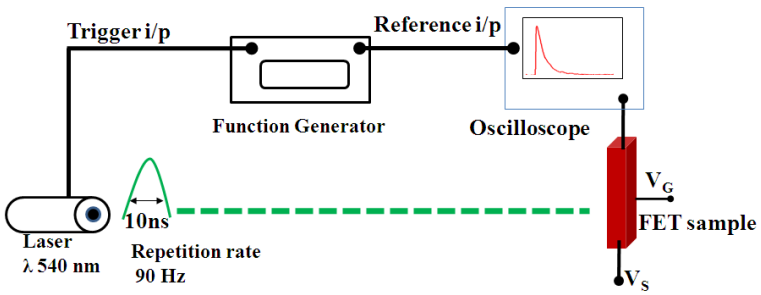

Figure 4.13: **Schematic diagram for single pulse planar transient-TOF measurement set-up for bilayer FET.**

Transient photocurrent measurement is a useful technique in the time domain to study the dynamics of photoinduced charge carriers. This technique is a powerful tool to estimate the charge carrier generated within a short time and can be used to find out the quantum yield of the device under test. Planar transient-TOF single pulse photocurrent measurement allows us to temporally characterize the

charge transport across the **D-A** interface and monitor the V_g dependent channel transport processes. The experimental setup is identical to TOF setup, where a sandwiched structure is replaced by a planar FET structure and instead of charge generating sheet and blocking contact, We have P3HT as the optically active donor forming a schottky contact with aluminum but a decent injecting contact with PCBM layer, thereby only allowing electron as the transporting carriers. The measurement was carried out both in dc and ac mode. In ac mode, single pulse [10 ns] Nd:YAG laser (543 nm) is used as the light source and current is measured across a high resistance resistor coupled to a 1 GHz sampling rate Le Croy Oscilloscope. The Oscilloscope and the function generator triggering the laser are synchronized with each other. The time resolution of data acquired in the oscilloscope was 50 ns, which was used to study the photoresponse of single pulse excitation of bilayer FET. Details of the experimental set-up are observed in the Fig. 4.13. Transient signal arising from bilayer FET in comparison to absence of signal from single PCBM layer FET for a light intensity of 100 μW/cm^2 incident on the sample can be noted in the Fig. 4.14. Incidenting higher light intensity and increasing V_{ds} do not give rise to transient signal in single PCBM layer FETs. This feature indicates the origin of excess carriers from the photogenerated process in P3HT into PCBM. The repetition rate of trigger before the next laser pulse was incident on the sample was adjusted such that the decay characteristics showed the I_{ds} reverted back to the dark current before the next light pulse was incident. For the given samples, the rep-rate was set to 90 Hz.

I_{ds}(t) profile was characterized at different V_g for the bilayer FET as seen in the Fig. 4.15. Several key features of carrier generation and transport are embedded in the transient profile. This features essentially indicates the origin of carriers from

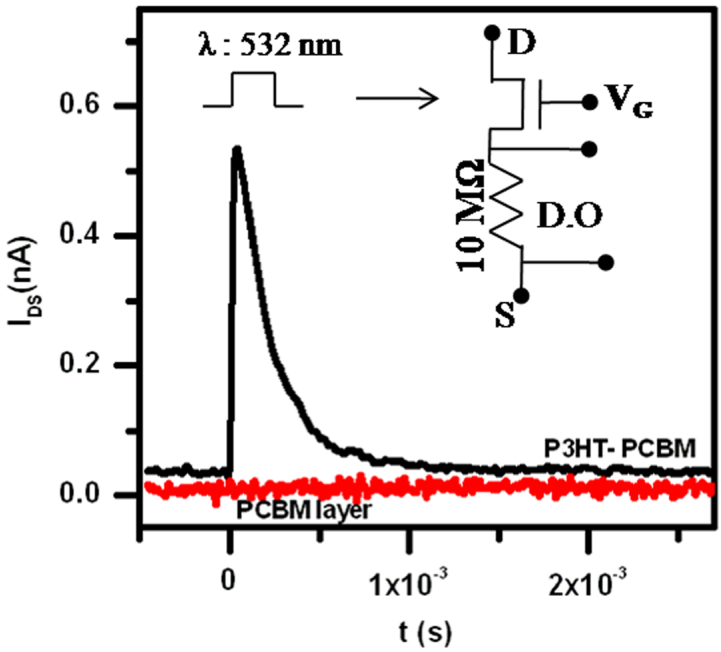

Figure 4.14: **Presence of transient signal from Bilayer FET and absence of signal from PCBM FET, Inset shows the schematics for transient measurement.**

photogenerated process at the **D-A** interface and is expectedly dependent on V_g. For t $<$ 0 s, implies before the light pulse has been incident on the sample, and we can see it follows a n-channel transport, and after t $>$ 0 s, there is increase in I_{ds} and a function of different V_g it shows different rise time, peak photocurrent value and decay characteristics.

The measured current provides a direct estimate of the excess electron introduced in the channel, $Q_{excess} = \int I(t)_{light} dt$. The Q_{excess} calculated for V_g 60 V was $\approx$ 5.9 x 10^{13} and for V_g 0 V was $\approx$ 2 x 10^{13}. The excess electron in turn quantifies the charge-transfer processes occurring at the **D-A** interface. The device active area consists of (40 μm x 2 mm) over which the entire light is incident corresponding to an incident photon flux of $10^{15}/cm^2s$. Efficiency can be defined

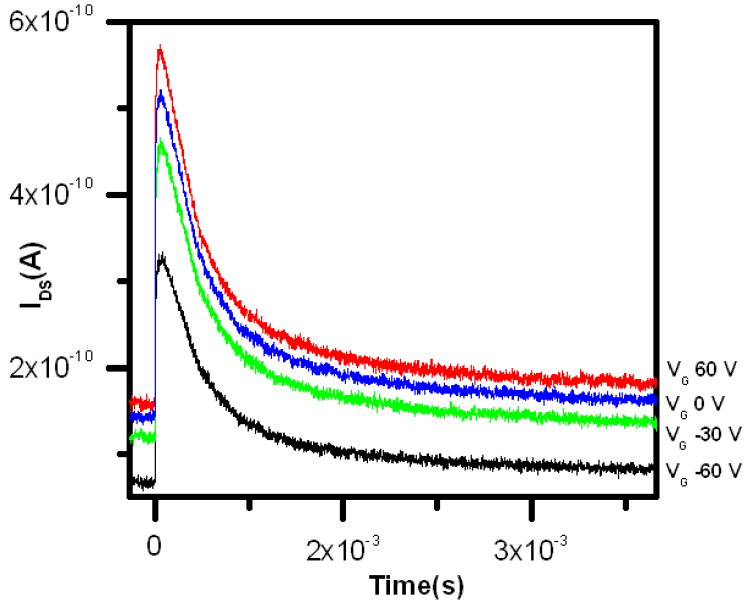

Figure 4.15: **Transient response of DA-FET to a single pulse photoexcitation (10 ns, 532 nm, 100 $\mu W/cm^2$) at V_{ds} 100 V and different V_g.**

as Q_{excess}/(photon flux) is observed to V_g dependent.

A schematics of I_{ds}(t) profile as seen in Fig. 4.16 is depicted for different regimes indicating the crossover of different process contributing to I_{ds}. The V_g independent regime 1, $(t_1 < t < t_{onset})$ is observed in the early stages after switching off the single pulse photoexcitation, which can be attributed to the diffusion of separated electrons from the **D-A** interface into the bulk. The diffusion length L_d estimate from $(D_n\tau)^{1/2}$, where $\tau \sim \tau_{onset}$ is found to be $\approx$ 4 nm. Since the time duration of light pulse is 10 ns, and the exciton generation and charge separation at **D-A** interface occurs within the first few picoseconds, the delayed current response that is observed is due to the diffusion of charge carriers from the **D-A** interface to the bulk. In order to verify the delayed response doesn't arises from external RC circuitry, care has been taken by adding a additional high resistance across the

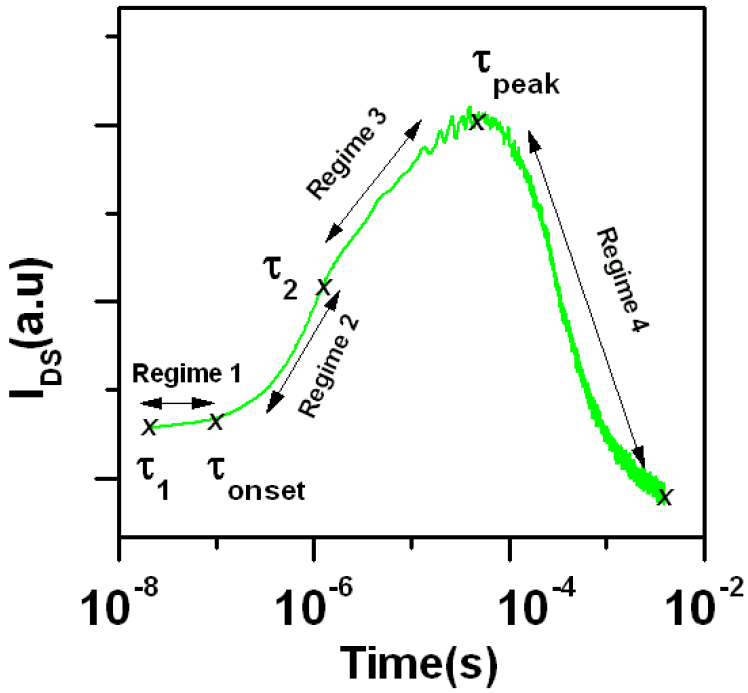

Figure 4.16: **Schematic representation of I_{ds}(t) profile indicating distinct regimes.**

input of the oscilloscope.

For $\tau > \tau_{onset}$ in regime 2, $d[I_{ds}(t)/dt]$ is V_g dependent and increases for a specified duration ($t_{onset} < t < t_2$). An inflexion point in the I_{ds}(t) buildup profile is observed with an abrupt change in $d[I_{ds}(t)/dt]$ in the regime 3 ($t_2 < t < t_{peak}$). $d[I_{ds}(t)/dt]$ discernibly decreases in this range and eventually I_{ds}(t) culminates in a rounded maxima. If τ_{peak} corresponding to this maxima is taken as a measure of transit time then μ can be estimated if the electric field across the interface and channel can be quantified, then $\mu_{min} \approx 10^{-6} cm^2/Vs$ assuming $V_d \approx V_g$.
Beyond the maxima, I_{ds}(t) decreases and the decay rate in this region is V_g dependent as seen in Fig. 4.17, which can be attributed to the barrier limited transport processes. In the present case, the decay rate fits to a sum of exponential processes,

$$y = A_1 exp(-x/\tau_1) + A_2 exp(-x/\tau_2) \tag{4.2}$$

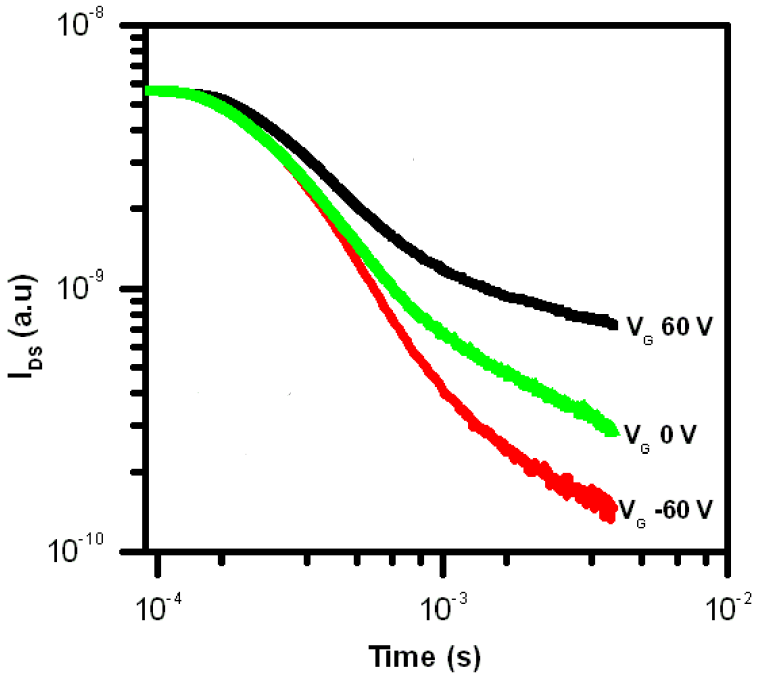

Figure 4.17: **Decay characteristics observed for DA-FET at different V_g.**

where τ_1 and τ_2 signifies a fast and slow decay. A single carrier two trap model corresponding to deep and shallow traps characterizing the decay kinetics of the PCBM layer can possibly explain the trend. This decay kinetics is in contrast to slow non-exponential relaxation processes observed in single layer PFET[125], where the relaxation processes were explained based in spatial separation of photo-generated positive and negative carriers and hierarchical sequential recombination mechanisms. The interpretation of decay of charge carriers in the molecular PCBM is quite complex due to combination of positional and energetic disorder[175]. The measured time constant (τ) is consistent with the values observed in electron decay due to traps measured using time resolved microwave conductivity techniques[176].

Voltage (V)	**Decay time $\tau_1 \vert \tau_2$**	**Rise time**
V_g60	278 μs/1.3 ms	2.6 μs
V_g0	300 μs/2.5 ms	2 μs
V_g-60	331 μs/0.6 ms	1 μs

Table 4.2: Rise and decay characteristics for P3HT-PCBM bilayer FET.

The fall in rise time in the depletion mode of operation indicates the extent of depletion of the PCBM layer, since the effective time taken by the charge carriers to reach the conducting channel in PCBM in depletion mode becomes smaller.

The observed photocurrent decay response is an indicator of kinetics of charge generation, transport and decay characteristics of bilayer FET. The transport equation for the excess photogenerated charge carriers (electrons) based on drift-diffusion model has been modeled to study the charge carriers under applied V_g given by the below equation,

$$\frac{dn}{dt} = -\frac{n}{\tau_n} + \frac{1}{q}\frac{dj_n}{dx} \tag{4.3}$$

and this can be rewritten using expression for current density as,

$$j_n = qn\mu_n F + qD_n\frac{dn}{dx} \tag{4.4}$$

$$D_n\frac{d^2n}{dx^2} + \mu_n F\frac{dn}{dx} = \frac{dn}{dt} + \frac{n}{\tau_n} \tag{4.5}$$

where D_n is the diffusion coefficient for the carriers and τ is the life time of the charge carriers, F is the applied electric field and n is the concentration of charge carriers.

Simulation solution shows the sheet of charge carriers that are generated at **D-A**

interface is then transported across the sample as they reach the channel. Photo-generated charge carriers at the **D-A** interface is normalized to unity and distribution of electrons along the various coordinates of the sample can be seen at various interval of time. The decay of charge carriers can be correlated to small life time and the trap distribution in the sample. Thus n(x=h,t) can capture some of the features such as broadening and attenuation of the propagating carrier-pulse in the profile as observed in Fig. 4.18. This observation is confirmed in the $I_{ds}(t)$ decay characteristics, where the charges decay rapidly after reaching the peak photocurrent value.

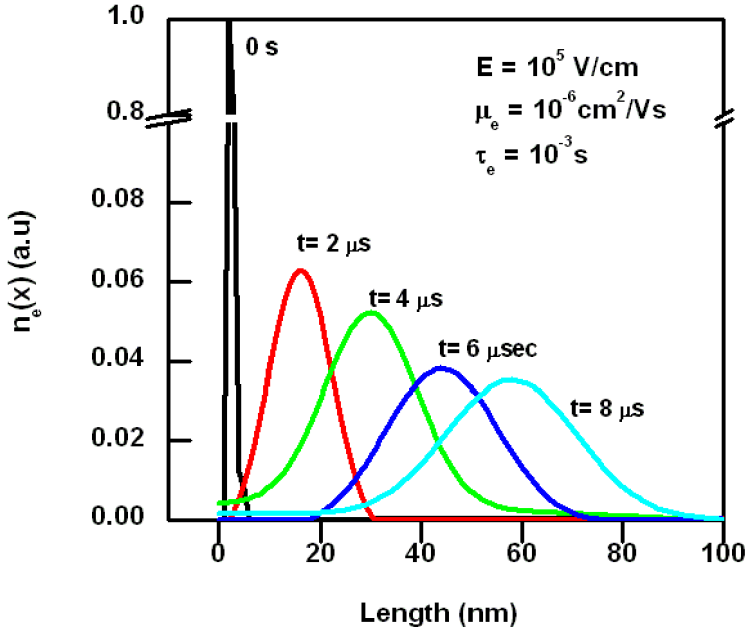

Figure 4.18: **Drift-diffusion solution of n(x) calculated at different cross-section of the sample at different interval of time. At (x=5, t=0) corresponds to initial photogenerated charges at the D-A interface.**

4.2.6 Summary for P3HT-PCBM bilayer FET

In summary, an illustrative experimental investigation has been studied on optically active donor and optically inactive acceptor based bilayer FET, by photoexciting the donor polymer and noting the change in acceptor based transistor characteristics. Charge transport efficiency within the PCBM-bulk is estimated from the current profiles and observed to gate voltage dependent. This studies can be extended to efficient, compatible and other robust system to study charge transfer and transport process across **D-A** interface. We extend the present studies to another optically active acceptor system, N2200 observed to be air stable and having high n-channel mobility.

4.3 Optically Active Acceptor-Donor

The stable n-channel FET characteristics can be used as an electrical template to observe changes introduced upon laminating the surface by a (D) polymer layer. The (D) polymer can be further perturbed by photoexcitation and the changes can be closely followed. The charge transport in these organic solar cells is largely governed by the energy barrier (bilayer) or the higher spatial disorder (bulk heterojunction). **D-A** interface plays an important role in determining the free charge carrier yield initiated by the excitonic processes in the donor media[177]. In bilayer structure the **D-A** interface is spatially well defined and since the photogenerated charges are confined to either side and the bimolecular recombination probability is minimized thereby facilitating the yield of free carriers available for extraction. There has been a recent revival of interest in solution-processed bilayer solar cell arising from the possibility of larger exciton diffusion lengths in

cleaner systems with lower defect concentrations and long range interactions promoting charge transfer over large length scales. There is considerable interest in examining the interfacial photophysical processes under different electrostatic conditions without invasive factors such as injection currents[170] in standard bilayer geometry. Exciton dissociation process at the interface competes with back recombination mechanism where charge separated states decays back to the ground state decreasing the free carrier yield[178].

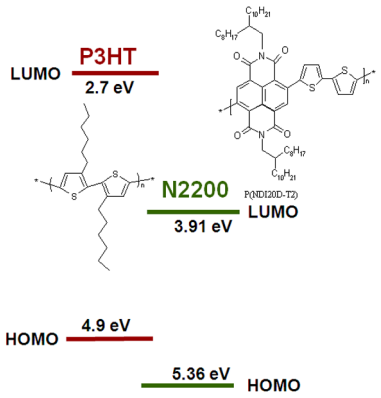

Figure 4.19: **Schematics depicting the HOMO(LUMO) energy level for P3HT and N2200 polymers along with its chemical structure.**

We fabricate a novel device structure consisting of a **D-A** bilayer where the A-layer forms the underlying n-channel FET device. Photogenerated charge carrier can be introduced in these devices, upon photoexciting the D-layer which leads to a charge transfer across the **D-A** heterojunction resulting in diffusion and drift of the electrons away from the interface and towards the channel region. Consequently, the charge carrier generation and charge transport can occur at spatially well separated zones We have previously utilized this approach on **D-A** bilayer n-transporting FET consisting of [6,6]-phenyl C61-butyric acid methyl ester (PCBM) as the A-layer[179]. The μ_{FET} was significantly lower and the PCBM does not have

a characteristic absorption window. In the present studies we utilize N2200 a high stability, high mobility, optically active (A) system with a characteristic absorption window which complements the (D) optical region. The complementarity in the optical absorption characteristics enables the distinction of carrier's contribution to the V_g dependent spectral response of the drain-source current I_{ds}. The dependent of photophysical process occurring at the **D-A** interface and semiconductor-dielectric interfaces are observed using combination of steady state and transient pulse excitation studies.

Model systems of regio-regular poly(3-hexylthiophene) RR-P3HT and naphthalene-bis(dicarboximide) NDI based polymer poly[N,N'-bis(2-octyldodecyl)-napthalene-1,4,5,8-bis(dicarboximide)-2,6-diyl-alt-5,5'-(2,2'-bithiophene), (P(NDI20D-T2), Polyera ActivInk N2200 is used as a (D) and (A) species respectively for the present studies, with both components exhibiting good film forming capability. N2200 is highly air stable, optically active n-type polymer exhibiting unprecedented OTFT characteristics under ambient conditions in combination with Au contacts and various polymeric dielectrics[180].

4.3.1 Optically active N2200 FET fabrication

Top contact FETs fabricated from N2200 on cross linked benzocyclobutene polymer dielectric (BCB) treated with 1 μm solution of octadecyltrichlorosilane (OTS) in n-hexane, and coated with Al as S-D electrodes exhibited n-type transport, as indicated from the output characteristics and transfer characteristics (inset) indicated in Fig. 4.20. Upon testing several devices and fitting them to the

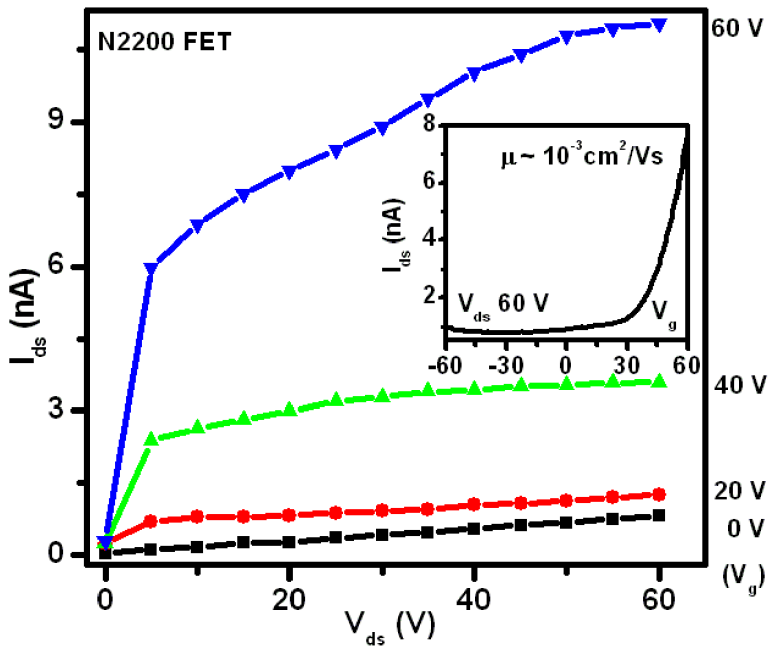

Figure 4.20: **n-channel FET characteristics of single layer N2200, observed at increasing V_g, Inset transconductance characteristics at V_{ds} 60 V.**

above model, the observed FET was found to be in the range of $\sim 10^{-3}$ cm^2/Vs. The observed V_{th} was found to be in the range of 0 to 20 V. Large V_{th} were observed in the sample, which could be attributed to imperfections in the soft-dielectric media and presence of traps at the dielectric-semiconductor interface.

P3HT-N2200 based bilayer structure was obtained using non-solvent methodology as reported for P3HT-PCBM bilayer FET. For bilayer structure the choice of Al as S-D electrode was used to ensure the complementarity of Al electrode in forming decent injecting contacts with N2200 while forming blocking contacts with P3HT is utilized to inject charge carriers into the N2200 film. It is to be noted that the blocking behavior of Al with P3HT is prominent for lateral transport compared to its ability to inject in carriers in a sandwich-diode configuration. FETs based on N2200 with Al as the S-D electrodes shows n-channel transfer response

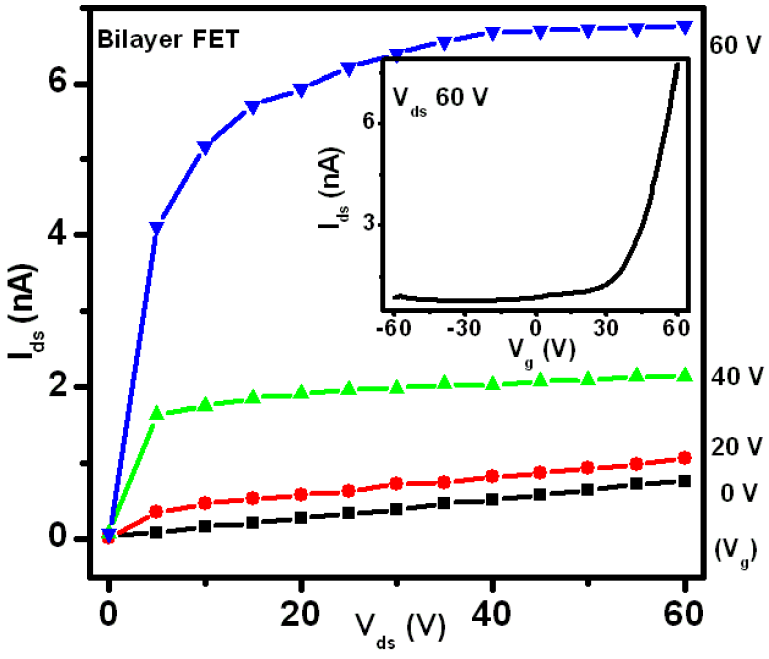

Figure 4.21: **n-channel FET characteristics of bilayer P3HT-N2200, observed at increasing V_g, Inset transconductance characteristics at V_{ds} 60 V.**

and introduction of an additional (D) polymer layer on N2200 merely introduces a marginal shift in the characteristics as seen in Fig. 4.21. The presence of P3HT (D) layer, does not adversely affect the n-transport characteristics of N2200 (A) based FET. In order to verify the active transport region in the bilayer FET, the output characteristics for drain current in positive and negative drain-source voltage were measured, Fig. 4.22. The results shows I_{ds} exhibiting saturation current in positive drain voltage and diverging I_{ds} in negative voltage, indicative of unipolar n-channel FET. The magnitude of the I_{ds} remains unchanged in all the donor laminated acceptor field effect transistor devices and corresponded to the single layer N2200 FET value. μ_e and on-off ratio obtained from the transistor characteristics of the bilayer devices in the dark was similar to that of single layer N2200 transistor.

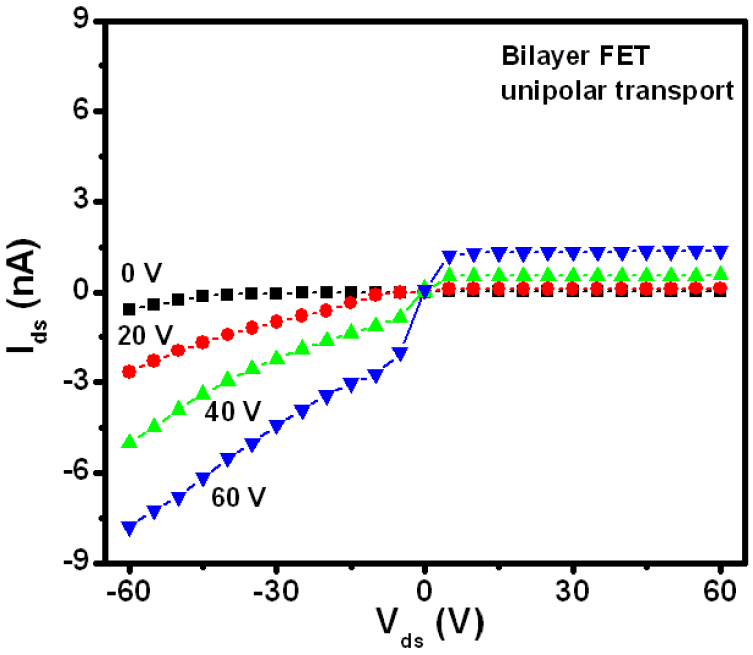

Figure 4.22: **I-V characteristics of single layer N2200 FET with positive and negative V_{ds} showing asymmetric response implying unipolar charge transport.**

4.3.2 Dark I-V characteristics

The electrical characteristic of the pristine-single layer N2200 FET changes upon photoexcitation of the device in a manner analogous to changes in p-channel FET[122]. The changes introduced for N2200 FET can be summarized by the following features: (i) The spectral response of the intensity modulated drain source $I_{ph}(\lambda)$ current largely follows the absorption profile of the N2200 as indicated in [Fig. 4.24(inset)] which consist of two distinct maxima. (ii) The I_{ds} changes with respect to intensity in the ON and OFF state can be described in terms of a photoconductive (linear responsivity) 60 μA/W) and photovoltaic type (log response) as observed in Fig. 4.23.

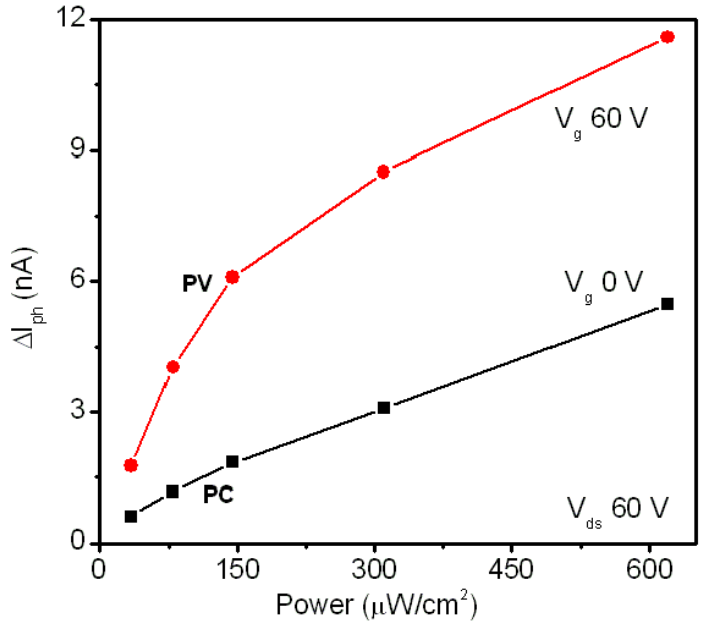

Figure 4.23: **Photocurrent as a function of incident light intensity in the on-state V_g 60 V and the off state V_g 0 V indicating photovoltaic and photoconductive effect.**

4.3.3 Photocurrent spectroscopy of Bilayer FET

Spectral investigation of DA-FET can provide more information about the origin of charge carriers apart from the electrostatic induced charge carriers at the dielectric-semiconductor interface. The presence of optically active donor and acceptor system will help us to identify the origin of photogenerated charge carriers from either component. In case of bilayer FET, both the N2200 and P3HT layers are optically active and have complimentary absorption features which is reflected in the spectral response of intensity modulated I_{ds}. It is to be noted that the photogenerated negative charge carriers can originate either in N2200 bulk or at the P3HT-N2200 interface which finally results in a contribution to the total channel current as observed in the Fig. 4.25. The spectral region corresponding to the N2200 absorption $300 < \lambda < 450$ nm is observed to have a stronger V_g dependence

compared to the carriers originating from P3HT absorption region $450 < \lambda < 600$ nm region as expected due to the proximity of the dielectric.

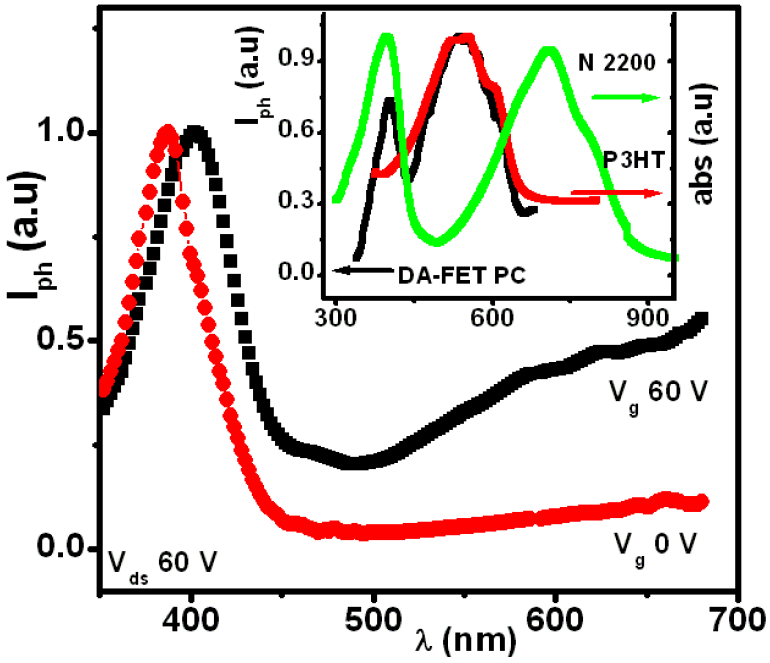

Figure 4.24: **Light intensity modulated $I_{ph}(\lambda)$ observed for single layer N2200 FET at V_g 60 V and V_g 0 V, (V_{ds} 60 V). Inset shows photocurrent spectra of bilayer FET(right) following the absorption profile for P3HT(left) and N2200(left).**

Since, the signal is in form of the I_{ds} primarily confined to the channel at the N2200/dielectric interface, the negative free carriers constitute the dominant species. The electrical transport process arising from the photogenerated positive carriers is a slower trap mediated process[125]. The differences in the carrier dynamics can also be adjudged by measuring an open circuit voltage developed at gate electrode with respect to shorted S-D electrodes. Signal in the range +70 mV is observed as seen in Fig. 4.26 upon illuminating the device (λ 532 nm, 100 μW/cm^2), indicative of an increase in the n-carrier density at the channel.

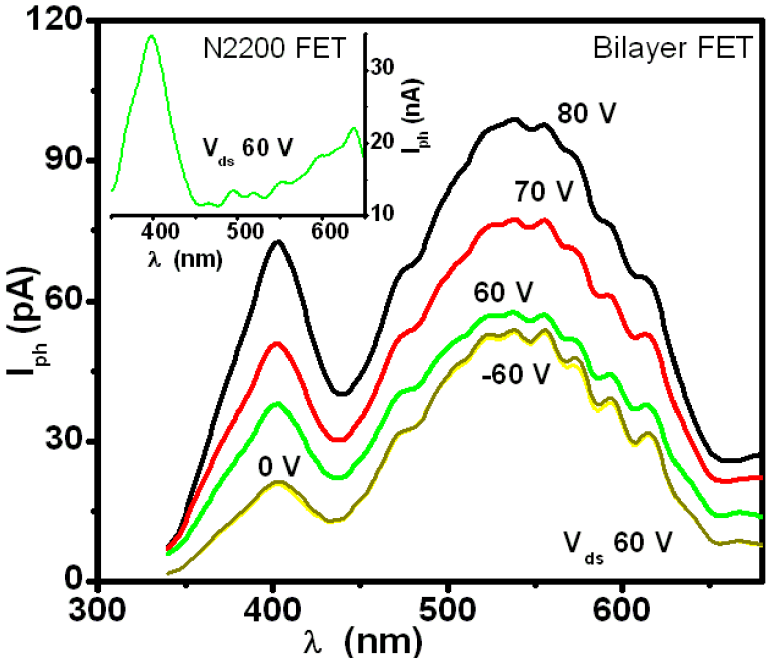

Figure 4.25: **Light intensity modulated $I_{ph}(\lambda)$ observed for Bilayer FET at different V_g, (V_{ds} 60 V, ω= 17 Hz) measured using Lock-in technique. Inset shows $I_{ph}(\lambda)$ for N2200 FET for (V_g 60 V, V_{ds} 60 V, ω= 17 Hz).**

4.3.4 Transient-TOF studies of Bilayer FET

Single pulse excitation is used to study the dynamics of charge transport in the bilayer FET structure. The time scale over which dynamics of charge transport in the bilayer are investigated should extend to the time taken for the device to reach the equilibrium in order to fully capture the behavior of the device. This allows us to study evolution of charge carriers from **D-A** interface to dielectric-semiconductor **D-S** interface. The $I_{ds}(t)$ measured upon a single pulse excitation is quite informative. The advantage of transient techniques over stationary I-V measurements is that one can study the dynamics of the processes which otherwise are integrated over time. Transient current measurements introduced by pulsing V_{ds} have been used in studying FETs to evaluate device parameters such as contact resistance and carrier mobility in polymers[181]. The present approach is based on

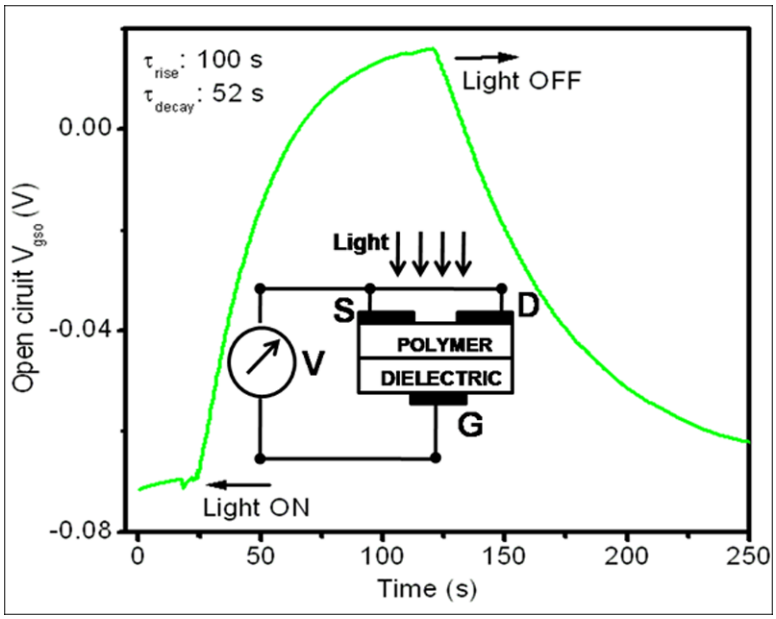

Figure 4.26: **Open-circuit voltage response measured between the gate electrode and shorted source-drain electrode for Bilayer FET upon illumination with 532 nm using a DC electrometer (Power = 100 $\mu W/cm^2$).**

studying transient I_{ds} induced by excess charge-carriers introduced by single pulse photoexcitation from the **D-A** interface. It is important to distinguish the present technique from the conventional time of flight (TOF) measurements employed for extracting mobility in thick polymer films sandwiched between electrodes. In the traditional TOF method, the charge carrier motion appears in the form of photocurrent, where the I_{ph}(t) represents the average charge carrier concentration and the mean velocity at a given time t, and the measured current density is in the direction of light propagation. While in the FET geometry, the excess carriers do not contribute to the current I_{ds} significantly till it is in the vicinity of the channel. We rely on the dominant signatures in this I_{ds}(t) to describe the underlying processes. The inflexion point in the I_{ds}(t) profile observed is taken as the carrier transit time and upon assuming uniform electric field (E), the mobility is estimated.

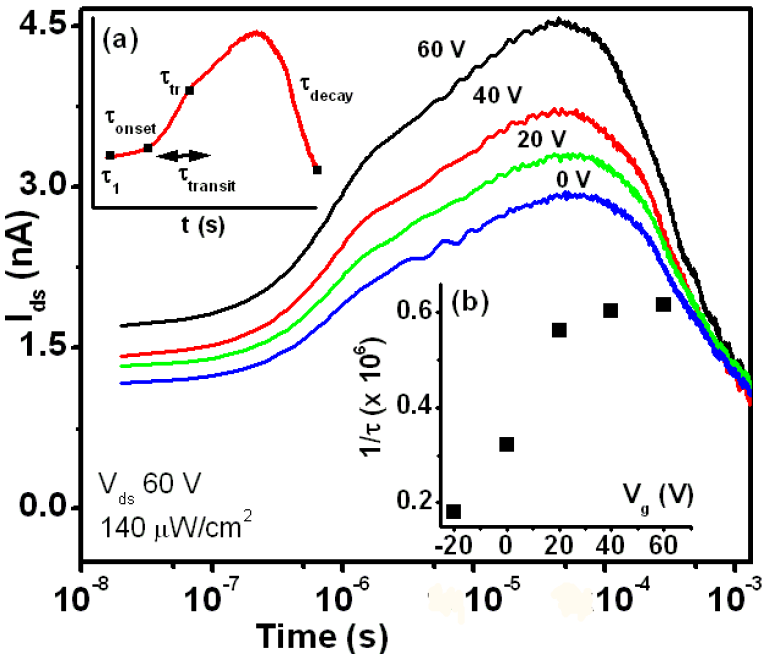

Figure 4.27: **Semi-log transient response of a bilayer FET to a single pulse photoexcitation (10 ns, 532 nm, 140 $\mu W/cm^2$) at different V_g(V_{ds} 60 V). Inset shows the schematics (a) semi-log plot indicating various time regimes, (b) Plot of reciprocal of rise time versus V_g.**

A typical I_{ds}(t) profile upon a single pulse photoexcitation on a bilayer N2200:P3HT device as observed in Fig. 4.27 exhibits the following features: (i) A distinct delay period prior to an increase in the I_{ds} following the 10 ns pulse is observed, denoted by a time-scale τ. The delay period was observed to be independent of V_g and can be attributed to the initial diffusion process after the interfacial C-T process. This appearance of delay is unlike the conventional TOF profiles where the current rise corresponds to the excitation pulse. (ii) I_{ds}(t) gradually rises beyond the τ_{onset} indicative of a current pathway for the photogenerated carriers. The electrical transport of the carriers in these systems can be described in the Gaussian disorder formalism. The initial narrow charge carrier pulse broadens as it propagates through the N2200 bulk. An inflexion point in the increasing I_{ds}(t) at τ_{tr} indicates the culmination of the carrier pulse at the channel. We attribute this zone in I_{ds}(t)

as a measure of the transit time τ_{tr}. $1/\tau_{tr}$ scales linearly with the field E, indicative of the independence of μ on E in the limited-low E regime as observed in the inset (b) Fig. 4.27. The variation of the field within the bulk semiconductor region is limited to a considerable extent. (iii) The equilibration of the photocarriers as it approaches of the zone of V_g influence (dielectric-semiconductor interface), further modifies the dispersive transient profile. The rate of increase in I_{ds}(t) gets progressively slow and the I_{ds}(t) goes through a broad maxima before it decays gradually to the original state. Transit time τ_{tr} can be used to estimate the bulk mobility of N2200 and upon assuming a value of E to be 4 x 10^4 V/cm, $\mu \sim$ 2.5 x 10^{-3} cm^2/Vs. Recent measurements for bulk electron transport in N2200 semiconductor have been studied. These results from both time-of-flight and electron-only current measurements suggest a bulk mobility of $\sim$ 5 x 10^3 cm^2/Vs[182]. The present approach permits mobility estimates in thinner samples. The I_{ds}(t) are inherently low field measurements since the voltages utilized for drawing the carriers to the channel is significantly << V_g. This value of transverse field across the N2200 layer can be justified by noting that V_g drop is largely across the dielectric, and the potential difference across the photocarrier transport region constitutes a fraction of the actual bias. The transit time decreases with increasing bias voltage as expected. It may be possible to arrive at an accurate value of the vertical field using numerical simulation procedures and scanning potentiometry experiments[154] using a localized region for the incident light and scanning it across the channel. This estimated mobility is similar to the reported bulk mobility measured using TOF set-up[182]. It may not be appropriate to compare the absolute value of μ_{FET} ($\sim 10^{-2}$ cm^2/Vs) to the present estimate with an assumed value of E. However, this range of bulk points to a 3-dimensional order in N2200 thin films.

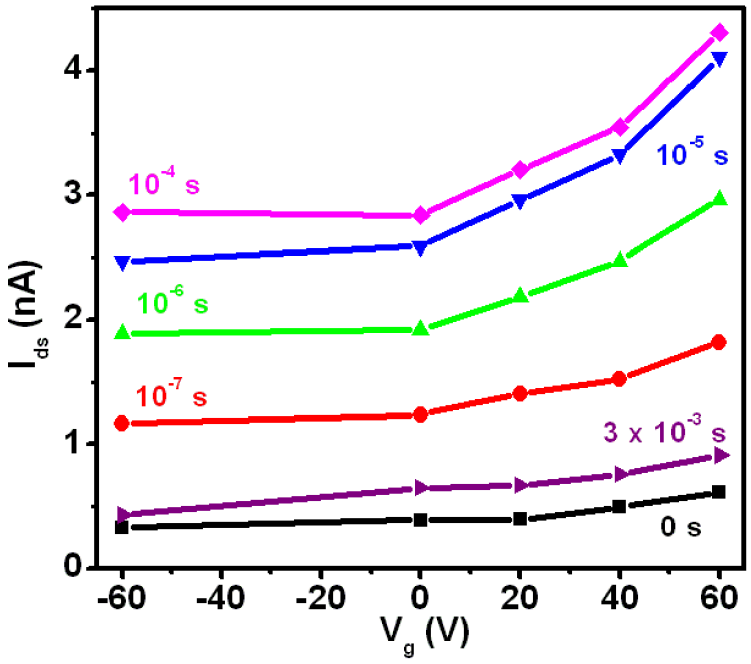

Figure 4.28: **Dynamic transconductance $I_{ds} - V_g$ responses for bilayer FET obtained from transient measurement at increasing time interval, data was constructed from I_{ds}(t) at different V_g.**

4.3.5 Dynamic Transconductance of Bilayer FET

The I_{ds}(t) obtained at different V_g can be utilized to reconstruct a dynamical transconductance $(I_{ds} - V_g)$(t). Fig. 4.28 depicts the $I_{ds}(V_g)$ at different t, with t = 0 corresponding to the dark state. The $I_{ds}(V_g)$ at different t is also a measure of the trajectory of photocarriers. The characteristic square law $I_{ds}(V_g)$ dependence is modified to a more exponential dependence from beyond t $> 10^{-6}$ s. The effective on-off ratio of the device in this interim period ($10^{-6}s<t<10^{-4}s$) increases along with a shift in V_{th}. These trends can be qualitatively explained on the basis of the carrier density increase. The effective on-off ratio of the sample also improves at different interval of time. The increase in the off current at different interval of time arises due to the net increase in the carrier density coming from the **D-A** interface, while the change in threshold voltage and transconductance arises due

to the increase in net effective internal electric field as the photogenerated charge carriers are swept from one interface to another interface.

It is instructive to compare the results of N2200 bilayer FET with that of PCBM:P3HT bilayer FET. The photoinduced I_{ds} is orders of magnitude larger in N2200 than in PCBM-C60 FETs[179]. The net excess charge upon a single-pulse photoexcitation for N2200:P3HT device can be estimated by the $\int I(t)dt$. For a typical response at V_g = 60 V, the integral corresponds to 2.6 x $10^{13}/cm^3$, which corresponds to charge collection efficiency of 0.01 charge/photon compared 10^{-3} charge/photon in PCBM:P3HT device for similar device and experimental parameters. The transit time in N2200 layer is also observed to be consistently smaller than in PCBM layer (with all other device parameters being equivalent). This feature points to a higher bulk mobility in N2200 than PCBM-C60. The other factors contributing to the significant photoinduced I_{ds} in N2200:P3HT can also arise from a more efficient primary steps in the C-T and charge separation processes. The origin of this trend can arise from compatibility of the electronic structure of the D and A systems leading to an optimum interface, and/or from mechanical aspects of a well structured bilayer interface formation as in case of P3HT-N2200 compared to P3HT:PCBM. These results suggest the possibility that optimized bilayer structure may be more suitable for P3HT:N2200 than bulk heterostructure for photovoltaic solar cells.

4.4 Summary

In conclusion, we have fabricated a n-channel bilayer FET with optically active donor P3HT on optically inactive acceptor PCBM, and optically active acceptor N2200 using non-solvent methodology. Combination of steady state illumination and single pulse transient measurement allows us study the photogenerated charge carriers at the D-A interface. The charge generation and separation occuring at the D-A interface are observed to be V_g dependent. The device allows us to simultaneously measure bulk and field effect mobility of the A-layer from $I_{ds}(t)$ profile.

CHAPTER 5

Summary and Future Directions

Important interface such as metal semiconductor interface which determine the efficiency of charge injection and donor acceptor interface crucial for understanding photovoltaic operation have been studied in field effect transistor geometry. Top contact PFET have been fabricated from single layer P3HT, P3HT-PCBM blend and bilayer consisting of P3HT-PCBM and P3HT-N2200.

In order to investigate the metal polymer interface, P3HT and P3HT-PCBM FETs have been fabricated in top contact geometry with large electrode span, in order to allow illuminating the polymer under the source drain electrode, without affecting the channel region. The P3HT and the blend devices showed a hole mobility of μ_{FET} 10^{-3} cm^2/Vs and on/off ratio greater than 10^3. The polymer has been selectively excited with $\lambda \approx 633$ nm corresponding to low absorption for P3HT and noted for its transconductance characteristics. For identical set of illumination intensity incident on the sample below the electrodes at equi distance and far away from the channel, larger I_{ds} is observed for drain excitation compared to source excitation. The transconductance behavior has been analyzed in linear, subthreshold and saturation regime and shows identical asymmetric response. Transconductance characteristics have been used to extract V_{th} shift upon photoexciting the polymer

under the electrodes. P3HT devices shows ΔV_{th} shift $\sim$ 3.1 V for source illumination and 8.1 V for drain illumination. P3HT-PCBM blend devices showed identical and large magnitude change of ΔV_{th} shift $\sim$ 9 V for source excitation and 20 V for drain excitation. A linear dependence of V_{th} shift with incident power is observed for both S-D excitation, with drain electrode showing larger slope in comparison to source electrode. V_{th} shift due to polymer excitation under the metal electrodes has been interpreted based on the contribution coming from the change in flat band potential, which arises due to mismatch between metal fermi level and semiconductor. The observation of asymmetric response, highlight the presence of larger barrier for charge injection at source electrode compared to the barrier required for charge collection at the drain electrode. The total contact resistance has been analytically modeled to extract the CR of the device in dark to be 9000 KΩ, 7100 KΩ for source excitation and 6000 KΩ for drain excitation.

Bilayer FET consisting of optically active donor P3HT and PCBM, N2200 as the acceptor have been fabricated using non-solvent methodology. The device architecture allows us to optically excite the donor polymer, and follow the excess charge introduced in acceptor bulk that can be monitored using FET measurement. The photogenerated charge carriers arising from the D-A interface are spatially separated from the electrostatic induced charges at the dielectric semiconductor interface. Steady state illumination allows monitoring the excess charges introduced from the donor to acceptor layer. The presence of donor layer does not alter the electrical characteristics of underlying acceptor FET. Photocurrent measurement of bilayer FET for P3HT-PCBM follows the absorption profile of P3HT, while for P3HT-N2200 bilayer FET has contribution coming from optically active N2200 as well as P3HT layer. The spectral region corresponding to N2200 absorption shows

large V_g dependence due to its proximity to dielectric interface compared to the spectral region for P3HT absorption in the photocurrent measurement. Transient measurement have been carried out and reveals V_g independent and dependent regimes from the I_{ds}(t) profile. V_g independent regime has been attributed to diffusion dominated process, and the various time regime observed to be V_g dependent has been used to estimate bulk mobility of PCBM and N2200. Bulk transverse mobility in PCBM was observed to be lower than field effect mobility, while in N2200 samples revealed identical bulk and field effect mobility implying 3-dimensional ordering in N2200 thin films.

The studies on bilayer FET can be further taken up to study charge transfer complexes, such as exciplexes present only at the (D-A) interface. Time resolved photocurrent spectrum along with combination of absorption studies at various V_g voltages on the bilayer FET can be used to estimate the presence of CT complexes at the interface. Exciplexes studies at interfaces are important in understanding the efficiency of free charge carrier generation upon photoexcitation of the donor polymer, and can be used to understand the limiting factors that affect the efficiency of organic photovoltaics.

Appendix 1

TCAD Device Simulation

We have adopted Synopsys Sentaurus Technology CAD tool[183] developed essentially for silicon based electronic devices to model the organic devices. Two-dimensional and three-dimensional virtual OFET structures have been designed and generated using structure editor of sentaurus tool suite, in accordance with the experimentally obtained geometry.

Numerical simulation for field effect devices can be done two dimensionally, Variable for this system are the electric potential φ and the hole and electron quasi-Fermi potential φ_{Fp} and φ_{Fn}, depending upon position and time. For concentration of carriers in equilibrium the corresponding expression for holes in local equilibrium the three potentials are connected through,

$$p = n_i exp\left((\varphi_{Fp} - \varphi)/V_T\right) \tag{1}$$

$$n = n_i exp\left((\varphi - \varphi_{Fn})/V_T\right) \tag{2}$$

$$n_i = \sqrt{N_V N_C} exp{-}E_g/2eV_T \tag{3}$$

The intrinsic density n_i is connected with the gap energy E_g and N_V, while $V_T = k_B T/e$ is the thermal voltage. The system of partial diffrential equation consists of Poisson equation for the electrical potential φ and the continuity equation for the hole and electron densities is then given by,

$$\vec{J_p} = ep\mu_p\left(-\nabla\varphi_{Fp}\right) \tag{4}$$

$$\vec{J_n} = en\mu_n\left(-\nabla\varphi_{Fn}\right) \tag{5}$$

can be then written into continuity equations, the system of equation can be then read as

$$\nabla ep\mu_p\left(-\nabla\varphi_{Fp}\right) = -e\frac{\partial}{\partial t}p - e(U_{SRH} + U_{direct}) \tag{6}$$

$$\nabla en\mu_n\left(-\nabla\varphi_{Fn}\right) = -e\frac{\partial}{\partial t}n + e(U_{SRH} + U_{direct}) \tag{7}$$

The direct radiative recombination rates are relevant only in ambipolar or double injection FET[184]. For organic devices and the device dimensions used recombination and generation process such as Auger recombination and avalanche generation are negligible. Numerical two dimensional simulation of Drift-Diffusion model has been carried out with device simulation program ISE TCAD[183]. The material parameters as specified for P3HT polymer used for device simualtion are as follow, Poole-Frenkel mobility has been implemented, given by

$$\mu = \mu_o exp(-E_o/kT)exp(\sqrt{F}((\beta/T) - \gamma) \tag{8}$$

where μ_0 is the low-field mobility, β and γ are the fitting parameters, E_0 is the effective activation energy and F is the electric field. The energy distribution of hole traps and electron traps are assumed to be Gaussian with mean zero centered at the band edge and standard deviation of 0.2 eV.

The I-V characteristics have been generated by solving Poisson equation, hole and electron continuity equations concurrently for a drift-diffusion transport model. The performance characteristics of OFETs are modeled and are found to be consistent with experimentally obtained current characteristics for P3HT FET.

TCAD Code

The code used to generate IV characteristics for P3HT FET.

Parameter	**values**
Permittivity ϵ	3
Bandgap E_g	1.7 eV
Electron affinity χ	3.15 eV
Refractive index (n)	1.65
Absorption coefficient α	1e5/cm
Density of States (N_C, N_V)	$10^{21}\ cm^{-3}$
Concentration of traps	$10^{16} cm^{-3}$(holes), $10^{17} cm^{-3}$(electron)
Trap activation energy	0.1 eV (hole), 0.3 eV (electron)

Table 1: Standard P3HT parameter used for simulation, adapted from reference[185]

.

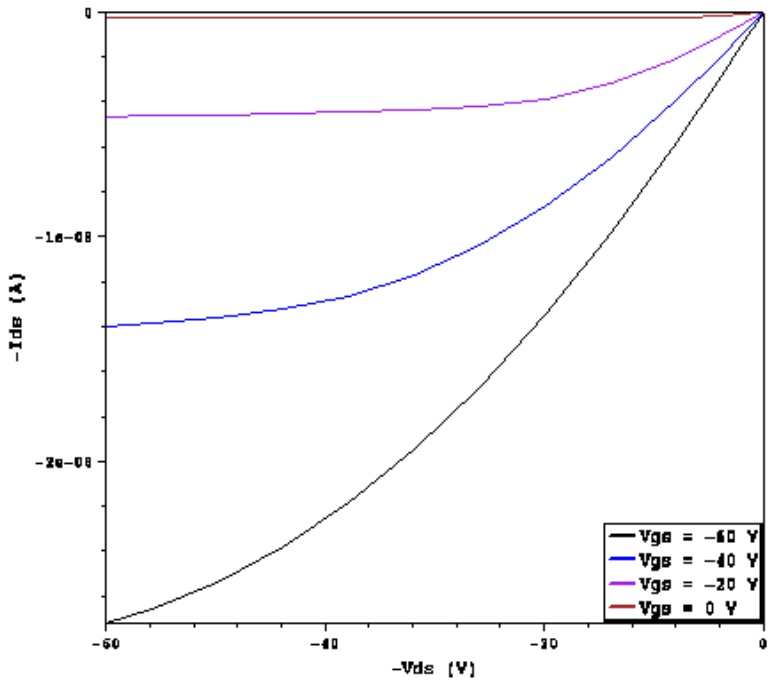

Figure 1: **Drain-Source current characteristics for simulated P3HT FET.**

File (

Grid= ofet-P3HT-msh.grd

Doping= ofet-P3HT-msh.dat

Parameter= models.par

Plot= Id-Vg-des.dat

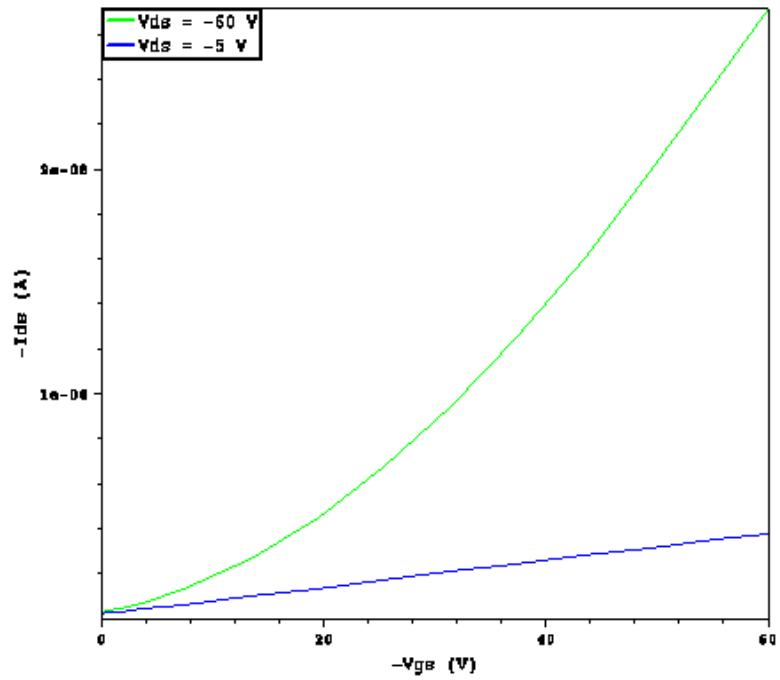

Figure 2: **Transfer Characteristics for simulated P3HT FET.**

Current= Id-Vg-des.plt

Output= Id-Vg-des.log)

Electrode (

Name= "'Source" Voltage=0.0

Name= "Drain" Voltage=0.0

Name= "Gate" Voltage=0.0)

Physics

(AreaFactor=1

SemAbsorption)

Physics(Material=Anysemiconductor)

Mobility (HighFieldSaturation(PFMob Eparallel))

Traps((eNeutral Gaussian fromCondBand Conc=1e15 ActEnergy=0.05 EnergyMid=0

EnergySig=0.035 eXsection=1e-10 hXsection=1e-12)

(hNeutral Gaussian fromValBand Conc=1e15 ActEnergy=0.05 EnergyMid=0 EnergySig=0.035 eXsection=1e-12 hXsection=1e-10))

Physics(Region=P3HT-channel-region)

OptBeam (

WaveLength = 632e-07 [cm]

WavePower = 5000e-6 [W/cm2]a

SemAbs (model= parameter) ODB or parameter

Semsurf = 0.0

SemWind = (-20.0 20.0))

Plot

(eDensity hDensity)

(eCurrent hCurrent)

(eQuasiFermi hQuasiFermi)

(ElectricField eEparallel hEparallel)

(Potential SpaceCharge)

(OptBeam)

(BeamGeneration)

(SRHRecombination Auger AvalancheGeneration)

(eMobility hMobility eVelocity hVelocity)

(Doping DonorConcentration AcceptorConcentration)

Math

(Extrapolate)

(Derivatives)

(Newdiscretization)

(RelErrControl)

(Iterations=30)

(NotDamped=50)

(-CheckUndefinedModels)

(Digits=4)

(RecBoxInteger (1e-3 10 1000)

(Traps(Damping=100) Default is 10; used when initial convergence is an issue.)

Solve

(initial gate voltage Vgs=0.0V)

(Optics)

(Poisson)

(Coupled (Poisson Hole))

(Coupled (Poisson Electron Hole))

Ramp gate voltage to -40V

(QuasiStationary)

(InitialStep=0.05 Maxstep=0.1 MinStep=0.00000001

Goal name= Drain voltage=-40) Coupled (Poisson Electron Hole)

Ramp drain voltage to -40V

(QuasiStationary)

(InitialStep=0.01 Maxstep=0.1 MinStep=0.00000001

Goal { name=Gate voltage=-40)

Coupled (Poisson Electron Hole)

END

"Note the syntax of the TCAD code has been ignored in order to accomodate the error resulting from LaTex compilation."

Appendix 2
MATLAB code

MATLAB code used to simulate the drift-diffusion of charge carriers from D-A interface to the electrodes. The code has been modified and adapted from reference[186].

```
PI = 3.1415926; Q=10e-6;
E = 1e5; (Applied Electric field)
Ebi = 2.5 * 10e4; (Built in Field)
Mh = 1e-4; (hole mobility)
Me = 1e-6; (electron mobility)
Dh = 26e-3 * Mh; (Einstein Relationship for hole)
De = 26e-3 * Me; (Einstein Relationship for electron)
TAUh = 1e-3; (Life time for holes)
TAUe = 1e-3; (Life time for electrons)
TMax = 1; (time window for carrier distribution)
L = 2e-5; (Sample thickness in cm)
Thickness=input('Enter thickness in nm ');
L=Thickness*1e-7;
S = 0; (Initial HOLE CONCENTRATION at electrodes)
SS = 0; (Intial ELECTRON CONCENTRATION at electrodes)
J = 1; (Initializing)
for X=0 : 5e-3 : 1
MATCARRIER(J,1) =X*2000; (unit:angstrom)
J = J + 1;
```

end

J = 1; K = 1;

STEPCOUNT = TMax/5;

for T = .001 : STEPCOUNT: TMax

K = K + 1;

SUM = 0;

for X =0: 0.005: 1

for n =0: 200

M = n;

S = $(-1)^M$*sin((2*n+1)*PI*(X*L-Mh*(E+Ebi)*T*10e-6)/L)* exp(-((1/TAUh)+Dh*((2∗ $n + 1) * PI/L)^2$)*T*10e-6);

SS = $(-1)^M$∗sin((2*n+1)*PI*(X*L+Me*(E+Ebi)*T*10e-6)/L)*exp(-((1/TAUe)+De*((2∗ $n + 1) * PI/L)^2$)*T*10e-6);

SUM = SUM+(S+SS)*2/L;

end (end for n loop)

if (SUM ¡ 0)

SUM = 0;

end

MATCARRIER(J, K) = SUM*L;

J = J + 1; S = 0; SS = 0; SUM = 0;

end (for x loop)

J = 1;

end (for T loop)

J = 1;

RC = 0.0095;

TMax = 1;

for T = .000001 : (TMax)/1000: TMax

MATCURRENT(J, 1) = T; (units: microsec)

J = J + 1;

end

J = 1; I=1;

for T = .001 : (TMax)/1000: TMax

time(I)=T;

DRIFHOLE = 0;

DIFFHOLE = 0;

CURRENTHOLE = 0;

DRIFELEC = 0;

DIFFELEC = 0;

CURRENTELEC = 0;

CURRENT = 0;

for X =0 : .01 : 1

for n = 0 : 20

M = n;

S = $(-1)^M$*sin((2*n+1)*PI*(X*L-Mh*(E+Ebi)*T*10e-6)/L)*exp(-((1/TAUh)+Dh*((2*$n+1)*PI/L)^2$*T*10e-6);

S1 = $(-1)^M$*((2*n+1)*PI)*cos((2*n+1)*PI*(X*L-Mh*(E+Ebi)*T*10e-6)/L)*exp(-((1/TAUh)+Dh*$((2*n+1)*PI/L)^2$)*T*10e-6);

SS = $(-1)^M$*sin((2*n+1)*PI*(X*L+Me*(E+Ebi)*T*10e-6)/L)*exp(-((1/TAUe)+De*((2*$n+1)*PI/L)^2$)*T*10e-6);

SS1 = $(-1)^M$*((2*n+1)*PI)*cos((2*n+1)*PI*(X*L+Me*(E+Ebi)*T*10e-6)/L)*exp(-((1/TAUe)+De*$((2*n+1)*PI/L)^2$)*T*10e-6);

DRIFHOLE = DRIFHOLE + S*(2/L);

```
DIFFHOLE = DIFFHOLE + S1*(2/L);
DRIFELEC = DRIFELEC + SS*(2/L);
DIFFELEC = DIFFELEC + SS1*(2/L);
end
CURRENTHOLE = (Q/L)*(CURRENTHOLE+(E+Ebi)*Mh*10e-2*L*DRIFHOLE-
Dh*10e-2*L*DIFFHOLE);
CURRENTELEC = (Q/L)*(CURRENTELEC+(E+Ebi)*Me*10e-2*L*DRIFELEC+
De*10e-2*L*DIFFELEC);
end
CURRENT = -1*(CURRENTHOLE + CURRENTELEC);
RCCURRENT = CURRENT*(1 - exp(-T / RC));
current-array(I)=CURRENT;
MATCURRENT(J, 2) = RCCURRENT * 10000;
MATCURRENT(J, 3) = CURRENT * 10000;
I = I + 1;
J = J + 1;
end
plot(MATCURRENT(1:size(MATCURRENT,1),1),MATCURRENT(1:size(MATCURRENT,1),3)
plot(MATCURRENT(1:size(MATCURRENT,1),1),MATCURRENT(1:size(MATCURRENT,1),2))
```

References

[1] Zheng-Tao, Z., Jeffrey, T., Rudiger, D. and George, G. M. "Humidity sensors based on pentacene thin-film transistors", *Appl. Phys. Lett.* **81**, 4643 (2002).

[2] Heuer, H. W., Wehrmann, R. and Kirchmeyer, S. "Electrochromic Window Based on Conducting Poly(3,4-ethylenedioxythiophene)-Poly(styrene sulfonate)", *Adv. Mater.* **12**, 89 (2002).

[3] Friend, R. H., Gymer, R., Holmes, A., Burroughes, J., Marks, R., Taliani, C., Bradley, D. D. C., Santos, D., Bredas, J., Logdlund, M. and Salaneck, M. "Electroluminescence in conjugated polymers", *Nature* **397**, 121 (1999).

[4] Tang, C. "Two-layer organic photovoltaic cell", *Appl. Phys. Lett.* **48**, 183 (1986).

[5] Anton, U., Angelika, B., Karl-Heinz, K., Herbert, N., Hans-Joachim, R. and Klaus, M. "On the relation between charge-storage capacity and π topology of different oligonaphthylenes", *Adv. Mater.* **4**, 91 (1991).

[6] Burroughes, J. H., Jones, C. A. and Friend, R. H. "New semiconductor device physics in polymer diodes and transistors", *Nature* **335**, 137 (1988).

[7] Baude, P. F., Ender, D. A., Haase, M. A. Kelley, T. W., Muyres, D. V. and Theiss, S. D. "Pentacene-based radio-frequency identification circuitry", *Appl. Phys. Lett.* **82**, 3964 (2003).

[8] Smilowitz, L. B. "Conjugated polymers: modern electronic materials", *Circuits and Devices Magazine, IEEE* **10**, 19 (1994).

[9] Chiang, C. K., Fincher, C. R., Park, Y. W., Heeger, A. J., Shirakawa, H., Louis, E. J., Gau, S. C. and MacDiarmid, A. G. "Electrical Conductivity in Doped Polyacetylene", *Phys. Rev. Lett.* **39**, 1098 (1977).

[10] Kohlman, R. S., Joo, J. and Epstein, A. J. *"Physical properties of polymers handbook"*. AIP press, New York, (1996).

[11] Anderson, P. W. "Absence of Diffusion in Certain Random Lattices", *Phys. Rev.* **109**, 1492 (1958).

[12] Miller, A. and Abrahams, E. "Impurity Conduction at Low Concentrations", *Phys. Rev.* **120**, 745 (1960).

[13] Bassler, H. "Charge Transport in Disordered Organic Photoconductors a Monte Carlo Simulation Study", *Phys. Status Solidi B* **175**, 15 (1993).

[14] Gartstein, Y. N. and Conwell, E. M. "High-field hopping mobility in molecular systems with spatially correlated energetic disorder", *Chem. Phys. Lett.* **245**, 351 (1995).

[15] Novikov, S. V., Dunlap, D. H., Kenkre, V. M., Parris, P. E. and Vannikov, A. V. "Essential Role of Correlations in Governing Charge Transport in Disordered Organic Materials", *Phys. Rev. Lett.* **81**, 4472 (1998).

[16] Dunlap, D. H., Kenkre, V. M. and Parris, P. E. "Charge-Dipole Model for the Universal Field Dependence of Mobilities in Molecularly Doped Polymers", *Phys. Rev. Lett.* **77**, 542 (1996).

[17] Le Comber, P. G. and Spear, W. E. "Electronic Transport in Amorphous Silicon Films", *Phys. Rev. Lett.* **25**, 509 (1970).

[18] Vissenberg, M. and Matters, M. "Theory of the field-effect mobility in amorphous organic transistors", *Phys. Rev. B* **57**, 12964 (1998).

[19] Tanase, C., Meijer, E. J., Blom, P. W. M. and de Leeuw, D. M. "Unification of the Hole Transport in Polymeric Field-Effect Transistors and Light-Emitting Diodes", *Phys. Rev. Lett.* **91**, 216601 (2003).

[20] Goldie, D. M. "The implication of Meyer-Neldel behaviour for oxidising gas detection in phthalocyanine thin-films", *J. Mat. Sci* **37**, 33323 (2002).

[21] Kondo, M., Chida, Y. and Matsuda, A. "Observation of Meyer-Neldel rule in extended energy regime using novel a-Si:H TFTs", *Journal of Non-Crystalline Solids* **198**, 178 (1996).

[22] Stallinga, P., Gomes, H. L., Biscarini, F., Murgia, M. and de Leeuw, D. M. "Electronic transport in field-effect transistors of sexithiophene", *J. Appl. Phys.* **96**, 5277 (2004).

[23] Ebisawa, F., Kurokawa, T. and Nara, S. "Electrical properties of polyacetylene/polysiloxane interface", *J. Appl. Phys.* **54**, 3255 (1983).

[24] Koezukaa, H., Tsumura, A. and Ando, T. "Field effect transistor with polythiophene thin film", *Synth. Met.* **18**, 699 (1986).

[25] Garnier, F., Horowitz, G., Peng, X. and Ichou, D. "An all-organic soft thin film transistor with very high carrier mobility", *Adv. Mater.* **2**, 592 (1990).

[26] Garnier, F., Hajlaoui, R., Yassar, A. and Srivastava, P. "All-Polymer Field-Effect Transistor Realized by Printing Techniques", *Science* **265**, 1684 (1994).

[27] Drury, C. J., Mutsaers, C. M. J., Hart, C. M., Matters, M. and de Leeuw, D. M. "Low-cost all-polymer integrated circuits", *Appl. Phys. Lett.* **73**, 108 (1998).

[28] Crone, B., Dodabalapur, A., Lin, Y., Filas, R., Bao, Z., LaDuca, A., Sarpeshkar, R., Katz, H. and Li, W. "Large-scale complementary integrated circuits based on organic transistors", *Nature* **403**, 521 (2000).

[29] Rogers, J. A., Bao, Z. and Dodabalapur, A. "Organic smart pixels and complementary inverter circuits formed on plastic substrates by casting and rubber stamping", *IEEE Electron Device Lett.* **21**, 100 (2000).

[30] Ziernelis, K. "Putting it on plastic", *Nature* **393**, 619 (1998).

[31] Torsi, L., Dodabalapur, A., Sabbatini, L. and Zambonin, P. G. "Multi-parameter gas sensors based on organic thin film transistors", *Sens. Actuators, B* **67**, 312 (2000).

[32] Shimoda, T., Kimura, M., Seki, S., Kobaysshi, H., Kanbe, S., Miyashita, S., Friend, R. H., Burroughes, J. H., Towns, C. R. and Millard, I. S. *IEDM* **107** (1999).

[33] Sirringhaus, H., Tessler, N. and Friend, R. H. "Integrated Optoelectronic Devices Based on Conjugated Polymers", *Science* **280**, 1741 (1998).

[34] Lilienfield, J. E. *US patent.* 1745175, (1930).

[35] Christopher, R. N., Reid J, C., Matthew J, P. and Daniel, C. F. "High mobility top-gated pentacene thin-film transistors", *J. Appl. Phys.* **98**, 084506 (2005).

[36] Roichman, Y. and Tessler, N. "Structures of polymer field-effect transistor: Experimental and numerical analyses", *Appl. Phys. Lett.* **80**, 151 (2002).

[37] Henrik, G. O. S., Tomas, G. B., Ronald, O., Maxim, S., David, S., McCulloch, I. and Henrik, S. "Insulators and device geometry in polymer field effect transistors", *Org. Elec.* **6**, 142 (2005).

[38] Horowitz, G., Peng, X. Z., Fichou, D. and Garnier, F. "The oligothiophene based field effect transistor: How it works and how to improve it", *J. Appl. Phys.* **67**, 528 (1990).

[39] Shur, M. *"Physics of Semiconductor Devices".* (1990).

[40] Veres, J., Simon, O., Giles, L. and Dago de, L. "Gate Insulators in Organic Field Effect Transistors", *Chem. Mater.* **16**, 4543 (2004).

[41] Yang, Y. S., Kim, S. H., Lee, J. I., Chu, H. Y., Do, L. M., Lee, H., Oh, J., Zyung, T., Ryu, M. K. and Jang, M. S. "Deep-level defect characteristics in pentacene organic thin films", *Appl. Phys. Lett.* **80**, 1595 (2002).

[42] Egginger, M., Bauer, S., Schwodiauer, R., Neugebauer, H. and Sariciftci, N. S. "Current versus gate voltage hysteresis in organic field effect transistors", *Monatsh Chem.* **140**, 735 (2009).

[43] Naber, R. C. G., Cristina, T., Blom, P. W. M., Gerwin, H. G., Albert, W. M., Fred J, T., Sepas, S. and de Leeuw Dago, M. "High-performance solution-processed polymer ferroelectric field-effect transistors", *Nat. Mater.* **4**, 243 (2005).

[44] Xie, Z., Abdou, M. S. A., Lu, X., Deen, M. J. and Holdcroft, S. "Electrical characteristics and photolytic tuning of poly(3-hexylthiophene) thin film metal insulator semiconductor field effect transistors (MISFETs)", *Can. J. Phys.* **70**, 1171 (1992).

[45] Willander, M., Assadi, A. and Svensson, C. "Polymer based devices their function and characterization", *Synth. Met.* **57**, 4099 (1993).

[46] Fuchigami, H., Tsumura, A. and Koezuka, H. "Polythienylenevinylene thin-film transistor with high carrier mobility", *Appl. Phys. Lett.* **63**, 1372 (1993).

[47] Brown, A. R., Pomp, A., Hart, C. M. and de Leeuw, D. M. "Logic Gates Made from Polymer Transistors and Their Use in Ring Oscillators", *Science* **270**, 972 (1995).

[48] Paloheimo, J., Kuivalainen, P. Stubb, H. and Vuorimaa, P. Lahti, Y. "Molecular field-effect transistors using conducting polymer Langmuir Blodgett films", *Appl. Phys. Lett.* **56**, 1157 (1990).

[49] Horowitz, G. and Hajlaoui, M. E. "Mobility in Polycrystalline Oligothiophene Field-Effect Transistors Dependent on Grain Size", *Adv. Mater.* **12**, 1046 (2000).

[50] Bao, Z., Lovinger, A. J. and Dodabalapur, A. "Organic field-effect transistors with high mobility based on copper phthalocyanine", *Appl. Phys. Lett.* **69**, 3066 (1996).

[51] Bao, Z., Lovinger, A. J. and Dodabalapur, A. "Highly ordered vacuum-deposited thin films of metallophthalocyanines and their applications in field effect transistors", *Adv. Mater.* **9**, 42 (1997).

[52] Xiao, K., Liu, Y. Q., Qi, T., Zhang, W., Wang, F., Gao, J. H., Qiu, W. F., Ma, Y. Q., Cui, G. L., Chen, S. Y., Zhan, X. W., Yu, G., Qin, J. G., Hu, W. P. and Zhu, D. B. "A Highly π Stacked Organic Semiconductor for Field-Effect Transistors Based on Linearly Condensed Pentathienoacene", *J. Am. Chem. Soc.* **127**, 13281 (2005).

[53] Dimitrakopoulos, C. D. and Malenfant, P. R. L. "Organic Thin Film Transistors for Large Area Electronics", *Adv. Mater.* **14**, 99 (2002).

[54] Gundlach, D. J., Lin, Y. Y., Jackson, T. N., Nelson, S. F. and Schlom, D. G. "Pentacene organic thin film transistors molecular ordering and mobility", *Electron Dev. Lett. IEEE* **18**, 87 (1997).

[55] Lin, Y. Y., Gundlach, D. J., Nelson, S. F. and Jackson, T. N. "Pentacene based organic thin film transistors", *IEEE Trans. Electron Dev.* **44**, 1325 (1997).

[56] Yang, S. Y., Shin, K. and Park, C. E. "The Effect of Gate-Dielectric Surface Energy on Pentacene Morphology and Organic Field-Effect Transistor Characteristics", *Adv. Func. Mater.* **15**, 1806 (2005).

[57] Kang, S. J., Noh, M., Park, D. S., Kim, H. J., Kim, S. Y., Koo, B. W., Kang, I. N. and Whang, C. N. "Geometric Effect of Channel on Device Performance in Pentacene Thin-Film Transistor", *Jpn. J. Appl. Phys.* **43**, 7718 (2004).

[58] Dimitrakopoulos, C. D., Brown, A. R. and Pomp, A. "Molecular beam deposited thin films of pentacene for organic field effect transistor applications", *J. Appl. Phys.* **80**, 2501 (1996).

[59] Kymissis, I., Dimitrakopoulos, C. D. and Purushothaman, S. "High-performance bottom electrode organic thin film transistors", *IEEE Trans. Electron Dev.* **48**, 1060 (2001).

[60] Garnier, F., Yassar, A., Hajlaoui, R., Horowith, G., Deloffre, F., Servet, B., Ries, S. and Alnot, P. "Molecular engineering of organic semiconductors: design of self-assembly properties in conjugated thiophene oligomers", *J. Am. Chem. Soc.* **115**, 8716 (2003).

[61] Halik, M., Klauk, H., Zschieschang, U., Schmid, G., Ponomarenko, S., Kirchmeyer, S. and Weber, W. "Relationship Between Molecular Structure and Electrical Performance of Oligothiophene Organic Thin Film Transistors", *Adv. Mater.* **15**, 917 (2003).

[62] Hajlaoui, M. E., Garnier, F., Hassine, L., Kouki, F. and Bouchriha, H. "Growth conditions effects on morphology and transport properties of an oligothiophene semiconductor", *Synth. Met.* **129**, 215 (2002).

[63] McCullough, R. D. "The Chemistry of Conducting Polythiophenes", *Adv. Mater.* **10**, 93 (1998).

[64] Sirringhaus, H., Brown, P., Friend, R. H., Nielsen, M. M., Bechgaard, K., Langeveld-Voss, B. M. W., Spiering, A. J. H., Janssen, R. J., Meijer, E. W., Herwig, P. and de Leeuw, D. M. "Two dimensional charge transport in self organized, high mobility conjugated polymers", *Nature* **401**, 685 (1999).

[65] Bao, Z. and Lovinger, A. J. "Soluble Regioregular Polythiophene Derivatives as Semiconducting Materials for Field Effect Transistors", *Chem. Mater.* **11**, 2607 (1999).

[66] Donat, B. P., Panozzo, S., Vial, J. C., Beigne, C. and Rieutord, R. "Increased field effect mobility from linear to branched thiophene-based polymers", *Synth. Met.* **146**, 225 (2004).

[67] Lim, W. Y., Nagamatsu, S., Takashima, W., Endo, T., Rikukawa, M. and Kaneto, K. "Dependencies of Field Effect Mobility on Regioregularity and Side Chain Length in Poly(Alkylthiophene) Films", *IEICE Trans. Electron.* **1071**, E83C (2000).

[68] Zen, A., Pflaum, J., Hirschmann, S., Zhuang, W., Jaiser, F., Asawapirom, U., Rabe, J. P., Scherf, U. and Neher, D. "Effect of Molecular Weight and Annealing of Poly(3-hexylthiophene)s on the Performance of Organic Field-Effect Transistors", *Adv. Func. Mater.* **14**, 757 (2004).

[69] Kline, R. J., McGehee, M. D., Kadnikova, E. N., Liu, J. S. and Frechet, J. M. J. "Controlling the Field-Effect Mobility of Regioregular Polythiophene by Changing the Molecular Weight", *Adv. Mater.* **15**, 1519 (2003).

[70] Kaneto, K., Lim, W. M., Takashima, W., Endo, T. and Rikukawa, M. "Alkyl Chain Length Dependence of Field-Effect Mobilities in Regioregular Poly(3-Alkylthiophene) Films", *Jap. J. Appl. Phys.* **39-part2**, L872 (2000).

[71] Babel, A. and Jenekhe, S. A. "Alkyl chain length dependence of the field-effect carrier mobility in regioregular poly(3-alkylthiophene)s", *Synt. Met.* **148**, 169 (2005).

[72] Ong, B. S., Wu, Y. L. and Liu, P. "Design of High-Performance Regioregular Polythiophenes for Organic Thin-Film Transistors", *Proc. IEEE* **93**, 1412 (2005).

[73] Chen, X. L., Lovinger, A. J., Bao, Z. and Sapjeta, J. "Morphological and Transistor Studies of Organic Molecular Semiconductors with Anisotropic Electrical Characteristics", *Chem. Mater.* **13**, 1341 (2001).

[74] Natali, D., Sampietro, M., Franco, L., Bolognesi, A. and Botta, C. "Mobility anisotropy in Langmuir Blodgett deposited poly(3-methoxypentyl-tiophene) based thin film transistors", *Thin Solid Films* **472**, 238 (2005).

[75] Sirringhaus, H., Kawase, T., Friend, R. H., Shimoda, T., Inbasekaran, M., Wu, W. and Woo, E. P. "High-Resolution Inkjet Printing of All-Polymer Transistor Circuits", *Science* **290**, 2123 (2000).

[76] Abdou, M. S. A., Orfino, F. P., Son, Y. and Holdcroft, S. "Interaction of Oxygen with Conjugated Polymers: Charge Transfer Complex Formation with Poly(3-alkylthiophenes)", *J. Am. Chem. Soc* **119**, 4518 (1997).

[77] McCulloch, I., Bailey, C., Giles, M., Heeney, M., Love, I., Shkunov, M., Sparrowe, D. and Tierney, S. "Influence of Molecular Design on the Field-Effect Transistor Characteristics of Terthiophene Polymers", *Chem. Mater.* **17**, 1381 (2005).

[78] Ong, B., Wu, Y. L., Jiang, L., Liu, P. and Murti, K. "Polythiophene-based field-effect transistors with enhanced air stability", *Synth. Met.* **142**, 49 (2004).

[79] Murphy, A. R., Chang, P. C., VanDyke, P., Liu, J. S., Frechet, J. M. J., Subramanian, V., DeLongchamp, D. M., Sambasivan, S., Fischer, D. A. and Lin, E. K. "Self-Assembly, Molecular Ordering, and Charge Mobility in Solution-Processed Ultrathin Oligothiophene Films", *Chem. Mater.* **17**, 6033 (2005).

[80] Newman, C. R., Chesterfield, R. J., Merlo, J. A. and Frisbie, C. D. "Transport properties of single-crystal tetracene field-effect transistors with silicon dioxide gate dielectric", *Appl. Phys. Lett.* **85**, 422 (2004).

[81] Facchetti, A., Mushrush, M., Yoon, M. H., Hutchison, G. R., Ratner, M. A. and Marks, T. J. "Building Blocks for n-Type Molecular and Polymeric Electronics. Perfluoroalkyl- versus Alkyl-Functionalized Oligothiophenes (nT; n = 2-6). Systematics of Thin Film Microstructure, Semiconductor Performance, and Modeling of Majority Charge Injection in Field-Effect Transistors", *J. Am. Chem. Soc.* **126**, 13859 (2204).

[82] Katz, H. E., Lovinger, A. J., Johnson, J., Kloc, C., Siegrist, T., Li, W., Lin, Y. Y. and Dodabalapur, A. "A soluble and air-stable organic semiconductor with high electron mobility", *Nature* **404**, 478 (2000).

[83] Katz, H. E., Johnson, J., Lovinger, A. J. and Li, W. J. "Naphthalenetetracarboxylic Diimide-Based n-Channel Transistor Semiconductors: Structural Variation and Thiol-Enhanced Gold Contacts", *J. Am. Chem. Soc.* **122**, 7787 (2000).

[84] Laquindanum, J. G., Katz, H. E., Dodabalapur, A. and Lovinger, A. J. "n-Channel Organic Transistor Materials Based on Naphthalene Frameworks", *J. Am. Chem. Soc.* **118**, 11331 (1996).

[85] Jones, B. A., Ahrens, M. J., Yoon, M. H., Facchetti, A., Marks, T. J. and Wasielewski, M. R. "High-Mobility Air-Stable n-Type Semiconductors with Processing Versatility: Dicyanoperylene-3,4:9,10-bis(dicarboximides)", *Angew. Chem. Int. Ed.* **43**, 6363 (2004).

[86] Chesterfield, R. J .and Newman, C. R., Pappenfus, T. M., Ewbank, P. C., Haukaas, M. H., Mann, K. R., Miller, L. L. and Frisbie, C. D. "High Electron Mobility and Ambipolar Transport in Organic Thin-Film Transistors Based on a π Stacking Quinoidal Terthiophene", *Adv. Mater.* **15**, 1278 (2003).

[87] Zhihua, C., Yan, Z., He, Y. and Antonio, F. "Naphthalenedicarboximide- vs Perylenedicarboximide-Based Copolymers. Synthesis and Semiconducting Properties in Bottom Gate N Channel Organic Transistors", *J. Am. Chem. Soc.* **131**, 8 (2009).

[88] Astrov, D. N. *Sov. Phys. JETP* **11**, 708 (1960).

[89] Waldauf, C., Schilinsky, P., Perisutti, M., Hauch, J. and Brabec, C. J. "Solution-Processed Organic n-Type Thin-Film Transistors", *Adv. Mater.* **15**, 2084 (2003).

[90] Stassen, A. F., de Boer, R. W. I., Iosad, N. N. and Morpurgo, A. F. "Influence of the gate dielectric on the mobility of rubrene single-crystal field-effect transistors", *Appl. Phys. Lett.* **85**, 3899 (2004).

[91] Veres, J., Ogier, S. D., Leeming, S. W., Cupertino, D. C. and Khaffaf, S. M. "Low-k Insulators as the Choice of Dielectrics in Organic Field-Effect Transistors", *Adv. Func. Mater.* **13**, 199 (2003).

[92] Hulea, I. N., Fratini, S., Xie, H., Mulder, C. L., Iossad, N. N., Rastelli, G., Ciuchi, S. and Morpurgo, A. F. "Tunable Frohlich polarons in organic single-crystal transistors", *Nat. Mat.* **5**, 982 (2006).

[93] Dimitrakopoulos, C. D., Puroshothaman, S., Kymissis, J., Callegari, A. and Shaw, J. M. "Low-Voltage Organic Transistors on Plastic Comprising High-Dielectric Constant Gate Insulators", *Science* **283**, 822 (1999).

[94] Dimitrakopoulos, C. D., Kymissis, I., Purushothaman, S., Neumayer, D. A., Duncombe, P. R. and Laibowitz, R. B. "Low-Voltage, High-Mobility Pentacene Transistors with Solution-Processed High Dielectric Constant Insulators", *Adv. Mater.* **11**, 1372 (1999).

[95] Chua, L. L., Ho, P. K. H., Sirringhaus, H. and Friend, R. H. "High-stability ultrathin spin-on benzocyclobutene gate dielectric for polymer field-effect transistors", *Apl. Phys. Lett.* **84**, 3400 (2004).

[96] Chua, L. L., Zaumseil, J., Chang, J. F. Ou, E. C. W., Ho, P. K. H., Sirringhaus, H. and Friend, R. H. "General observation of n-type field-effect behaviour in organic semiconductors", *Nature* **434**, 194 (2005).

[97] Bao, Z. N., Feng, Y., Dodabalapur, A., Raju, V. R. and Lovinger, A. J. "High-Performance Plastic Transistors Fabricated by Printing Techniques", *Chem. Mater.* **9**, 1299 (1997).

[98] Bao, Z. N., Kuck, V., Rogers, J. A. and Paczkowski, M. A. "Silsesquioxane Resins as High-Performance Solution Processible Dielectric Materials for Organic Transistor Applications", *Adv. Func. Mater.* **12**, 526 (2002).

[99] Peng, X. Z., Horowitz, G., Fichou, D. and Garnier, F. "All-organic thin-film transistors made of alpha-sexithienyl semiconducting and various polymeric insulating layers", *Appl. Phys. Lett.* **57**, 2013 (1990).

[100] Ishii, H., Sugiyama, K., Ito, E. and Seki, K. "Energy Level Alignment and Interfacial Electronic Structures at Organic/Metal and Organic/Organic Interfaces", *Adv. Mater.* **11**, 605 (1999).

[101] Wan, A., Hwang, J., Amy, F. and Kahn, A. "Impact of electrode contamination on the NPD/Au hole injection barrier", *Org. Electron* **6**, 47 (2005).

[102] de Boer, B., Hadipour, A., Mandoc, M. M., van Woudenbergh, T. and Blom, P. W. M. "Tuning of Metal Work Functions with Self-Assembled Monolayers", *Adv. Mater.* **17**, 621 (2005).

[103] Hamadani, B. H., Corley, D. A., Ciszek, J. W., Tour, J. M. and Natelson, D. "Controlling Charge Injection in Organic Field-Effect Transistors Using Self-Assembled Monolayers", *Nano Lett.* **6**, 1303 (2006).

[104] Klauk, H., Gundlach, D. J. and Jackson, T. N. "Fast organic thin-film transistor circuits", *IEEE Electron Device Lett.* **20**, 289 (1999).

[105] Garnier, F., Hassine, L., Kouki, F., Bouchriha, H. and Hajlaoui, M. E. " Growth conditions effects on morphology and transport properties of an oligothiophene semiconductor", *Synth. Met.* **129**, 215 (2002).

[106] Halik, M., Klauk, H., Zschieschang, U., Schmid, G., Ponomarenko, S. A. and Kirchmeyer, S. "Oligothiophene Organic Thin Film Transistors and Circuits", *MRS Symp-Proc.* **771**, 11 (2003).

[107] Bao, Z., Lovinger, A. J. and Dodabalapur, A. "Organic field-effect transistors with high mobility based on copper phthalocyanine", *Appl. Phys. Lett.* **69**, 3066 (1996).

[108] Scheinert, S. and Schliefke, W. "Analyzes of field effect devices based on poly(3-octylthiophene)", *Synth. Met.* **139**, 501 (2003).

[109] Liang, G. and Cui, T. "Fabrication and characterization of poly(3,4-ethylenedioxythiophene) field-effect transistors", *Solid-State Electron.* **48**, 87 (2004).

[110] Arias, A. C., Ready, S. E., Lujan, R., Wong, W. S., Paul, K. E., Salleo, A., Chabinyc, M. L., Apte, R. and Street, R. A. "All jet-printed polymer thin-film transistor active-matrix backplanes", *Appl. Phys. Lett.* **85**, 3304 (2004).

[111] Sirringhaus, H. and Tessler, N.and Friend, R. H. "Integrated, high-mobility polymer field-effect transistors driving polymer light-emitting diodes", *Synth. Met.* **102**, 857 (1999).

[112] Kuo, C. "Field-effect transistor with the water-soluble self-acid-doped polyaniline thin films as semiconductor", *Synth. Met.* **93**, 155 (1998).

[113] Brown, A. R., de Leeuw, D. M., Lous, E. J. and Havinga, E. E. "Organic n-type field-effect transistor", *Synth. Met.* **66**, 257 (1994).

[114] Peterson, P. F., Gutmann, M., Proffen, T. and Billinge, S. J. L. "New Air-Stable n-Channel Organic Thin Film Transistors", *J. Am. Chem. Soc.* **120**, 207 (1998).

[115] Smits, E. C. P., Anthopoulos, T. D., Setayesh, S., van Veenendaal, E., Coehoorn, R., Blom, P. W. M., de Boer, B. and de Leeuw, D. M. "Ambipolar charge transport in organic field-effect transistors", *Phys. Rev. B* **73**, 205316 (2006).

[116] Dodabalapur, A., Katz, H. E., Torsi, L. and Haddon, R. C. "Organic Heterostructure Field-ffect Transistors", *Science* **269**, 1560 (1995).

[117] Rost, C., Gundlach, D. J. and Karg, S.and Riess, W. "Ambipolar organic field-effect transistor based on an organic heterostructure", *J. Appl. Phys.* **95**, 5782 (2004).

[118] Arias, A. C., Corcoran, N., Banach, M., Friend, R. H., MacKenzie, J. D. and Huck, W. T. S. "Vertically segregated polymer-blend photovoltaic thin-film structures through surface-mediated solution processing", *Appl. Phys. Lett.* **80**, 1695 (2002).

[119] Meijer, E. J., de Leeuw, D. M., Setayesh, S., van Veenendaal, E., Huisman, B. H., Blom, P. W. M., Hummelen, J. C., Scherf, U. and Klapwijk, T. M. "Solution-processed ambipolar organic field-effect transistors and inverters", *Nat. Mater.* **2**, 678 (2003).

[120] Zaumseil, J. and Sirringhaus, H. "Electron and Ambipolar Transport in Organic Field-Effect Transistors", *Chem. Rev.* **107**, 1296 (2007).

[121] Zaumseil, J., Donley, C. L., Kim, J. S., Friend, R. H. and Sirringhaus, H. "Efficient Top-Gate, Ambipolar, Light-Emitting Field-Effect Transistors Based on a Green-Light-Emitting Polyfluorene", *Adv. Mater.* **18**, 2708 (2006).

[122] Narayan, K. S. and Kumar, N. "Light responsive polymer field-effect transistor", *Appl. Phys. Lett.* **79**, 1891 (2001).

[123] Forrest, S. R. "Active optoelectronics using thin-film organic semiconductors", *IEEE J. Select. Topics Quantum Electron* **6**, 1072 (2000).

[124] Peumans, P., Yakimov, A. and Forrest, S. R. "Small molecular weight organic thin-film photodetectors and solar cells", *J. Appl. Phys.* **93**, 3693 (2003).

[125] Soumya, D. and Narayan, K. S. "Nonexponential relaxation of photoinduced conductance in organic field effect transistors", *Phys. Rev. B* **68**, 125208 (2003).

[126] Soumya, D. and Narayan, K. S. "Gate-Voltage Control of Optically- Induced Charges and Memory Effects in Polymer Field-Effect Transistors", *Adv. Mater.* **16**, 2151 (2004).

[127] Yong-Young, N., Dong-Yu, K., Yuji, Y., Kiyoshi, Y., Byung-Jun, J., Eunhee, L. and Hong-Ku, S. "Organic thin film phototransistors: materials and mechanism", *Proceeding of SPIE* **5724**, 172 (2005).

[128] Wudl, F. "Fullerene materials", *Journal of Materials Chemistry* **12**, 1959 (2002).

[129] Shigenori, M., Anvar, Z. and Katsumi, Y. "Doping effect of buckminsterfullerene in conducting polymer: Change of absorption spectrum and quenching of luminescene", *Solid state commnunications* **82**, 249 (1992).

[130] Saricftci, N. S., Smilowitz, L., Heeger, A. J. and Wudl, F. "Photoinduced Electron Transfer from a Conducting Polymer to Buckminsterfullerene", *Science* **258**, 1474 (1992).

[131] Dhritiman, G., Monojit, B. and Narayan, K. S. "Area dependent efficiency of organic solar cells", *Appl. Phys. Lett.* **93**, 163301 (2008).

[132] Mills, M. E., Townsend, P., Castillo, D., Martin, S. and Achen, A. "Benzocyclobutene (DVS-BCB) polymer as an interlayer dielectric (ILD) material", *Microelectronic Engineering* **33**, 327 (1997).

[133] Salleo, A., Chabinyc, M. L., Yang, M. S. and , Street, R. A. "Polymer thin-film transistors with chemically modified dielectric interfaces", *Appl. Phys. Lett.* **81**, 4383 (2002).

[134] Vogt, B. D., Soles, C. L., Lee, H. J., Lin, E. K. and Wu, W. "Moisture absorption into ultrathin hydrophilic polymer films on different substrate surfaces", *Polymer* **46**, 1635 (2005).

[135] Pisula, W., A. Menon, A., Stepputat, M., Lieberwirth, I., Kolb, U., Tracz, A., Sirringhaus, H., Pakula, T. and Mullen, K. "A Zone-Casting Technique for Device Fabrication of Field-Effect Transistors Based on Discotic Hexa-peri-hexabenzocoronene", *Adv. Mater.* **17**, 684 (2005).

[136] Soumya, D. *"Polymer Field Effect Transistor, Electrical Transport properties and studies of photoinduced charge generation and relaxation processes"*. Ph.D Thesis, JNCASR, (2006).

[137] Harrison, M. G., Gruner, J. and Spencer, G. C. W. "Analysis of the photocurrent action spectra of MEH-PPV polymer photodiodes", *Phys. Rev. B: Condens. Matter* **55**, 7831 (1997).

[138] Sze, S. M. *Physics of Semiconductor Devices.* John-Wiley and Sons, New Jersey, (1981).

[139] Kahn, A., Koch, N. and Gao, W. "Electronic structure and electrical properties of interfaces between metals and π conjugated molecular films", *J. Polym. Sci. B: Polym. Phys.* **41**, 2529 (2003).

[140] Lyon, J. E., Cascio, A. J., Beerbom, M. M., Schlafb, R., Zhu, Y. and Jenekhe, S. A. "Photoemission study of the poly3-hexylthiophene/Au interface", *Appl. Phys. Lett.* **88**, 222109 (2006).

[141] Weiying, G. and Antoine, K. "Controlled p doping of the hole-transport molecular material N,N'-diphenyl-N,N'-bis(1-naphthyl)-1,1'-biphenyl-4,4'-diamine with tetrafluorotetracyanoquinodimethane", *J. Appl. Phys.* **94**, 359 (2003).

[142] Arkhipov, V. I., Emelianova, E. V. and Adriaenssens, G. J. "Effective transport energy versus the energy of most probable jumps in disordered hopping systems", *Phys. Rev. B* **64**, 125125 (2001).

[143] Street, R. A. and Salleo, A. "Contact effects in polymer transistors", *Appl. Phys. Lett.* **81**, 2887 (2002).

[144] Horowitz, G., Lang, P., Mottaghi, M., and Aubin, H. "Extracting Parameters from the Current-Voltage Characteristics of Organic Field-Effect Transistors", *Adv. Func. Mater.* **14**, 1069 (2004).

[145] Klauk, H., Schmid, G., Radlik, W., Weber, W., Zhou, L., Sheraw, C. D., Nichols, J. A. and Jackson, T. N. "Contact resistance in organic thin film transistors", *Solid-state Electron.* **47**, 297 (2003).

[146] Necliudov, V., Shur, M. S., Gundlach, D. J. and Jackson, T. N. "Contact resistance extraction in pentacene thin film transistors", *Solid-state Electron.* **47**, 259 (2003).

[147] Pesavento, P. V., Chesterfield, R. J., Newman, C. R. and Frisbie, C. D. "Gated four-probe measurements on pentacene thin-film transistors: Contact resistance as a function of gate voltage and temperature", *J. Appl. Phys.* **96**, 7312 (2004).

[148] Chesterfield, R. J., McKeen, J. C., Newman, C. R., Frisbie, C. D., Ewbank, P. C., Mann, K. R. and Miller, L. L. "Variable temperature film and contact resistance measurements on operating n-channel organic thin film transistors", *J. Appl. Phys.* **95**, 6396 (2004).

[149] Burgi, L., Richards, T. J., Friend, R. H. and Sirringhaus, H. S. "Close look at charge carrier injection in polymer field-effect transistors", *J. Appl. Phys.* **94**, 6129 (2003).

[150] Puntambekar, K. P., Pesavento, P. V. and Frisbie, C. D. "Surface potential profiling and contact resistance measurements on operating pentacene thin-film transistors by Kelvin probe force microscopy", *Appl. Phys. Lett.* **83**, 5539 (2003).

[151] Gao, W. and Kahn, A. "Effect of electrical doping on molecular level alignment at organicorganic heterojunctions", *Appl. Phys. Lett.* **82**, 4815 (2003).

[152] Reucroft, P. J. *Photocarrier generation mechanism in polymers.* Photoconductivity in polymers: An Interdisciplinary Approach, (1976).

[153] Horowitz, G., Hajlaoui, R., Bouchriha, H., Bourguiga, R. and Hajlaoui, M. "Potentiometry of an operating organic semiconductor field-effect transistor", *Adv. Mater.* **10**, 923 (1998).

[154] Seshadri, K. and Frisbie, C. D. "Potentiometry of an operating organic semiconductor field-effect transistor", *Appl. Phys. Lett.* **78**, 993 (2001).

[155] Natali, D., Fumagalli, L. and M., S. "Modeling of organic thin film transistors: Effect of contact resistances", *J. Appl. Phys.* **101**, 014501 (2007).

[156] Onsager, L. "Initial recombination of ions", *Physical Review* **54**, 554 (1938).

[157] Braun, C. L. "Electric field assisted dissociation of charge transfer states as a mechanism of photocarrier production", *Journal of Chemical Physics* **80**, 4157 (1984).

[158] Sariciftci, N. S. and Heeger, A. J. "Reversible metastable ultrafast photoinduced electron transfer from semiconducitng polymers to buckminsterfullerene and in the corresponding donor acceptor heterojunctions", *Int. J. Mod. Phys. (B)* **8**, 237 (1994).

[159] Morteani, A. C., Sreearunothai, P., Herz, L. M., Friend, R. H. and Silva, C. "Exciton Regeneration at Polymeric Semiconductor Heterojunctions", *Phys. Rev. Lett.* **92**, 247402 (2004).

[160] Benson-smith, J. J., Goris, L., Vandewal, K., Haenen, K., Manca, J. V., Vanderzande, D., Bradley, D. D. C. and Nelson, J. "Formation of a Ground-State Charge-Transfer Complex in Polyfluorene-[6,6]-Phenyl-C61 Butyric

Acid Methyl Ester (PCBM) Blend Films and Its Role in the Function of Polymer PCBM Solar Cells", *Adv. Func. Mater.* **17**, 451 (2007).

[161] Drori, T., Sheng, C. X., Ndobe, A., Singh, S., Holt, J. and Vardeny, Z. V. "Below-Gap Excitation of π Conjugated Polymer-Fullerene Blends: Implications for Bulk Organic Heterojunction Solar Cells", *Phys. Rev. Lett.* **101**, 037401 (2008).

[162] Lloyd-Hughes, J., Richards, T. Sirringhaus, H., Johnston, M. B. and Herz, L. M. "Exciton dissociation in polymer field-effect transistors studied using terahertz spectroscopy", *Phys. Rev. B* **77**, 125203 (2008).

[163] Shi, J. W., Wang, H. B., Song, D., Tian, H. K., Geng, Y. H. and Yan, D. H. "n-Channel, Ambipolar, and p-Channel Organic Heterojunction Transistors Fabricated with Various Film Morphologies", *Adv. Func. Mater.* **17**, 397 (2007).

[164] Babel, A., Wind, J. D. and Jenekhe, S. A. "Ambipolar Charge Transport in Air-Stable Polymer Blend Thin-Film Transistors", *Adv. Func. Mater.* **14**, 891 (2004).

[165] Rost, C., Karg, S., Riess, W., Loi, M. A., Murgia, M. and Muccini, M. "Ambipolar light-emitting organic field-effect transistor", *Appl. Phys. Lett.* **85**, 1613 (2004).

[166] Capelli, R., Toffanin, S., Generali, G., Usta, H., Facchetti, A. and Muccini, M. "Organic light-emitting transistors with an efficiency that outperforms the equivalent light-emitting diodes", *Nat. Mater.* **AOL**, 1 (2010).

[167] Kersting, R., Lemmer, U., Deussen, M., Bakker, H. J., Mahrt, R. F., Kurz, H., Arkhipov, V. I., Bassler, H. and Gobel, E. O. "Ultrafast Field-Induced Dissociation of Excitons in Conjugated Polymers", *Phys. Rev. Lett.* **73**, 1440 (1994).

[168] Blom, P. W. M., Mihailetchi, V. D., Koster, L. J. A. and Markov, D. E. "Device Physics of Polymer:Fullerene Bulk Heterojunction Solar Cells", *Adv. Mater.* **19**, 1551 (2007).

[169] Astrid, G., Morteani, A. C. and Friend, R. H. "Correlation of Heterojunction Luminescence Quenching and Photocurrent in Polymer-Blend Photovoltaic Diodes", *Adv. Mater.* **21**, 3924 (2009).

[170] Barth, S., Bassler, H., Rost, H. and Horhold, H. H. "Extrinsic and intrinsic dc photoconductivity in a conjugated polymer", *Phys. Rev. B* **56**, 3844 (1997).

[171] Barth, S. and Bassler, H. "Intrinsic Photoconduction in PPV-Type Conjugated Polymers", *Phys. Rev. Lett.* **79**, 4445 (1997).

[172] Hamilton, M. and Kanicki, J. "Organic polymer thin-film transistor photosensors", *IEEE J. Sel. Top. Quantum Electron.* **10**, 840 (2004).

[173] Lloyd-Hughes, J., Richards, T., Sirringhaus, H., Castro-Camus, E., Herz, L. M. and Johnston, M. B. "Charge trapping in polymer transistors probed by terahertz spectroscopy and scanning probe potentiometry", *Appl. Phys. Lett.* **89**, 112101 (2006).

[174] Kim, K. H., Zheng, Z. amd Lang, Z., Friend, R. H., Huck, W. T. S. and Kim, J. S. "Efficient Conjugated-Polymer Optoelectronic Devices Fabricated by Thin-Film Transfer-Printing Technique", *Adv. Func. Mater.* **18**, 1012 (2008).

[175] Mihailetchi, V. D., van Duren, J. K. J., Blom, P. W. M., Hummelen, J. C., Janssen, R. A. J., Kroon, J. M., Rispens, M. T., Verhees, W. J. H. and Wienk, M. M. "Electron Transport in a Methanofullerene", *Adv. Func. Mater.* **13**, 43 (2003).

[176] Quist, P. A. C., Savenije, T. J., Schins, J. M., Kroeze, J. E., Rijkers, P. A. and Siebbeles, L. D. A. "Electron diffusion in polymer:fullerene bulk heterojunctions", *Phys. Rev. B* **75**, 195317 (2007).

[177] G. Yu, J. Gao, J. C. H. F. W. and Heeger, A. J. "Polymer Photovoltaic Cells: Enhanced Efficiencies via a Network of Internal Donor-Acceptor Heterojunctions", *Science* **270**, 1789 (1995).

[178] Lemaur, V., Steel, M., Beljonne, D., Bredas, J. L. and Cornil, J. "Photoinduced Charge Generation and Recombination Dynamics in Model Donor/Acceptor Pairs for Organic Solar Cell Applications: A Full Quantum-Chemical Treatment", *J. Am. Chem. Soc.* **127**, 6077 (2005).

[179] Manohar, R. and Narayan, K. S. "Studies of charge transfer processes across donor-acceptor interface using a field effect transistor geometry", *Appl. Phys. Lett.* **95**, 183306 (2009).

[180] Yan, H., Chen, Z., Zheng, Y., Newman, C., Quinn, J. R., Dotz, F., Kastler, M. and Facchetti, A. "A high-mobility electron-transporting polymer for printed transistors", *Nature* **457**, 679 (2009).

[181] Weis, M., Lin, J., Taguchi, D., Manaka, T. and Iwamoto, M. "Analysis of Transient Currents in Organic Field Effect Transistor: The Time-of-Flight Method", *J. Phys. Chem. C* **113**, 18459 (2009).

[182] Steyrleuthner, R., Schubert, M., Jaiser, F., Blakesley, J. C., Chen, Z., Facchetti, A. and Neher, D. "Bulk Electron Transport and Charge Injection in a High Mobility n-Type Semiconducting Polymer", *Adv. Func. Mater.* **AOL**, 1 (2010).

[183] ISE TCAD, Zurich, Switzerland. *Integrated System Engineering AG*, (1998).

[184] Meijer, E. J., deLeeuw, D. M., Setayesh, S., Veenendaal, E. V., Huisman, B. H., Blom, P. W. M., Hummelen, J. C., Scherf, U. and Klapwijk, T. P. M. "Solution-processed ambipolar organic field-effect transistors and inverters", *Nat. Mat.* **2**, 678 (2003).

[185] Scheinert, S. and Paasch, G. "Fabrication and analysis of polymer field-effect transistors", *Phys. Stat. Sol. (a)* **201**, 1263 (2004).

[186] Tan, L., Curtis, M. D. and Francis, A. H. "Simulation of Transient Photoconduction in Organic p-n Junction Bilayer Photodiodes", *Chem. Mater.* **16**, 2134 (2004).